Mon. Not. R. Astron. Soc. **329,** 897–928 (2002)

Evolution of binary stars and the effect of tides on binary populations

Jarrod R. Hurley,[1★]† Christopher A. Tout[1★] and Onno R. Pols[2★]‡
[1]*Institute of Astronomy, Madingley Road, Cambridge CB3 0HA*
[2]*Department of Mathematics, PO Box 28M, Monash University, Victoria 3800, Australia*

Accepted 2001 October 11. Received 2001 September 20; in original form 2000 August 7

ABSTRACT

We present a rapid binary-evolution algorithm that enables modelling of even the most complex binary systems. In addition to all aspects of single-star evolution, features such as mass transfer, mass accretion, common-envelope evolution, collisions, supernova kicks and angular momentum loss mechanisms are included. In particular, circularization and synchronization of the orbit by tidal interactions are calculated for convective, radiative and degenerate damping mechanisms. We use this algorithm to study the formation and evolution of various binary systems. We also investigate the effect that tidal friction has on the outcome of binary evolution. Using the rapid binary code, we generate a series of large binary populations and evaluate the formation rate of interesting individual species and events. By comparing the results for populations with and without tidal friction, we quantify the hitherto ignored systematic effect of tides and show that modelling of tidal evolution in binary systems is necessary in order to draw accurate conclusions from population synthesis work. Tidal synchronism is important but, because orbits generally circularize before Roche lobe overflow, the outcome of the interactions of systems with the same semilatus rectum is almost independent of eccentricity. It is not necessary to include a distribution of eccentricities in population synthesis of interacting binaries; however, the initial separations should be distributed according to the observed distribution of semilatera recta rather than periods or semimajor axes.

Key words: methods: analytical – methods: statistical – binaries: general – stars: evolution – stars: variables: other – galaxies: stellar content.

1 INTRODUCTION

The evolution of binary stars does not differ from that of single stars unless they get in each other's way. If the binary orbit is wide enough, the individual stars are not affected by the presence of a companion, so that standard stellar evolution theory is all that is required to describe their evolution. However, if the stars become close, they can interact, with consequences for the evolution and appearance of the stars, as well as the nature of the orbit.

The effective gravitational potential in a frame rotating with a circular binary system forms equipotential surfaces called Roche surfaces. A sphere of the volume enclosed by the critical Roche surface defines the Roche lobe radius of each star. If either star fills its Roche lobe, then gas flows from the outer layers of that star through the inner Lagrangian point that connects the two Roche lobes. Some or all of this gas may be captured by the companion star so that mass transfer occurs and, as a result, the subsequent evolution of both stars takes a different course from that of isolated stars. When the Roche lobe-filling star is a giant, with a convective envelope, or is significantly more massive than its companion, then, as described by Paczyński (1976), the transferred mass may not be captured by the companion, but instead accumulates in a common envelope (CE) surrounding both stars. The outcome of CE evolution is still not fully understood, but possible scenarios include loss of the envelope as the two cores spiral in to form a closer binary or coalescence of the two stars.

Even in a detached system it is still possible for the stars to interact tidally. Tides can synchronize the spin of the stars with the orbit and circularize an eccentric orbit as the binary tends towards an equilibrium state of minimum energy. Further, if one star is losing mass in a stellar wind, the companion may accrete some of the material, with consequences for the orbit. For a discussion and review of the processes involved in close binary evolution and the various kinds of binaries or exotic stars that can result see Pringle & Wade (1985) and Wijers, Davies & Tout (1996).

★E-mail: jhurley@amnh.org (JRH); cat@ast.cam.ac.uk (CAT); O.R.Pols@astro.uu.nl (ORP)
† Present address: Department of Astrophysics, American Museum of Natural History, Central Park West at 79th Street, New York, NY 10024, USA.
‡ Present address: Astronomical Institute, Utrecht University, Postbus 80000, 3508 TA Utrecht, the Netherlands.

The effects of close binary evolution are observed in many systems, such as cataclysmic variables, X-ray binaries and Algols, and in the presence of stars such as blue stragglers, which cannot be explained by single-star evolution. While many of the processes involved are not understood in detail, we do have a qualitative picture of how binaries evolve, and we can hope to construct a model that correctly follows them through the various phases of evolution. Initial conditions are the mass and composition of the stars, the period (or separation) and eccentricity of the orbit. In order to conduct statistical studies of complete binary populations, i.e., population synthesis, such a model must be able to produce any type of binary that is observed in enough detail, but at the same time be computationally efficient. By comparing results from the model with observed populations, we can enhance our understanding of both binary evolution and the initial distributions (e.g. Eggleton, Fitchett & Tout 1989; Tutukov & Yungelson 1996; Terman, Taam & Savage 1998; Nelson & Eggleton 2001).

Models for binary evolution have been presented in the past (e.g. Whyte & Eggleton 1985; Pols & Marinus 1994; Portegies Zwart & Verbunt 1996, hereafter PZV). The model we present here supersedes the work of Tout et al. (1997), primarily by including eccentric orbits and stellar spins, which are subject to tidal circularization and synchronization. Amongst other improvements, the possibility of mass accretion from a wind is included. Our model incorporates the detailed single-star evolution (SSE) formulae of Hurley, Pols & Tout (2000, hereafter Paper I), which allow for a wider range of stellar types than the description of stellar evolution used by Tout et al. (1997). This requires an updating of the treatment of processes such as Roche lobe overflow, CE evolution and coalescence by collision.

Throughout this paper we refer to one star as the primary, mass M_1, stellar type k_1, etc., and the other as the secondary (or companion), mass M_2 and stellar type k_2. At any time the primary is the star filling, or closest to filling, its Roche lobe. Numerical values of mass, luminosity and radius are in solar units unless indicated otherwise. The stellar types correspond to the evolutionary phases designated by the rapid SSE algorithm of Paper I, which are:

0 = MS star $M \lesssim 0.7$ deeply or fully convective
1 = MS star $M \gtrsim 0.7$
2 = Hertzsprung Gap (HG)
3 = First Giant Branch (GB)
4 = Core Helium Burning (CHeB)
5 = Early Asymptotic Giant Branch (EAGB)
6 = Thermally Pulsing AGB (TPAGB)
7 = Naked Helium Star MS (HeMS)
8 = Naked Helium Star Hertzsprung Gap (HeHG)
9 = Naked Helium Star Giant Branch (HeGB)
10 = Helium White Dwarf (HeWD)
11 = Carbon/Oxygen White Dwarf (COWD)
12 = Oxygen/Neon White Dwarf (ONeWD)
13 = Neutron Star (NS)
14 = Black Hole (BH)
15 = massless remnant.

The SSE algorithm provides the stellar luminosity L, radius R, core mass M_c, core radius R_c, and spin frequency $\Omega_{\rm spin}$, for each of the component stars as they evolve. A prescription for mass loss from stellar winds is included in the SSE algorithm. The algorithm covers all the evolution phases from the zero-age main sequence (ZAMS) up to and including the remnant stages, and is valid for all masses in the range 0.1 to 100 $M_\odot$ and metallicities from $Z = 10^{-4}$ to 0.03. This rapid binary-evolution algorithm is a natural extension of the SSE algorithm. Many of the formulae and much of the terminology contained in Paper I are utilized in this current paper and therefore the interested reader is encouraged to review Paper I.

In Section 2 we describe the binary-evolution algorithm in detail. Section 3 contains illustrative examples of Algol and cataclysmic variable (CV) evolution, and also compares our model with the results of certain binary cases highlighted by Tout et al. (1997) and other authors. We present the results of population synthesis to examine the effects of tides on binary evolution in Section 4, and conclusions are given in Section 5.

2 BINARY EVOLUTION

Before describing our treatment of Roche lobe overflow (RLOF) in detail, we describe interaction in detached systems, via wind accretion and tides. We also consider how mass and angular momentum loss from an individual component affects the system.

Two stars, bound through their mutual gravity, move in elliptical orbits about their common centre of mass. In plane polar coordinates, r, the separation of the stars, and θ, the phase angle, the equations of motion for an elliptical orbit are

$$r = \frac{a(1-e^2)}{1+e\cos\theta} \tag{1}$$

and

$$h = r^2\dot{\theta}, \tag{2}$$

where a is the semimajor axis of the ellipse, and e the eccentricity. The specific angular momentum of the system, $h = |\boldsymbol{h}|$, is given by

$$\boldsymbol{h} = \boldsymbol{r}\times\boldsymbol{v}, \tag{3}$$

where both $\boldsymbol{r}$ and $\boldsymbol{v} = \dot{\boldsymbol{r}}$ lie in the orbital plane. Note that the semilatus rectum

$$l = a(1-e^2) = \frac{h^2}{GM_{\rm b}}, \tag{4}$$

where

$$M_{\rm b} = M_1 + M_2, \tag{5}$$

the total mass of the system, is constant if orbital angular momentum is conserved. These equations consider the stars as point masses interacting by gravity alone. Perturbing effects, such as tidal forces, are not taken into account.

2.1 Wind accretion

If the primary star loses mass in a wind at a rate $\dot{M}_{1\rm W}$, which is determined according to a prescription for single stars such as that given in Paper I, the secondary can accrete some of the material as it orbits through it. Wind accretion is important for the evolution of ζ Aurigae and VV Cephei systems (Che-Bohnenstengel & Reimers 1986; Hack et al. 1992), symbiotic stars (Kenyon 1986; Iben & Tutukov 1996) and massive X-ray binaries (Lamers, van den Heuvel & Petterson 1976).

The mean accretion rate, on to the secondary, can be estimated according to a Bondi & Hoyle (1944) mechanism to be

$$\langle\dot{M}_{2\rm A}\rangle = \frac{-1}{\sqrt{1-e^2}}\left(\frac{GM_2}{v_{\rm W}^2}\right)^2\frac{\alpha_{\rm W}}{2a^2}\frac{1}{(1+v^2)^{3/2}}\dot{M}_{1\rm W}, \tag{6}$$

where

$$v^2 = \frac{v_{\rm orb}^2}{v_{\rm W}^2}, \tag{7}$$

$$v_{\rm orb}^2 = \frac{GM_{\rm b}}{a}. \tag{8}$$

The wind velocity is difficult to determine accurately from observations. We set it proportional to the escape velocity from the surface,

$$v_{\rm W}^2 = 2\beta_{\rm W}\frac{GM_1}{R_1}, \tag{9}$$

where the value of $\beta_{\rm W}$ must depend on the spectral type. Observations of luminous stars indicate that $\beta_{\rm W}$ decreases from about 7 for O stars to about 0.5 for A and F stars (Lamers, Snow & Lindholm 1995). Cool supergiant wind velocities are observed to be $5-35\,{\rm km\,s^{-1}}$ (Kučinskas 1999), where the lower limit should roughly correspond to the wind from the largest stars, about $900\,{\rm R}_\odot$. This suggests $\beta_{\rm W} \simeq 1/8$.

Averages over an orbital period are justified, because the duration of mass loss is typically much greater than *P*. Equation (6) is strictly valid only under the fast wind assumption ($v_{\rm W} \gg v_{\rm orb}$). If the orbital and wind velocities are comparable in size, then the binary motion disturbs the shape of the wind, and the assumption of spherical symmetry is violated. The parameter $\alpha_{\rm W}$ is taken to be 3/2 appropriate for Bondi–Hoyle accretion, and agrees with the lower limit found by Boffin & Jorissen (1988) when modelling wind accretion from a supergiant to explain the barium star ζ Capricorni.

It is necessary that the secondary does not accrete more mass than is lost by the primary, as may follow from equation (6) for highly eccentric orbits, so we enforce the condition

$$|\dot{M}_{2\rm A}| \leq 0.8|\dot{M}_{1\rm W}| \tag{10}$$

to ensure this, and for orbital angular momentum considerations (see Section 2.2). Use of this condition is rare, because we expect any system with appreciable mass accretion to also be experiencing strong tidal evolution (see Section 2.3). We note that there is no special reason for the choice of 0.8 as the upper limit. If the mass ratio of the binary system is close to unity, it is possible for both stars to lose mass at the same time, and the primary may accrete some mass from the secondary. In this case any interaction between the wind material from the two stars is ignored, and equation (6) is simply repeated with the roles of the stars reversed.

If a star loses mass in a stellar wind, then angular momentum is lost too. When the companion accretes some of the material, a fraction of the angular momentum lost from the intrinsic spin of the primary goes into the spin angular momentum of the companion. Therefore

$$\dot{J}_{\rm spin1} = \frac{2}{3}\dot{M}_{1\rm W}h_1 + \frac{2}{3}\mu_{\rm W}\dot{M}_{1\rm A}h_2, \tag{11}$$

where $\dot{M}_{1\rm W} < 0$ and $\dot{M}_{1\rm A} > 0$ (see also section 7.2 of Paper I). We assume that the specific angular momentum in the wind is transferred with perfect efficiency, i.e., $\mu_{\rm W} = 1$, whereas Ruffert (1999), who performed a numerical 3D study of wind accretion using a high-resolution hydrodynamic code, found that the efficiency is roughly between 0 and 70 per cent, depending on model parameters.

Motivated by observations of RS CVn binaries in which the more evolved star becomes the less massive before Roche lobe overflow has begun, Tout & Eggleton (1988) suggested that mass loss may be tidally enhanced by the presence of a moderately close companion. They give a simple descriptive formula

$$\dot{M} = \dot{M}_{\rm R}\left[1 + B_{\rm W}\max\left(\frac{1}{2}, \frac{R}{R_{\rm L}}\right)^6\right] \tag{12}$$

for the enhanced mass-loss rate, where $\dot{M}_{\rm R}$ is the Reimers rate (cf. Paper I), $R_{\rm L}$ is the Roche lobe radius, and $B_{\rm W} \simeq 10^4$. It is uncertain whether such enhanced mass-loss rates are realistic for a wide range of binary systems, so we include equation (12) in the model with $B_{\rm W}$ as a variable parameter, but typically $B_{\rm W} = 0$ is used.

2.2 Orbital changes due to mass variations

The orbital angular momentum can be expressed as

$$J_{\rm orb} = M_1 a_1^2 \Omega_{\rm orb} + M_2 a_2^2 \Omega_{\rm orb}, \tag{13}$$

which naively gives

$$\dot{J}_{\rm orb} = [(\dot{M}_{1\rm W} + \dot{M}_{2\rm A})a_1^2 + (\dot{M}_{2\rm W} + \dot{M}_{1\rm A})a_2^2]\Omega_{\rm orb}, \tag{14}$$

so that if the primary loses mass in a wind, the orbit loses an amount $\Delta M_1 a_1^2 \Omega_{\rm orb}$ of angular momentum, but if the secondary accretes some of this mass, then an amount $\Delta M_2 a_1^2 \Omega_{\rm orb}$ of angular momentum is returned to the orbit. This is exactly the case of conservative mass exchange where the momentum gained by the secondary must be taken from the primary. However, if the fast wind approximation is considered more carefully (Gair & Snellgrove, private communication; for details see Hurley 2000), then, averaged over an orbit,

$$\frac{\langle\delta e\rangle}{e} = -\langle\delta M_2\rangle\left(\frac{1}{M_{\rm b}} + \frac{1}{2M_2}\right), \tag{15}$$

and

$$\frac{\langle\delta a\rangle}{a} = -\frac{\delta M_1}{M_{\rm b}} - \left(\frac{2-e^2}{M_2} + \frac{1+e^2}{M_{\rm b}}\right)\frac{\langle\delta M_2\rangle}{1-e^2}. \tag{16}$$

The change to the orbital angular momentum is then

$$\frac{\langle\delta J\rangle}{J} = \frac{\delta M_1 M_2 - \langle\delta M_2\rangle M_1}{M_1 M_{\rm b}}, \tag{17}$$

and

$$\langle\delta J\rangle = \left[\left(\frac{M_2}{M_{\rm b}}\right)^2\delta M_1 - \left(\frac{M_1}{M_{\rm b}}\right)^2\frac{M_2}{M_1}\langle\delta M_2\rangle\right]a^2\Omega_{\rm orb}, \tag{18}$$

where

$$a_1^2 = \left(\frac{M_2}{M_{\rm b}}\right)^2 a^2 \quad , \quad a_2^2 = \left(\frac{M_1}{M_{\rm b}}\right)^2 a^2, \tag{19}$$

so that

$$\dot{J}_{\rm orb} = \left(\dot{M}_{1\rm W}a_1^2 - \frac{M_2}{M_1}\dot{M}_{2\rm A}a_2^2\right)\Omega_{\rm orb}. \tag{20}$$

This breaks down if $|\Delta M_2| \rightarrow |\Delta M_1|$, which should occur only in extreme cases, e.g., when $R \sim R_{\rm L}$ so that $v_{\rm orb} \sim v_{\rm W}$. The restriction to equation (6) avoids this problem. If mass loss from

both stars is considered, then

$$\dot{J}_{\rm orb} = \left[\left(\dot{M}_{\rm 1W} - \frac{M_1}{M_2}\dot{M}_{\rm 1A}\right)a_1^2 + \left(\dot{M}_{\rm 2W} - \frac{M_2}{M_1}\dot{M}_{\rm 2A}\right)a_2^2\right]\Omega_{\rm orb}. \quad (21)$$

In an eccentric orbit this model takes into account the fact that more matter is accreted at periastron than apastron, so that mass accretion results in circularization of the orbit. The secondary loses momentum owing to the drag it experiences in moving through the primary wind, and it is assumed that these losses are taken from the system in the wind. The model gives $\dot{e}/e < 0$ in all cases. Boffin & Jorissen (1988) predicted a modest increase in eccentricity, based on Huang (1956), due to neglecting changes to the orbital velocity. This was subsequently corrected by Theuns, Boffin & Jorissen (1996), although their treatment still allows eccentricity growth in certain cases. Another difference stems from the time averages, where Huang seems to assume, incorrectly, that the time average operator is multiplicative. equation (15) gives a circularization time-scale which, for small eccentricity, is

$$\frac{1}{\tau_{\rm circ}} = \frac{|\dot{e}|}{e} \approx q_2^2\left(\frac{R_1}{a}\right)^2\frac{|\dot{M}_{\rm 1W}|}{M_{\rm b}}, \quad (22)$$

where $q_2 = M_2/M_1$ is the mass ratio of the secondary star. For a 2.0-$M_\odot$ star on the giant branch the time-scale is

$$\tau_{\rm circ} \sim 1.263\times10^{10}\frac{1}{q_2^2}\left(\frac{a}{R_1}\right)^2 {\rm yr}, \quad (23)$$

and we show in Section 2.3 that the equivalent time-scale due to damping of tides raised on the surface of the 2.0-$M_\odot$ star is

$$\tau_{\rm circ} \sim 0.43\frac{1}{q_2^2}\left(\frac{a}{R_1}\right)^2 {\rm yr}. \quad (24)$$

Therefore the changes in eccentricity owing to mass variations are very small compared to the orbital changes brought about tidal friction. Even on the asymptotic giant branch, where the mass-loss rates increase significantly, this is still true because the deep convective envelope damps the tides even more rapidly.

2.3 Tidal evolution

Observations of close binary stars reveal that stellar rotation tends to synchronize with the orbital motion and can be slower (Levato 1974) or faster (Strassmeier 1996) than for single stars of the same type. The stars do not need to be in contact for this corotation to be achieved, so a mechanism such as tidal friction must be the cause. Tidal interaction is important in changing the orbit of a close detached binary. The degree of interaction is critically dependent on the ratio of the stellar radius to the separation of the stars (Zahn 1977; Hut 1981). The presence of a companion introduces a tidal, or differential, force, which acts to elongate the star along the line between the centres of mass, producing tidal bulges. If the rotational period of the star is shorter than the orbital period, then frictional forces on the surface of the star will drag the bulge axis ahead of the line of centres.

The tidal field can be decomposed into two parts: the *equilibrium tide* which, if all forms of dissipation are neglected, is described by assuming that the star is always in hydrostatic equilibrium, and the *dynamical tide* which arises from stellar oscillations. If dissipative processes are at work within the star, the equilibrium tide will lag or precede the line of centres. The resulting torque transfers angular momentum between the stellar spin and the orbit. Energy is dissipated in the tides, and this diminishes the total energy. Thus the orbital parameters change, and either asymptotically approach an equilibrium state or lead to an accelerated spiralling-in of the two stars (Hut 1980). The equilibrium state is characterized by corotation and a circular orbit, corresponding to a minimum energy for a given total angular momentum and alignment of the spin–orbit axes (which we do not consider in detail).

The main difficulty in a treatment of tidal evolution arises in identifying the physical processes which are responsible for the tidal torque, i.e., the dissipation mechanisms which cause the tides to deviate from an instantaneous equilibrium shape and thus to be misaligned with the line of centres (see Zahn 1992 and Tassoul & Tassoul 1996 for recent reviews of tidal evolution theory).

2.3.1 *The equilibrium tide with convective damping*

The most efficient form of dissipation that may operate on the equilibrium tide is turbulent viscosity in the convective regions of a star. All other forms of dissipation produce time-scales that normally exceed stellar nuclear lifetimes. This mechanism provides a satisfactory interpretation of the behaviour of stars possessing relatively deep convective envelopes. However, it should be noted that this is only an interpretation, because no completely satisfactory description of stellar convection is available. Nevertheless, estimates based on the eddy-viscosity treatment of convection, i.e., the mixing-length theory, seem to adequately represent the tidal time-scales for such stars (Zahn 1989).

To investigate the change of binary parameters due to tidal friction, Hut (1981) considers a simple model in which only equilibrium tides are described, with very small deviations in position and amplitude with respect to the equipotential surfaces. The resulting tidal evolution equations for the tide raised on a star of mass M due to the presence of its companion with mass m are

$$\frac{{\rm d}e}{{\rm d}t} = -27\left(\frac{k}{T}\right)_{\rm c} q(1+q)\left(\frac{R}{a}\right)^8\frac{e}{(1-e^2)^{13/2}} \times\left[f_3(e^2) - \frac{11}{18}(1-e^2)^{3/2}f_4(e^2)\frac{\Omega_{\rm spin}}{\Omega_{\rm orb}}\right], \quad (25)$$

$$\frac{{\rm d}\Omega_{\rm spin}}{{\rm d}t} = 3\left(\frac{k}{T}\right)_{\rm c}\frac{q^2}{r_g^2}\left(\frac{R}{a}\right)^6\frac{\Omega_{\rm orb}}{(1-e^2)^6} \times\left[f_2(e^2) - (1-e^2)^{3/2}f_5(e^2)\frac{\Omega_{\rm spin}}{\Omega_{\rm orb}}\right], \quad (26)$$

where the f_ns are polynomial expressions in e^2 given by Hut (1981). The apsidal motion constant of the primary k takes into account the structure of the star, and T is the time-scale on which significant changes in the orbit take place through tidal evolution, i.e., the damping time-scale defined in terms of the time it takes for the tidal bulge to catch up with the current position of the line of centres. Furthermore, $q = m/M$ ($= q_2$ as defined in this work) is the mass ratio of the stars, and $r_{\rm g}$ is the radius of gyration, where $r_{\rm g}^2 = I/(MR^2)$. This set of equations is valid for any value of the eccentricity, and further discussion of the weak friction model can be found in Alexander (1973) and Kopal (1978).

From equation (26) the synchronization time-scale can be defined as

$$\frac{1}{\tau_{\rm sync}} = \frac{\dot{\Omega}_{\rm spin}}{(\Omega_{\rm spin} - \Omega_{\rm orb})} = 3\left(\frac{k}{T}\right)_{\rm c} q_2^2\frac{MR^2}{I}\left(\frac{R}{a}\right)^6, \quad (27)$$

and from equation (25) the circularization time-scale is

$$\frac{1}{\tau_{\rm circ}} = \frac{21}{2}\left(\frac{k}{T}\right)_{\rm c} q_2(1+q_2)\left(\frac{R}{a}\right)^8 \tag{28}$$

when $e \simeq 0$ and, in the case of $\tau_{\rm circ}$, when $\Omega_{\rm spin} = \Omega_{\rm orb}$. Because $a > R$, $\tau_{\rm sync} < \tau_{\rm circ}$ and corotation is achieved before the orbit circularizes. When the orbit is nearly circular, $e \simeq 0$, it is stable ($\dot{e} < 0$) if $\Omega_{\rm spin}/\Omega_{\rm orb} < 18/11$, in agreement with Zahn (1977). If $\Omega_{\rm spin} > \Omega_{\rm orb}$, then $\dot{\Omega}_{\rm spin} < 0$ and $\dot{a} > 0$, which is as expected, i.e., transfer of angular momentum from the star to the orbit.

In this work it is more convenient to use the tidal circularization time-scale in the form given by Rasio et al. (1996),

$$\frac{1}{\tau_{\rm circ}} = \frac{f_{\rm conv}}{\tau_{\rm conv}}\frac{M_{\rm env}}{M} q_2(1+q_2)\left(\frac{R}{a}\right)^8, \tag{29}$$

so we use

$$\left(\frac{k}{T}\right)_{\rm c} = \frac{2}{21}\frac{f_{\rm conv}}{\tau_{\rm conv}}\frac{M_{\rm env}}{M}\,{\rm yr}^{-1} \tag{30}$$

in Hut's equations. Here

$$\tau_{\rm conv} = 0.4311\left[\frac{M_{\rm env}R_{\rm env}\left(R - \frac{1}{2}R_{\rm env}\right)}{3L}\right]^{1/3}\,{\rm yr} \tag{31}$$

is the eddy turnover time-scale (the time-scale on which the largest convective cells turnover), and $R_{\rm env}$ is the depth of the convective envelope. Equation (31) is essentially the same as equation (4) of Rasio et al. (1996), except that we use the radius in the middle of the convective zone, i.e., $r \simeq \left(R - \frac{1}{2}R_{\rm env}\right)$, rather than at the base, as the typical position of a convective element. The numerical factor $f_{\rm conv}$ is

$$f_{\rm conv} = \min\left[1, \left(\frac{P_{\rm tid}}{2\tau_{\rm conv}}\right)^2\right], \tag{32}$$

where $P_{\rm tid}$ is the tidal pumping time-scale given by

$$\frac{1}{P_{\rm tid}} = \left|\frac{1}{P_{\rm orb}} - \frac{1}{P_{\rm spin}}\right|. \tag{33}$$

As noted by Rasio et al., theoretically and observationally, $f_{\rm conv} = 1$ as long as $\tau_{\rm conv} \ll P_{\rm orb}$. However, if $P_{\rm tid} < \tau_{\rm conv}$, then the largest convective cells can no longer contribute to viscosity, because the velocity field they are damping changes direction before they can transfer momentum. Only the eddies that turn over in a time less than the pumping time-scale contribute, so that the average length and the velocity of these cells are both smaller by the same factor $2\tau_{\rm conv}/P_{\rm tid}$. The factor of 2 arises because tides come around twice in each period.

We implement tidal evolution during a time-step Δt by calculating $\dot{e}$ and $\dot{\Omega}_{\rm spin}$ from equations (25) and (26) and ensuring that the star is not spun down (or up) past the equilibrium spin at which no angular momentum can be transferred,

$$\Omega_{\rm spin,eq} = f_2(e^2)\Omega_{\rm orb}\left[\frac{1}{f_5(e^2)(1-e^2)^{3/2}}\right]. \tag{34}$$

The rate of change of the rotational angular momentum is then given by

$$\dot{J}_{\rm spin} = [k_2'(M - M_{\rm c})R^2 + k_3' M_{\rm c} R_{\rm c}^2]\dot{\Omega}_{\rm spin}, \tag{35}$$

where $k_2' = 0.1$ and $k_3' = 0.21$ (see section 7.2 of Paper I, which contains a description of how $J_{\rm spin}$ and $\Omega_{\rm spin}$ are calculated), so that

$$J_{\rm orb} = J_{\rm orb} - \dot{J}_{\rm spin}\Delta t,$$

$$J_{\rm spin} = J_{\rm spin} + \dot{J}_{\rm spin}\Delta t,$$

$$e = e + \dot{e}\Delta t,$$

and the change in semimajor axis is taken care of by the change in orbital angular momentum. A description of this type has been used successfully for red giants by Karakas, Tout & Lattanzio (2000) to model the eccentricities of barium stars.

The procedure for tidal circularization and synchronization given above is valid for all stars with convective envelopes. These have stellar types

$$k = 1 \quad \text{and} \quad M < 1.25,$$

$$k \in \{0, 2, 3, 5, 6, 8, 9\}.$$

If the companion has an appreciable convective envelope too, then the roles of the two stars can be reversed and the process repeated. Details of how to obtain the mass of the convective envelope can be found in section 7.2 of Paper I. The radial extent of the convective envelope is calculated in a similar fashion. For all giant-like stars ($k \in \{3, 5, 6, 8, 9\}$) $R_{\rm env} = R - R_{\rm c}$. For main-sequence (MS) stars

$$R_{\rm env,0} = \begin{cases} R & M \leq 0.35 \\ R'\left(\frac{1.25-M}{0.9}\right)^{1/2} & 0.35 < M < 1.25 \\ 0.0 & M \geq 1.25 \end{cases}, \tag{36}$$

and then

$$R_{\rm env} = R_{\rm env,0}(1-\tau)^{1/4}, \tag{37}$$

where

$$\tau = \frac{t}{t_{\rm MS}} \tag{38}$$

and R' is the radius of an MS star with $M = 0.35\,{\rm M}_\odot$ at τ (see Paper I). For Hertzsprung gap stars the convective envelope grows as the stars evolve so that

$$R_{\rm env} = \tau^{1/2}(R - R_{\rm c}) \tag{39}$$

with

$$\tau = \frac{t - t_{\rm MS}}{t_{\rm BGB} - t_{\rm MS}}. \tag{40}$$

The main-sequence lifetime, $t_{\rm MS}$, and the time taken for a star to reach the base of the GB, $t_{\rm BGB}$, are given by equations (4) and (5) of Paper I.

2.3.2 *The dynamical tide with radiative damping*

For stars with radiative envelopes, another mechanism is required to explain the observed synchronization of close binaries. A star can experience a range of oscillations that arise from, and are driven by, the tidal field: the dynamical tide (Zahn 1975).

Zahn (1977) derived a circularization time-scale

$$\frac{1}{\tau_{\rm circ}} = \frac{21}{2}\left(\frac{GM}{R^3}\right)^{1/2} q_2(1+q_2)^{11/6}E_2\left(\frac{R}{a}\right)^{21/2} \tag{41}$$

for radiative damping of the dynamical tide. Comparison with

equation (28) gives

$$\left(\frac{k}{T}\right)_{\rm r} = 1.9782\times10^{4}\frac{MR^{2}}{a^{5}}(1+q_{2})^{5/6}E_{2}\,{\rm yr}^{-1}, \quad (42)$$

where E_2 is a second-order tidal coefficient which can be fitted to values given by Zahn (1975),

$$E_{2} = 1.592\times10^{-9}M^{2.84}. \quad (43)$$

We use $(k/T)_{\rm r}$, along with $r_g^2 = k_2'$, in Hut's equations to model tides raised on stars with a radiative envelope. These have types

$k = 1 \quad M \geq 1.25,$

$k \in \{4, 7\}.$

The corresponding synchronization time-scale is given by

$$\frac{1}{\tau_{\rm synch}} = 52^{5/3}\left(\frac{GM}{R^{3}}\right)^{1/2}\frac{MR^{2}}{I}q_{2}^{2}(1+q_{2})^{5/6}E_{2}\left(\frac{R}{a}\right)^{17/2}, \quad (44)$$

so that

$$\frac{1}{\tau_{\rm circ}} = K\frac{1}{\tau_{\rm synch}} \quad , \quad K \approx 0.075\frac{1+q_{2}}{q_{2}}\left(\frac{R}{a}\right)^{2}, \quad (45)$$

and once again $\tau_{\rm circ} > \tau_{\rm synch}$ for realistic mass ratios.

2.3.3 *Tides on degenerate stars*

Campbell (1984) examined the tidal effects in double-degenerate binaries, and derived a synchronization time-scale

$$\frac{1}{\tau_{\rm synch}} = \frac{1}{1.3\times10^{7}}q_{2}^{2}\left(\frac{L}{M}\right)^{5/7}\left(\frac{R}{a}\right)^{6}{\rm yr}^{-1} \quad (46)$$

for a tide raised on a white dwarf (WD) of mass M. This assumes that the WD on which the tides act is initially non-rotating in inertial space, and $\tau_{\rm synch}$ provides an upper limit if this is not true. The synchronization time-scale would also be shorter if tidally excited non-radial oscillations in the star were considered. For WD–WD binaries the orbit should already be circular, and a circularization time-scale is not relevant. However, a synchronization time-scale is applicable, because the companion may be spun up by mass transfer. The formulation also applies to WD–NS binaries, which are in most cases initially eccentric so that a circularization mechanism is required.

Comparing the synchronization time-scale with that from equation (27) for convective damping gives

$$\left(\frac{k}{T}\right)_{\rm d} = 2.564\times10^{-8}r_{\rm g}^{2}\left(\frac{L}{M}\right)^{5/7}{\rm yr}^{-1}, \quad (47)$$

which can be used along with $r_{\rm g}^2 = k_3'$ in Hut's equations to give an estimate of the effect of tidal forces on the orbital parameters owing to degenerate damping.

In most cases a WD primary is expected to be effectively non-rotating, because the progenitor star would have spun down considerably on the AGB through mass loss and a large increase in radius. However, it should be noted that if the primary is initially rotating, it may be better to take equation (46) as representative of the circularization time. Assuming similar results to those derived for convective and radiative damping, this would mean an underestimate of $\tau_{\rm circ}$. Therefore, as equation (46) is an overestimate of $\tau_{\rm synch}$, and in the absence of a better understanding, we can hope that one approximation corrects for the other.

2.3.4 *Relative strengths of the damping mechanisms*

Time-scales for the synchronization and circularization of binary stars with radiative envelopes are generally orders of magnitude larger than those characterizing the equilibrium tide in convective-envelope stars. As an illustration, consider a binary consisting of two MS stars, with masses of 1.0 and 2.0 $\rm M_\odot$ respectively, separated by a distance of 10.0 $\rm R_\odot$. The circularization time-scale owing to tides raised on the 1.0-$\rm M_\odot$ star is $\tau_{\rm circ,c} \simeq 2.5\times10^{8}$ yr as given by equation (28) for convective damping, while that due to radiative damping of the tides on the 2.0-$\rm M_\odot$ star is, according to equation (41), $\tau_{\rm circ,r} \simeq 1.8\times10^{10}$ yr, an order of magnitude greater than the nuclear lifetime of the star. Tidal friction on the 1.0-$\rm M_\odot$ star dominates changes to the orbital parameters, because the convective time-scale, $\tau_{\rm circ,c}$, is an order of magnitude less than the MS lifetime of the 2.0-$\rm M_\odot$ star. For comparison, a WD–NS binary with a separation 10 times the WD radius would have $\tau_{\rm circ,d} \gtrsim 10^{14}$ yr.

Comparing the circularization time-scales for a binary consisting of a 0.5-$\rm M_\odot$ MS star and a 0.8-$\rm M_\odot$ WD gives

$$\tau_{\rm circ,c} \approx 60(a/{\rm R}_\odot)^{8}\,{\rm yr},$$

$$\tau_{\rm circ,d} \approx 10^{19}(a/{\rm R}_\odot)^{6}\,{\rm yr},$$

and thus the degenerate damping is dominant only for WD–WD and WD–NS systems in which the separation can become very small.

Following Zahn (1977), the limiting separations for synchronization and circularization can be defined as the initial separations $(a/R)_{\rm sync}$ and $(a/R)_{\rm circ}$ for which the characteristic time-scales are equal. As an example, consider equal-mass MS binaries with both $\tau_{\rm sync}$ and $\tau_{\rm circ}$ set equal to one-quarter of the MS lifetime. The results are given in Table 1. The tidal damping is clearly more efficient for stars with convective envelopes, and only becomes more so if the binary includes a giant-like star.

We note that Zahn (1977) obtains larger values of $(a/R)_{\rm circ}$ for radiative stars than those given in Table 1. This seems to arise from using MS lifetimes up to 6 times greater than those found here. However, using his $(a/R)_{\rm circ}$ with $\tau_{\rm sync} = \tau_{\rm circ}$ gives larger $(a/R)_{\rm sync}$ values than he records, with the end result that, while the values of $(a/R)_{\rm circ}$ calculated here are lower than his, the values of $(a/R)_{\rm sync}$ are much the same.

2.4 Gravitational radiation and magnetic braking

Coalescing neutron stars are a source of gravitational waves and may produce γ-ray bursts (Hartmann 1996). Such merging requires angular momentum loss from the system. This can be achieved by gravitational radiation from close binary systems driving the system to a mass transfer state, possibly followed by coalescence. It is also necessary for the formation of AM CVn systems (González Pérez 1999), and adequate for cataclysmic variables (CVs) below the period gap (Faulkner 1971). Eggleton (private communication) uses the weak-field approximation of general relativity to derive the orbital changes due to gravitational radiation from two point masses as

$$\frac{\dot{J}_{\rm gr}}{J_{\rm orb}} = -8.315\times10^{-10}\frac{M_{1}M_{2}M_{\rm b}}{a^{4}}\frac{1+\frac{7}{8}e^{2}}{(1-e^{2})^{5/2}}{\rm yr}^{-1}, \quad (48)$$

$$\frac{\dot{e}}{e} = -8.315\times10^{-10}\frac{M_{1}M_{2}M_{\rm b}}{a^{4}}\frac{\frac{19}{6}+\frac{121}{96}e^{2}}{(1-e^{2})^{5/2}}{\rm yr}^{-1}. \quad (49)$$

These formulae do not take into account any contribution from distortions in spherical symmetry of the stars. Kuznetsov et al. (1998) show that for a binary consisting of two neutron stars this contribution becomes noticeable only when the separation decreases to less than 7 times the size of the neutron star. Neglecting it then causes less than a 10 per cent error in the small time remaining to coalescence.

Gravitational radiation is efficient only for CVs with orbital periods less than 3 h, and so cannot explain the mass transfer rates of such objects with periods up to 10 h (Faulkner 1971; Zangrilli, Tout & Bianchini 1997). However, it is possible for orbital angular momentum to be lost from the system via magnetic braking of the tidally coupled primary by its own magnetic wind. Rappaport, Verbunt & Joss (1983) used mass-transfer rates deduced from observations of CVs, and the Skumanich (1972) braking law, to parametrize the rate of angular momentum loss by magnetic braking. We use

$$\dot{J}_{\rm spin} = \dot{J}_{\rm mb} = -5.83\times10^{-16}\frac{M_{\rm env}}{M}(R\Omega_{\rm spin})^3\,{\rm M}_\odot\,{\rm R}_\odot^2\,{\rm yr}^{-2}, \qquad (50)$$

where all masses and the radius are in solar units, and $\Omega_{\rm spin}$ is in units of years, to alter the spin angular momentum of the component star and allow tides to alter $J_{\rm orb}$. This is effective for any star with an appreciable convective envelope. We note that the non-parametric formulation for magnetic braking given by Stępień (1995), derived and calibrated from observations of spin-down of single stars, should be investigated in future versions of our binary model.

The MS primary in a CV has $R_1 \simeq R_{\rm L1} \simeq M_1$, so it is possible to derive the relation $P/{\rm h} \approx 10.0 M_1/{\rm M}_\odot$ for the period (Verbunt 1984). This with equations (48) and (50) gives

$$\frac{|\dot{J}_{\rm mb}|}{|\dot{J}_{\rm gr}|} = 9.815\times10^9\,\frac{(M_{\rm b}M_1^2)^{2/3}}{M_2^2}, \qquad (51)$$

so that magnetic braking dominates even as $M_1 \rightarrow 0.0$. Observations of CVs reveal a gap between 2 and 3 h in the otherwise smooth period–mass distribution. This period gap can be explained if magnetic braking becomes less effective when the orbital period falls below 3 h, corresponding roughly to an MS primary which has just become fully convective (Rappaport, Verbunt & Joss 1983; Zangrilli et al. 1997). We therefore do not apply magnetic braking when the primary is a fully convective MS star, $M_1 < 0.35$. Braking proceeds only by gravitational radiation for such systems.

Table 1. The fractional separations at which the synchronization and circularization time-scales are equal to 1/4 of the main-sequence lifetime for equal-mass binaries starting on the ZAMS. Only the contribution from one star has been taken into account. Column 2 gives the ZAMS radius of the star.

M	$R_{\rm ZAMS}$	$t_{\rm MS}$/yr	$(a/R)_{\rm sync}$	$(a/R)_{\rm circ}$
0.5	0.46	1.29×10^{11}	125.46	32.76
0.8	0.73	2.65×10^{10}	109.81	24.64
1.0	0.89	1.10×10^{10}	107.61	20.36
1.2	1.14	5.62×10^{9}	124.58	14.71
1.6	1.48	2.25×10^{9}	6.80	3.94
2.0	1.61	1.16×10^{9}	6.75	3.92
3.2	2.05	3.18×10^{8}	6.69	3.89
5.0	2.64	1.04×10^{8}	6.68	3.88
7.0	3.20	4.89×10^{7}	6.74	3.91
10.0	3.94	2.43×10^{7}	6.89	3.98

2.5 Supernovae kicks

When a star explodes as a supernova and becomes a neutron star or black hole it receives a velocity kick, due to any asymmetry in the explosion (Lyne & Lorimer 1994). This may disrupt the binary. Evidence for such a kick includes observations of pulsars with velocities in excess of those of ordinary stars (Hansen & Phinney 1997), double-NS binaries (Fryer & Kalogera 1997) and X-ray binaries with large eccentricities (Kaspi et al. 1996). The state of the binary post-supernova depends on the orbital parameters at the moment of explosion and the kick velocity. A complete derivation is given in Appendix A1.

If the binary survives the supernova explosion, then it is quite likely that the orbital parameters, a and e, change markedly from those of the initial orbit. In addition, the mass lost by the primary star carries away an amount $\Delta J_{\rm orb} = \Delta M_1 a_1^2 \Omega_{\rm orb}$ of orbital angular momentum from the system. Before the primary core collapses, it has spin angular momentum

$$J_{\rm spin} = k_3' M_{\rm c} R_{\rm c}^2 \Omega_{\rm spin}, \qquad (52)$$

which we conserve in the neutron star, spinning it up as it shrinks.

2.6 Roche lobe overflow

Mass transfer occurs in close binary systems following the onset of Roche lobe overflow (RLOF). This can be triggered either by a star expanding to fill its Roche lobe as a result of stellar evolution, or by angular momentum losses causing contraction of the orbit. The Roche lobe radius of a star is fitted by Eggleton (1983) with

$$\frac{R_{\rm L1}}{a} = \frac{0.49q_1^{2/3}}{0.6q_1^{2/3} + \ln(1+q_1^{1/3})}, \qquad (53)$$

in terms of the semimajor axis of the orbit and the mass ratio $q_1 = M_1/M_2$ of the primary star, accurate to within 2 per cent for $0 < q_1 < \infty$. Note that equation (53) may also be used to obtain the Roche lobe radius of the secondary by using the appropriate mass ratio, i.e., q_2. The theory of RLOF is based on two stars in a circular orbit in which complete corotation has been achieved. In most cases this is adequate, because tidal friction generally acts to remove any eccentricity on a time-scale shorter than the evolution time-scale of the binary. However, it may be possible for RLOF to occur in an eccentric orbit if the binary is formed by tidal capture so that the primary, the more evolved star, has not spent all its life as part of the present system. It is also possible that stars may form in a close eccentric binary, but it is generally expected that some initial circularization occurs as part of the formation process. Eccentric RLOF could also be envisaged if a star in an eccentric orbit is rapidly expanding, such as on the AGB, so that the nuclear and circularization time-scales are similar. If any of these rare cases arise, then, for want of a more detailed treatment, we subject them to instant synchronization at the onset of RLOF.

When $R_1 > R_{\rm L1}$ mass is transferred to the companion star, with the primary losing an amount of mass $\Delta M_{1\rm R}$ and the secondary gaining some fraction $\Delta M_{2\rm R}$ of this mass. All normal processes of binary evolution, as described in the preceding sections of this paper, are also treated during RLOF. This means that mass variations due to stellar winds and the related changes to $J_{\rm orb}$ and $J_{\rm spin}$ are still accounted for, as are changes resulting from tidal friction. In addition, if a degenerate secondary star is not altered by the tidal evolution treatment, then its spin is changed according to

$$\Delta J_{\rm spin2} = k_3' \Delta M_{2\rm R} R_2^2 \Omega_{\rm K2}, \qquad (54)$$

where we assume that the accreted material comes from the inner edge of an accretion disc which has

$$\Omega_{\rm K2} = \sqrt{\frac{GM_2}{R_2^3}}. \tag{55}$$

Care is taken to conserve the total angular momentum of the system. Independent of the transfer, the tides should maintain corotation of the primary and the orbit during the Roche phase. We assume that mass changes due to RLOF do not affect the orbital angular momentum if the mass transfer is conservative. Any material not accepted by the secondary is lost from the system, taking with it specific angular momentum from the primary so that $a(M_1 + M_2) =$ constant. During RLOF $R_{\rm L1}$ is used as the effective radius of the primary when calculating $\dot{M}_{\rm 1W}$ and any associated angular momentum changes, as well as in the tidal expressions.

The treatment of RLOF presented here is a substantially revised version of that described by Tout et al. (1997), including essential changes required to make it compatible with the updated stellar evolution treatment and the explicit treatment of angular momentum. Following Tout et al., we describe the stability of mass transfer using the radius–mass exponents ζ defined by Webbink (1985).

2.6.1 *Dynamical mass transfer*

If $\zeta_{\rm ad} < \zeta_{\rm L}$ the radius of the primary increases faster than the Roche lobe on conservative mass transfer. The mass-loss rate from the primary is limited only by the sonic expansion rate of its envelope, as mass is transferred through the inner Lagrangian point connecting the Roche lobes of the two stars. Stars with deep surface convection zones, and degenerate stars, are unstable to such dynamical time-scale mass-loss, unless the primary is rather less massive than the secondary so that $\zeta_{\rm L}$ is more negative than $\zeta_{\rm ad}$. Thus dynamical mass transfer occurs for giants ($k_1 \in \{3, 5, 6, 8, 9\}$), low-mass MS stars ($k_1 = 0$) and WDs ($k_1 \in \{10, 11, 12\}$) when $q_1 > q_{\rm crit}$. This critical mass ratio is defined by $\zeta_{\rm ad} = \zeta_{\rm L}$, where $\zeta_{\rm L} \approx 2.13q_1 - 1.67$ (Tout et al. 1997) for conservative mass transfer. For normal giants $R \propto M^{-x}$, where $x \simeq 0.3$ varies with composition (as given by equation 47 of Paper I), so that $\zeta_{\rm ad} = -x$ if $\zeta_{\rm ad} \approx \zeta_{\rm eq}$. However, the behaviour of the radius deviates from this relation when the mass of the giant envelope is small. To detailed stellar models we fit

$$\zeta_{\rm ad} \approx \zeta_{\rm eq} \approx -x + 2\left(\frac{M_{\rm c}}{M}\right)^5, \tag{56}$$

and use

$$q_{\rm crit} = \left[1.67 - x + 2\left(\frac{M_{\rm c1}}{M_1}\right)^5\right]/2.13 \tag{57}$$

for the critical mass ratio above which mass transfer proceeds on a dynamical time-scale. We note that a modified criterion is required in cases of non-conservative mass transfer, and that the assumption of $\zeta_{\rm ad} \approx \zeta_{\rm eq}$ is not always true (Hjellming 1989). Naked helium giants have $\zeta_{\rm ad} \approx 0$, so that $q_{\rm crit} = 0.784$. We treat all cases with $q_1 > q_{\rm crit}$ in which the primary star is a giant as CE evolution, described in Section 2.7.1. For low-mass MS stars $q_{\rm crit} = 0.695$, and for white dwarfs $q_{\rm crit} = 0.628$ (see Tout et al. 1997). We describe treatment of these cases in Sections 2.6.4 and 2.6.5.

Based on models of condensed polytropes (Hjellming & Webbink 1987), an alternative condition for dynamical mass transfer from a giant primary,

$$q_{\rm crit} = 0.362 + [3(1 - M_{\rm c1}/M_1)]^{-1},$$

valid for $M_{\rm c1}/M_1 \gtrsim 0.2$, is given by Webbink (1988). This relation is similar to equation (57) for $M_{\rm c1}/M_1 = 0$, but quickly diverges as $M_{\rm c1}/M_1$ increases: it is a factor of 2 larger at $M_{\rm c1}/M_1 = 0.6$. For values of q_1 intermediate between the two conditions Tout et al. (1997) allow mass transfer to proceed on a thermal time-scale so that CE evolution is avoided. In the presence of mass loss, and particularly any enhanced mass loss, this would lead to a significant increase in the number of stable mass-transfer systems. The formation paths of many binary populations, such as CVs (which require a common-envelope phase) and symbiotic stars (which need to avoid common envelope), would therefore be affected if we were to follow the same scheme.

2.6.2 *Nuclear mass transfer*

If $\zeta_{\rm L} < (\zeta_{\rm ad}, \zeta_{\rm eq})$, then mass transfer is stable until nuclear evolution causes further expansion of the star, that is to say that the mass transfer is not self-stimulating. The radius of the primary remains constrained to that of its Roche lobe, and the star remains in thermal equilibrium. Mass transfer proceeds at a rate such that $R_1 \approx R_{\rm L1}$, so that the primary just overfills its Roche lobe. We achieve this by transferring mass at a rate that steeply increases with the amount by which the Roche lobe is overfilled,

$$\dot{M}_{\rm 1R} = F(M_1)[\ln(R_1/R_{\rm L1})]^3\ {\rm M}_\odot\ {\rm yr}^{-1}, \tag{58}$$

where

$$F(M_1) = 3 \times 10^{-6}[\min(M_1, 5.0)]^2 \tag{59}$$

is chosen by experiment to ensure that the mass transfer is steady. If the primary is a degenerate star ($k_1 \geq 10$), then it is necessary to increase equation (59) by the factor $10^3/\max(R_1, 10^{-4})$. In general, nuclear mass transfer occurs on a much longer time-scale than either dynamical or thermal mass transfer, so that systems such as Algols and CVs can be observed in this state.

2.6.3 *Thermal mass transfer*

If $\zeta_{\rm eq} < \zeta_{\rm L} < \zeta_{\rm ad}$ mass transfer is unstable on a thermal time-scale. The primary does not remain in thermal equilibrium as it loses mass: it contracts and remains just filling its Roche lobe. This is an awkward case to treat, because the thermal time-scale is long compared with the orbital period, but short compared with the time-scale for nuclear evolution. First, we calculate the mass-transfer rate at the full equilibrium rate using equation (58). This gives an upper limit. For giants and giant-like stars ($k_1 \in \{2, 3, 4, 5, 6, 8, 9\}$) we limit this to the thermal rate, which we approximate by

$$\dot{M}_{\rm KH} = \frac{M_1}{\tau_{\rm KH1}} \tag{60}$$

with

$$\frac{\tau_{\rm KH}}{\rm yr} = \frac{10^7 M}{RL}\begin{cases} M & k \in \{0, 1, 7, 10, 11, 12, 13, 14\} \\ (M - M_{\rm c}) & k \in \{2, 3, 4, 5, 6, 8, 9\} \end{cases}, \tag{61}$$

where $\tau_{\rm KH}$ is the Kelvin–Helmholtz time-scale. This still allows the possibility of $R_1 > R_{\rm L1}$ by quite a large fraction. The most common case of mass transfer at the thermal rate has a Hertzsprung

gap primary star ($k_1 = 2$), because $\zeta_{\rm ad}$ is quite large, while $\zeta_{\rm eq}$ is close to its giant branch value. For these stars $\zeta_{\rm L}$ can still exceed $\zeta_{\rm ad}$ when q_1 is large. We assume $\zeta_{\rm ad} \approx 6.85$ (Tout et al. 1997) so that if q_1 exceeds $q_{\rm crit} = 4$, CE evolution ensues as a result of dynamical mass transfer. We note that this assumption is rather approximate and can be improved in future versions of the algorithm by calibrating to detailed binary calculations. For all non-giant-like stars we allow mass transfer to proceed at the rate given by equation (58) but limited by the dynamical rate

$$\dot{M}_{\rm DYN} = \frac{M_1}{\tau_{\rm DYN1}}, \tag{62}$$

where

$$\tau_{\rm DYN} = 5.05 \times 10^{-5} \sqrt{\frac{R^3}{M}} {\rm yr}. \tag{63}$$

In this dynamically limited case, if $R_1 > 10 R_{\rm L1}$ as a result of significant orbital contraction, the stars are allowed to merge according to the appropriate collision prescription (see Section 2.7.3).

2.6.4 *Dynamical mass transfer from low-mass main-sequence stars*

Low-mass MS stars ($k_1 = 0$) are deeply convective, so that mass transfer to a companion proceeds dynamically if $q_1 > 0.695$. If this is the case, we assume that the entire star overflows its Roche lobe on a time-scale $\tau_{\dot{M}} = \tau_{\rm DYN1}$, and only a single star remains.

If the secondary star is fairly unevolved ($k_2 \in \{0, 1, 2\}$), its thermal time-scale will be relatively long, and it can accrete only a fraction

$$\Delta M_{\rm 2R} = \min\left(10 \frac{\tau_{\dot{M}}}{\tau_{\rm KH2}}, 1\right) \Delta M_{\rm 1R}, \tag{64}$$

of the mass, where $\Delta M_{\rm 1R} = M_1$. If the secondary is still on the MS, it must be rejuvenated (see Section 2.6.6). When the secondary is a giant or a CHeB star ($k_2 \in \{3, 4, 5, 6\}$), its envelope can easily absorb all of the primary mass on a dynamical time-scale. If the secondary is a naked He star or a WD ($k_2 \in \{7, 8, 9, 10, 11, 12\}$), then all the material is accreted dynamically and swells up to form a giant envelope around the degenerate star, which becomes the core of a new giant star. This is effectively a reverse of the process which formed the degenerate remnant star in the first place when a giant or CHeB star lost its envelope. The new star requires an age appropriate to its core, the calculation of which is described in Section 2.7 along with a detailed description of the outcome.

2.6.5 *Mass transfer from degenerate objects*

If a WD ($k_1 \in \{10, 11, 12\}$) evolves to fill its Roche lobe, then the secondary must be a more massive WD or possibly an NS or BH ($k_2 \in \{10, 11, 12, 13, 14\}$). Mass transfer proceeds at a steady rate according to equation (58), unless $q_1 > 0.628$ when the mass transfer becomes dynamical. In this case the entire mass is transferred on a time-scale $\tau_{\rm DYN1}$, as given by equation (63), leading to coalescence of the two stars.

When dynamical mass transfer leads to the coalescence of two HeWDs, we assume that the temperature produced is enough to ignite the triple-α reaction. If all the material in the new core were rapidly converted to CO, then the nuclear energy released would be greater than the binding energy of the core, so that no remnant is left ($k_2 = 15$). Here we follow this procedure, but it is possible that a naked helium star is produced (Webbink 1984). This alternative could easily be included. Dynamical mass transfer of helium on to a COWD or ONeWD causes the accreted material to swell up and form an envelope around the CO or ONe core (Iben, Tutukov & Yungelson 1996) so that a HeGB star is formed ($k_2 = 9$). If an ONeWD accretes CO or ONe material, this is simply added to the WD ($k_2 = 12$), unless the new mass exceeds the Chandrasekhar mass, $M_{\rm Ch}$, in which case electron capture on ^{24}Mg nuclei leads to an accretion-induced collapse (AIC) (Nomoto & Kondo 1991; van Paradijs et al. 1997) and the formation of an NS ($k_2 = 13$).

Dynamical mass transfer from a COWD to another COWD quickly leads to the formation of a thick accretion disc (as in all the above cases of dynamical transfer) around the more massive WD, followed by coalescence over a viscous time-scale. When two COWDs coalesce, we form a larger COWD ($k_2 = 11$) of mass $M_2 + \Delta M_{\rm 2R}$. If the mass exceeds $M_{\rm Ch}$, then it explodes as a possible type Ia SN (Branch 1998), leaving no remnant ($k_2 = 15$). However, whether a thermonuclear explosion actually occurs is not clear. The temperature produced at the core–disc boundary depends on the accretion rate, which in turn depends on the viscosity of the disc, all of which is uncertain. If the temperature is hot enough to ignite carbon and oxygen, whether the WD is converted to an ONeWD depends on competition between the rate of propagation of the flame inwards, which depends on the opacity, and the cooling rate of the WD. Saio & Nomoto (1998) used spherically symmetric evolution models of accreting WDs to show that carbon burning is ignited at the core–disc boundary and that the flame propagates all the way to the centre, by heat conduction, converting the material to ONeMg without causing an explosion. If this is indeed the case, then CO–CO WD merger products with a total mass greater than $M_{\rm Ch}$ would become AIC neutron stars rather than type Ia SNe.

When an NS or BH ($k_1 \in \{13, 14\}$) fills its Roche lobe, the secondary must be an NS or BH, and we allow the two stars to merge and form a single remnant of the combined mass. Alternatively, coalescing NSs may destroy themselves in a γ-ray burst (Hartmann 1996).

2.6.6 *The response of the secondary*

If the secondary is an MS, HG or CHeB star ($k_2 \in \{0, 1, 2, 4\}$) we transfer an amount of mass given by equation (64), limited by the thermal time-scale of the secondary

$$\tau_{\dot{M}} = \frac{M_2}{\dot{M}_{1R}} < \tau_{\rm KH2}. \tag{65}$$

A giant secondary can respond to mass transfer by dynamically shrinking, and no limitation need be applied. When a HeMS star accretes mass from a primary of the same type, we transfer an amount of mass given by equation (64). The HeMS star must then be rejuvenated. However, if mass is transferred to a naked helium star from a primary of any hydrogen-rich type, we put all the mass in an envelope around the helium core, and form a new CHeB or AGB star. Details of how the new star is made are given in Section 2.7.

At any time the secondary may respond to mass transfer by filling its own Roche lobe so that a contact binary is formed. If this occurs, we allow the two stars to coalesce (see Section 2.7.3). Generally, CE evolution arises before contact, unless the binary formed as a very close system.

2.6.6.1 *Rejuvenation*

We extend the rejuvanation described by Tout et al. (1997) for MS stars to include HG and HeMS stars. When such a primary transfers mass, it must be aged so that the fractional age of the star, in terms of its current evolution phase, remains unchanged. The process by which this is done is the same as that described in section 7.1 of Paper I. If any of these stars are accepting mass, then they rejuvenate. This we do simply by reversing the ageing process for MS stars with radiative cores ($0.35 \leq M \leq 1.25$) and for HG secondaries (see section 7.1 of Paper I). For MS stars with convective cores ($M > 1.25$), and fully convective stars ($M < 0.35$), the core grows and mixes in unburnt fuel as the star gains mass, so that the star appears even younger. The rejuvenation of MS stars is detailed by Tout et al. The core of a HeMS star is convective with $M_{\rm c} \propto M$, so these secondaries are rejuvenated in the same way.

2.6.6.2 *Steady accretion on to degenerate objects*

For transfer of mass to degenerate objects we follow Tout et al. (1997), but the greater variety of stars now makes the procedure more complex. Accretion of H-rich material leads to novae if $\dot{M} < 1.03 \times 10^{-7}\,{\rm M}_\odot\,{\rm yr}^{-1}$, and supersoft X-ray sources if $1.03 \times 10^{-7} \leq \dot{M} < 2.71 \times 10^{-7}\,{\rm M}_\odot\,{\rm yr}^{-1}$, in the same way, and for accretion rates $\dot{M} \geq 2.71 \times 10^{-7}\,{\rm M}_\odot\,{\rm yr}^{-1}$ HeWDs become GB stars while CO and ONeWDs become TPAGB stars (see Section 2.7 for details). For nova systems we assume that all but a fraction ϵ of the accreted material is ejected in the nova explosion, i.e.

$$\Delta M_{2{\rm R}} = \epsilon \Delta M_{1{\rm R}}, \tag{66}$$

where ϵ is an input parameter to the model and may be negative. Typically we take $\epsilon = 0.001$.

How the WD secondary responds to steady accretion of He-rich material, either directly ($7 \leq k_1 \leq 10$) or as a consequence of steady hydrogen burning on the surface of the WD, depends on its composition. Woosley, Taam & Weaver (1986) calculated thermonuclear explosions induced by the accretion of helium on to a HeWD. Their models showed that accretion at $2 \times 10^{-8}\,{\rm M}_\odot\,{\rm yr}^{-1}$ on to a 0.4-$\rm M_\odot$ HeWD leads to a violent, centrally ignited detonation when the mass of the star reaches $0.66\,{\rm M}_\odot$. Nomoto & Sugimoto (1977) had previously found detonations at $0.78\,{\rm M}_\odot$. Here a HeWD is allowed to accrete material until its mass reaches $0.7\,{\rm M}_\odot$, when it is destroyed ($k_2 = 15$).

A COWD accreting helium can accumulate about $0.15\,{\rm M}_\odot$ of helium-rich material, provided the total mass remains below $M_{\rm Ch}$, before helium ignites at the base of the accreted layer. This is an edge-lit detonation (ELD). The detonation front propagates outward through the helium layer, while an inward propagating pressure wave compresses the CO core which ignites off-centre, followed by an outward detonation which destroys the WD (Woosley & Weaver 1994; Livne & Arnett 1995). Kawai, Saio & Nomoto (1987), by considering steady state spherically accreting models, argue that if the accretion rate exceeds $3 \times 10^{-8}\,{\rm M}_\odot\,{\rm yr}^{-1}$ helium can burn steadily and non-degenerately. It is not clear that such steady burning is possible if accretion is from a disc leaving most of the WD photosphere free to radiate. Therefore, once a COWD has accumulated $0.15\,{\rm M}_\odot$ of accreted helium, we set off an ELD which destroys the WD in a type Ia SN. Livne & Arnett argue that the properties of type Ia SNe are diverse enough to suggest that the progenitors have a range of parameters, such as mass. The more luminous events might then correspond to more massive progenitors. They find that detonations in sub-Chandrasekhar mass WDs are a promising explanation for most, if not all, type Ia SNe. Such SNe are not standard candles (cf. Section 2.6.5): they exhibit considerable diversity in behaviour.

In the case of steady transfer of He-rich material on to an ONeWD, or steady transfer of C-rich material ($k_1 = 11, 12$) on to a COWD or ONeWD, we add the material to the degenerate core of the secondary. If the new mass of a white dwarf secondary exceeds the Chandrasekhar limit, $M_{\rm Ch}$, then we annihilate it in a type Ia SN, unless it is an ONeWD ($k_2 = 12$) which undergoes AIC leaving an NS remnant. When such a SN explodes as a result of steady mass transfer, the primary survives, having transferred only just enough material for the secondary mass to reach $M_{\rm Ch}$.

The amount of mass that a WD, NS or BH can accrete may be limited by the Eddington limit (Cameron & Mock 1967),

$$\dot{M}_{\rm Edd} = 2.08 \times 10^{-3}(1+X)^{-1} R_2\,{\rm M}_\odot\,{\rm yr}^{-1}, \tag{67}$$

where X is the hydrogen mass fraction, so that

$$\Delta M_{2{\rm R}} = \min(\dot{M}_{\rm Edd}\tau_{\dot{M}}, \Delta M_{1{\rm R}}). \tag{68}$$

There is some uncertainty as to whether the Eddington limit should actually be applied, because the energy generated in excess of the limit might be removed from the system in a strong wind or asymmetrically through a disc. Super-Eddington accretion rates may be important in the formation of low-mass X-ray binaries and millisecond pulsars (Webbink & Kalogera 1997) and in models of X-ray emission from quasars due to accretion from a disc on to a rapidly rotating BH (Beloborodov 1998). Imposing the Eddington limit significantly reduces the formation rate of Type Ia SNe (Livio 2000). For these reasons the Eddington limit, equation (68), is only optionally included. A NS may gain enough mass to exceed the maximum NS mass of $1.8\,{\rm M}_\odot$ (see Section 6.2.2 of Paper I), in which case it becomes a BH.

2.7 Common envelopes, coalescence and collisions

As a result of Roche lobe overflow, it is possible for the binary components to come into contact and coalesce, or for the binary to reach a common-envelope (CE) state. The most frequent case of CE evolution involves a giant transferring mass to a main-sequence star on a dynamical time-scale. Although the process is difficult to model, and therefore uncertain, it is envisaged that the secondary is not able to accept the overflowing material owing to its relatively long thermal time-scale. The giant envelope overfills the Roche lobes of both stars, so that the giant core and the MS star are contained within a common envelope. Owing to its expansion the envelope rotates more slowly than the orbit of the core and the MS star, so that friction causes them to spiral together and transfer energy to the envelope. This process may release sufficient energy to drive off the entire envelope, leaving a close binary containing a WD and an MS star, or it may lead to coalescence of the giant core and the MS star. Evidence for a mechanism such as CE evolution is provided by CVs and close double-degenerate binaries whose characteristics can be understood only if a significant amount of angular momentum and mass have been removed from the precursor system. Planetary nebulae containing a close binary at their centre are probably the result of a recent CE event (Bond, Liller & Mannery 1978).

In contrast to the relatively gentle nature of coalescence, it is possible that two stars in a close eccentric orbit could collide at

periastron before either star has a chance to fill its Roche lobe. Furthermore, in a dense environment such as the core of a star cluster, two individual stars may be involved in a hyperbolic collision. Generally this involves formation of a binary via tidal capture and then CE evolution or coalescence, owing to the relatively low velocity dispersion in star clusters. We assume that any collision involving a giant or giant-like star that has a dense core and an appreciable envelope leads to CE evolution. All other collisions simply result in a merger of the two stars. The outcome of a collision depends on the impact parameter, which in turn depends on the relative velocity and the relative sizes of the stars, as well as their structure. Detailed modelling of specific collision cases has been undertaken (Rasio & Shapiro 1991; Benz & Hills 1992; Bailey & Davies 1999), but in the absence of results covering the full parameter space we employ the simple treatment given in the following sections.

2.7.1 *Common-envelope evolution*

Common-envelope evolution occurs either as a result of a collision between a star with a dense core ($k_1 \in \{2,3,4,5,6,8,9\}$) and any other star, or at the onset of Roche lobe overflow where mass is transferred from a giant ($k_1 \in \{2,3,5,6,8,9\}$) on a dynamical time-scale and $q_1 > q_{\rm crit}$. The primary is therefore a giant or giant-like star with core mass $M_{\rm c1}$ and core radius $R_{\rm c1}$, and an envelope mass $M_{\rm env1} = M_1 - M_{\rm c1}$. To make the calculations simpler, we define effective values, marked with a prime ($'$), for the secondary. If the secondary is an MS star ($k_2 \in \{0,1,7\}$), then it has an effective core mass $M'_{\rm c2} = M_2$, and an effective core radius $R'_{\rm c2} = R_2$, but $M_{\rm c2} = 0.0$. For a giant or giant-like secondary ($k_2 \in \{2,3,4,5,6,8,9\}$) the effective values are the actual values, i.e., $M'_{\rm c2} = M_{\rm c2}$ and $R'_{\rm c2} = R_{\rm c2}$, and for degenerate secondaries ($k_2 \geq 10$) where $M_{\rm c2} = M_2$ and $R_{\rm c2} = R_2$. The effective envelope mass is given by $M'_{\rm env2} = M_2 - M'_{\rm c2}$.

Our treatment of CE evolution follows closely the description of Tout et al. (1997), where the outcome depends on the initial binding energy of the envelope and the initial orbital energy of the two cores. First, we calculate the total binding energy of the envelope,

$$E_{\rm bind,i} = -\frac{G}{\lambda}\left(\frac{M_1 M_{\rm env1}}{R_1} + \frac{M_2 M'_{\rm env2}}{R_2}\right), \tag{69}$$

with $\lambda = 0.5$. Note that we use the indices i and f to represent initial and final quantities respectively, in relation to the CE event. The initial orbital energy of the cores is

$$E_{\rm orb,i} = -\frac{1}{2}\frac{GM_{\rm c1}M'_{\rm c2}}{\rm a_i}, \tag{70}$$

where $a_{\rm i}$ is the semimajor axis at the onset of the CE phase. We assume that the cores spiral in, transferring orbital energy to the envelope with an efficiency $\alpha_{\rm CE}$, which is necessarily a free parameter due to uncertainty in its value. It is probably not a constant (Regős & Tout 1995), but generally $\alpha_{\rm CE} \approx 1$ is used. The final separation $a_{\rm f}$, if sufficient energy were released to drive away the entire envelope, can be calculated via

$$E_{\rm bind,i} = \alpha_{\rm CE}(E_{\rm orb,f} - E_{\rm orb,i}), \tag{71}$$

where

$$E_{\rm orb,f} = -\frac{1}{2}\frac{GM_{\rm c1}M'_{\rm c2}}{a_{\rm f}}. \tag{72}$$

Equation (53), in conjunction with $a_{\rm f}$, gives the Roche lobe of each core: $R_{{\rm L}1,f}$ uses $q_1 = M_{\rm c1}/M'_{\rm c2}$, and $R_{{\rm L}2,f}$ uses $q_2 = M'_{\rm c2}/M_{\rm c1}$. If neither core fills its Roche lobe, then a binary composed of the cores with separation $a_{\rm f}$ survives, and the entire envelope escapes the system. The envelope has been removed from one, or both, of the stars, leaving behind the appropriate remnant (see Section 6 of Paper I). We assume that the envelope ejection is isotropic, and that both cores emerge from the CE in corotation with the orbit. We note that HG stars ($k \in \{2,8\}$) have an evolving density profile that is not yet as steep as in giants. Our assumption that HG stars have a core mass growing linearly in time (see Paper I) mimics this to some extent, although the actual remnant mass in a detailed computation may still be somewhat different.

If Roche lobe overflow would have occurred for either core, then they could not have spiralled in so far, instead coalescing at an earlier time. We assume that this takes place when $R'_{\rm c2} = R_{\rm L2}$, or $R_{\rm c1} = R_{\rm L1}$, depending on which core fills its Roche lobe first, so that the corresponding $a = a_L$ can be found from equation (53), and then the binding energy left in the remaining envelope can be calculated according to

$$E_{{\rm bind},f} - E_{\rm bind,i} = \alpha_{\rm CE}\left(\frac{1}{2}\frac{GM_{\rm c1}M'_{\rm c2}}{a_L} + E_{\rm orb,i}\right). \tag{73}$$

This results in the formation of a new giant or giant-like star with

$$k_3 \in \{2,3,4,6,8,9\},$$

$$M_3 = M_{\rm f},$$

$$M_{\rm c3} = M_{\rm c1} + M_{\rm c2},$$

unless $k_2 = 7$ and $k_1 \in \{2,3,4,5,6\}$, in which case $M_{\rm c3} = M_{\rm c1} + M_2$ (see later). The resultant mass $M_{\rm f}$ must be determined. The star has an envelope binding energy

$$E_{{\rm bind},f} = -\frac{GM_{\rm f}M_{{\rm env},f}}{\lambda R_{\rm f}} = -\frac{GM_{\rm f}(M_{\rm f} - M_{\rm c3})}{\lambda R_{\rm f}}, \tag{74}$$

and $R_{\rm f}$ can be estimated by noting that on a dynamical time-scale the radius of a giant responds to changes in mass according to $R \propto M^{-x}$ (where x is given by equation 47 of Paper I). The radius $R_{\rm i}$ of the star, if the system were to coalesce immediately, satisfies

$$E_{\rm bind,i} = -\frac{G(M_1 + M_2)(M_1 + M_2 - M_{\rm c3})}{\lambda {\rm R_i}} \tag{75}$$

and, as CE evolution is over on a dynamical time-scale,

$$\frac{R_{\rm f}}{R_{\rm i}} = \left(\frac{M_1 + M_2}{M_{\rm f}}\right)^x. \tag{76}$$

Therefore

$$\frac{E_{{\rm bind},f}}{E_{\rm bind,i}} = \left(\frac{M_{\rm f}}{M_1 + M_2}\right)^{1+x}\frac{M_{\rm f} - M_{\rm c3}}{M_1 + M_2 - M_{\rm c3}}, \tag{77}$$

which we solve for $M_{\rm f}$ by a Newton–Raphson iteration. We assume that the new star rotates with the same period as the orbit immediately prior to coalesence.

A different treatment is described by Iben & Livio (1993). Their initial envelope binding energy is not that of the giant (or giants), but that of the initial configuration of the CE itself, which surrounds the cores with a diameter of about $2a_{\rm i}$. This amounts to

replacing equation (69) with

$$E_{\rm bind,i} = -G\frac{(M_1 + M_2)(M_{\rm env1} + M'_{\rm env2})}{a_{\rm i}} \quad (78)$$

(see Yungelson et al. 1994), giving a reduction in the envelope binding energy and therefore less likelihood that the process ends in coalescence of the cores. A similar effect can be mimicked in our treatment by increasing $\alpha_{\rm CE}$ to values greater than unity. At first sight this may seem unphysical given the definition, but as discussed by Iben & Livio (1993), an increase in $\alpha_{\rm CE}$ can be envisaged if additional energy sources other than the orbital energy are involved. Processes with potential to supply such energy include enhanced nuclear burning in shell-burning zones of giants, nuclear burning on the surface of a degenerate secondary, dynamo generation of magnetic fields, and recombination of the hydrogen and helium ionization zones in giants. Possibly the CE absorbs ordinary nuclear energy in the process of swelling up to a diameter of $2a_{\rm i}$, but this should occur on a thermal time-scale. Unfortunately, the theoretical determination of reliable values for $\alpha_{\rm CE}$ has proven difficult due to a lack of understanding of the processes involved, and our ability to model them.

2.7.2 *Coalescence of CE cores*

When two cores spiral into each other, the outcome depends on their relative density. If they are of similar *compactness*, we assume that they coalesce and mix completely. If one core is considerably more compact than the other, that core sinks to the centre without mixing, while the less dense core mixes with the envelope. All cores, including remnant stars, are considered to be compact unless the core is an MS star. The case of an EAGB star ($k = 5$) is particularly interesting, because it has a carbon core growing within a stationary helium core. Detailed models show that the mass inside the hydrogen shell is dense enough for the helium core to be used as the core for collision purposes.

In our model the stellar type k_3 of the new star produced as a result of coalescence is given by the intersection of the k_1th column and the k_2th row of the collision matrix in Table 2. The mass of the new star is $M_3 = M_{\rm f}$, and the core mass is $M_{\rm c3} = M_{\rm c1} + M_{\rm c2}$. If, by chance, there is no remaining envelope, the coalescence product is the remnant remaining if a star of type k_3 loses its envelope. Note that $k_3 \in \{13, 14\}$ signifies the creation of an unstable Thorne–Żytkow object (Thorne & Żytkow 1977) when the merger involves an NS or BH. For simplicity, our Thorne–Żytkow objects rapidly eject their envelopes, leaving only the NS or BH (Fryer, Benz & Herant 1996), so that $M_3 = M_2$.

If $k_1 \in \{2, 3, 4, 5, 6\}$ and $k_2 \in \{0, 1\}$, then $k_3 = k_1$, and the MS star is simply absorbed into the giant envelope. The initial mass and age of the giant are unaffected by the merger, because the core mass of the star is not changed. Similarly, if $k_1 \in \{8, 9\}$, then $k_2 = 7$, because the CO core of the giant sinks to the centre, becoming the core of the new star. If $k_1 \in \{8, 9\}$ and $k_2 \in \{0, 1\}$, then $k_3 = 6$, because the MS star mixes with the envelope of the helium giant to form a hydrogen-helium envelope around the CO core of the giant. An initial mass, $M_{0,3}$, and age, t_3, appropriate for the core mass and stellar type of the new star must be set. We describe our procedure in Section 2.7.4. This must be done in all merger cases where the new star is of a different type to either star involved in the merger, or if the core mass of the star has changed as a result of the merger.

If $k_1 \in \{2, 3\}$ and $k_2 \in \{2, 3, 10\}$, then $k_3 = 3$, because the two helium cores merge to form a larger helium core within the existing envelope (or mixed envelopes). If both merging cores are degenerate ($M_0 < M_{\rm HeF}$ for the giants), then enough heat is produced in the merger to ignite the triple-α reaction, and the nuclear energy released is greater than the binding energy of the new core, so $k_3 = 15$.

If $k_1 \in \{2, 3\}$ and $k_2 \in \{6, 11, 12\}$, then $k_3 = 5$, because the helium core surrounds the CO (or ONe) core within the envelope (or mixed envelopes) to form an EAGB star. The same occurs if $k_1 = 6$ and $k_2 = 10$.

If $k_1 = 6$ and $k_2 \in \{6, 8, 9\}$, then the two cores mix to form a larger CO core, surrounded by the mixed envelopes, so that $k_3 = 6$. This is also the result when $k_1 = 6$ and $k_2 \in \{11, 12\}$, although only one envelope is involved in this case. The binding energy of the new envelope must be reduced by the amount of energy liberated in merging the two degenerate cores. This removes the envelope in all cases, so that in fact $k_3 \in \{11, 12\}$.

If $k_1 \in \{8, 9\}$ and $k_2 \in \{8, 9, 11, 12\}$, then $k_3 = 9$, because the CO (and possibly neon) cores mix to form a larger core surrounded by a helium envelope. When $k_1 \in \{8, 9\}$ and $k_2 = 10$, we assume that the two stars mix to form an evolved HeMS star, $k_3 = 7$, with

Table 2. The stellar type of the new star k_3 produced when two stars merge as a result of a collision (normal type) or CE evolution (bold italic type).

		Primary Star k_1														
		0	1	2	3	4	5	6	7	8	9	10	11	12	13	14
Secondary Star k_2	0	1	1	***2***	***3***	***4***	***5***	***6***	4	***6***	***6***	3	6	6	13	14
	1	1	1	***2***	***3***	***4***	***5***	***6***	4	***6***	***6***	3	6	6	13	14
	2	***2***	***2***	***3***	***3***	***4***	***4***	***5***	***4***	***4***	***4***	***3***	***5***	***5***	***13***	***14***
	3	***3***	***3***	***3***	***3***	***4***	***4***	***5***	***4***	***4***	***4***	***3***	***5***	***5***	***13***	***14***
	4	***4***	***4***	***4***	***4***	***4***	***4***	***4***	***4***	***4***	***4***	***4***	***4***	***4***	***13***	***14***
	5	***5***	***5***	***4***	***4***	***4***	***4***	***4***	***4***	***4***	***4***	***4***	***4***	***4***	***13***	***14***
	6	***6***	***6***	***5***	***5***	***4***	***4***	***6***	***4***	***6***	***6***	***5***	***6***	***6***	***13***	***14***
	7	4	4	***4***	***4***	***4***	***4***	***4***	7	***8***	***9***	7	9	9	13	14
	8	***6***	***6***	***4***	***4***	***4***	***4***	***6***	***8***	***8***	***9***	***7***	***9***	***9***	***13***	***14***
	9	***6***	***6***	***4***	***4***	***4***	***4***	***6***	***9***	***9***	***9***	***7***	***9***	***9***	***13***	***14***
	10	3	3	***3***	***3***	***4***	***4***	***5***	7	***7***	***7***	15	9	9	13	14
	11	6	6	***5***	***5***	***4***	***4***	***6***	9	***9***	***9***	9	11	12	13	14
	12	6	6	***5***	***5***	***4***	***4***	***6***	9	***9***	***9***	9	12	12	13	14
	13	13	13	***13***	***13***	***13***	***13***	***13***	13	***13***	***13***	13	13	13	13	14
	14	14	14	***14***	***14***	***14***	***14***	***14***	14	***14***	***14***	14	14	14	14	14

$M_{0,3} = M_3$ and

$$t_3 = \left(\frac{M_{c1}}{M_{c1} + M_2}\right) t_{HeMS3}. \quad (79)$$

If $k_1 \in \{2, 3, 4, 5, 6\}$ and $k_2 = 7$, then $k_3 = 4$, because the giant core material mixes with the HeMS star to form a new core that contains some unburnt helium. All the remaining cases that arise as a result of CE evolution, i.e., $k_1 \in \{2, 3\}$ and $k_2 \in \{4, 5, 8, 9\}$ as well as $k_1 \in \{4, 5\}$ and $k_2 \in \{4, 5, 6, 8, 9, 10, 11, 12\}$, also have $k_3 = 4$, because the merged core is a mixture of processed and unprocessed helium. The age of the new CHeB star depends on how advanced, in terms of central helium burning, the two progenitor stars were. How this is taken into account is the subject of Section 2.7.4.

2.7.3 *Collision outcomes*

It now remains to describe the result of all collisions that do not proceed via CE evolution. We allow the stars to merge without mass-loss, $M_3 = M_1 + M_2$ (cf. Bailey 1999). The stellar type of the merged product is determined by the nature of the colliding stars as given by the collision matrix (Table 2).

As in Tout et al. (1997), the collision of two MS stars, $k_1 \in \{0, 1\}$ and $k_2 \in \{0, 1\}$, leads to $k_3 \in \{0, 1\}$, with $M_{0,3} = M_3$ and $k_3 \in \{0, 1\}$, with $M_{0,3} = M_3$ and

$$t_3 = 0.1 \frac{t_{MS3}}{M_3} \left(\frac{M_1 t_1}{t_{MS1}} + \frac{M_2 t_2}{t_{MS2}}\right), \quad (80)$$

where t_1 and t_2 are the ages of the colliding stars. When two HeMS stars collide, we apply the same, except that $k_1 = k_2 = k_3 = 7$ and the t_{MSi} are replaced by t_{HeMSi}. If $k_1 \in \{0, 1\}$ and $k_2 = 7$, then $k_3 = 4$, because the naked helium star sinks to the centre forming a CHeB star with $M_{c3} = M_2$. A HeWD, $k_1 = 10$, colliding with an MS star, $k_2 \in \{0, 1\}$, sinks to the centre of the MS star where hydrogen shell burning can begin at its surface. The result is a GB star, $k_3 = 3$, with core mass $M_{c3} = M_1$. Similarly, if $k_1 \in \{11, 12\}$ and $k_2 \in \{0, 1\}$, double shell burning begins at the WD surface, so that $k_3 = 6$. If $k_1 = 10$ and $k_2 = 7$, the naked helium star absorbs the HeWD, leaving a rejuvenated HeMS star, $k_3 = 7$, with $M_{0,3} = M_3$ and

$$t_3 = \frac{t_{HeMS3}}{M_3} \frac{M_2 t_2}{t_{HeMS2}}. \quad (81)$$

However, if $k_1 \in \{11, 12\}$ and $k_2 = 7$, then $k_3 = 9$, because the WD forms the core of an evolved helium giant with $M_{c3} = M_1$.

When two HeWDs, $k_1 = 10$ and $k_2 = 10$, collide, we assume that the temperature produced is hot enough to ignite the triple-α reaction, and that the subsequent nuclear runaway destroys the system, so that $k_3 = 15$ (cf. Section 2.6.5). If $k_1 = 10$ and $k_2 \in \{11, 12\}$, then $k_3 = 9$, with $M_{c3} = M_2$, because the helium material swells up to form an envelope around the CO (or ONe) core, which in general is smaller and denser by virtue of a larger mass. If $k_1 = 11$ and $k_2 = 11$, then a larger COWD is formed, $k_3 = 11$, unless $M_3 \geq M_{Ch}$, in which case the new star is destroyed in a type Ia SN and $k_3 = 15$. Similarly, if $k_1 = 12$ and $k_2 \in \{11, 12\}$, then $k_3 = 12$, unless $M_3 \geq M_{Ch}$, causing the ONeWD to undergo an AIC to an NS, $k_3 = 13$ (see Section 2.6.5).

If $k_1 \in \{13, 14\}$ and $k_2 \in \{0, 1, 7\}$, an unstable Thorne–Żytkow object results, i.e., $k_3 = k_1$ and $M_3 = M_1$. Finally, if $k_1 \in \{13, 14\}$ and $k_2 \in \{10, 11, 12, 13, 14\}$, then $k_3 = k_1$, unless the new mass of the NS exceeds the maximum allowable NS mass of $1.8\,M_\odot$, in which case we collapse it to a BH.

2.7.4 *The new star*

When a new giant or core-helium-burning star is made ($k_3 \in \{3, 4, 5, 6, 8, 9\}$), then an age, t_3, and an initial mass, $M_{0,3}$ must be assigned to the star appropriate to its type k_3, mass M_3 and core mass M_{c3}.

If $k_3 = 3$, then our goal is to find $M_{0,3}$ so as to place the star at the base of the GB with its correct core mass. The decision as to where the star should start its evolution is quite arbitrary, with the base of the GB (BGB) chosen, because it simplifies the process. As discussed in Section 5.2 of Paper I, the helium core of a GB star is degenerate if $M < M_{HeF}$ (where $M_{HeF} \simeq 2.0$ is the maximum initial mass for which He ignites degenerately in a helium flash) and non-degenerate otherwise. So the first step is to place M_{HeF} into equation (44) of Paper I to find the maximum degenerate BGB core mass. If M_{c3} is greater than this value, then $M_{0,3}$ can be fixed by setting $M_{c,BGB} = M_{c3}$ and inverting equation (44) of Paper I. Otherwise it is necessary to find the luminosity corresponding to M_{c3} using the GB M_c–L relation given by equation (37) of Paper I. We use a Newton–Raphson procedure to find $M_{0,3}$ such that the luminosity at the BGB (given by equation 10 of Paper I) equals that luminosity, taking $M_{0,3} = M_{HeF}$ as an initial guess. Once $M_{0,3}$ has been found, we set t_3 to the corresponding time taken for such a star to reach the BGB as given by equation (4) of Paper I. We note that stars with initial mass $M_0 > M_{FGB}$ (see Section 5 of Paper I) do not have a GB, which means that a GB star cannot be made with a core mass greater than the value given by inserting M_{FGB} into equation (44) of Paper I. Such a situation is extremely unlikely, but if it does occur, then we form an CHeB star.

We make a CHeB star, $k_3 = 4$, whenever the new core is composed of a mixture of burnt and unburnt helium and the surrounding envelope contains mostly hydrogen. The new core is assigned a fractional age, which we determine according to the amount of central helium burning that has already occurred in the colliding stars. Each of these stars is assigned a fraction y, where

$$y = \begin{cases} 0 & k \in \{0, 1, 2, 3, 10\} \\ 1 & k \in \{6, 8, 9, 11, 12\} \\ \frac{t - t_{HeI}}{t_{DU} - t_{HeI}} & k \in \{4, 5\} \\ \frac{t}{t_{HeMS}} & k = 7 \end{cases},$$

and then

$$y_3 = \frac{y_1 M_{c1} + y_2 M_{c2}}{M_{c3}}, \quad (82)$$

where M_c must be replaced by M for $k = 7$. The age of the new star is then

$$t_3 = t_{HeI3} + y_3 t_{He3}, \quad (83)$$

where t_{HeI3} and t_{He3} are dependent on $M_{0,3}$. The time of central helium ignition, t_{HeI}, the lifetime of the CHeB phase, t_{He}, the time taken to reach the second dredge-up phase at the start of the TPAGB, t_{DU}, and the MS lifetime of a naked helium star, t_{HeMS}, are given by equations (43), (57), (70) and (79) of Paper I. There is a minimum allowed core mass for CHeB stars, which corresponds to an initial mass of M_{HeF}. To find the minimum possible initial mass relevant to M_{c3}, corresponding to $y_3 = 1$, it is first necessary to find the base of the asymptotic giant branch (BAGB) core mass for $M_{0,3} = M_{HeF}$, using equation (66) of Paper I. If M_{c3} is larger than this value, we find M_{min} by setting $M_{c3} = M_{c,BAGB}$ and inverting equation (66) of Paper I, otherwise $M_{min} = M_{HeF}$. We find the

maximum possible initial mass corresponding to $y_3 = 0$ by setting $M_{c3} = M_{c,HeI}$ and solving for M_{max}. A bisection method can be used to find $M_{0,3}$, where $M_{min} \leq M_{0,3} \leq M_{max}$, and

$$M_{c3} = M_{c,HeI}(M_{0,3}) + y_3[M_{c,BAGB}(M_{0,3}) - M_{c,HeI}(M_{0,3})]. \quad (84)$$

If $k_3 = 5$, we assume that M_{c3} is representative of the helium core mass, $M_{c,He}$, of the new EAGB star, and find the initial mass by setting $M_{c3} = M_{c,BAGB}$ and solving equation (66) of Paper I for $M_{0,3}$. The age of the star is the time taken to reach the BAGB,

$$t_3 = t_{HeI3} + t_{He3}. \quad (85)$$

For a new TPAGB star, $k_3 = 6$, M_{c3} is the CO core mass, and our aim is to put the star at the start of the TPAGB phase, so we set $M_{c3} = M_{c,DU}$. To do this, it is necessary to find the corresponding helium core mass, $M_{c,He}$, just before the transition from the EAGB to the TPAGB. Stars with $0.8 < M_{c,He} < 2.25$ undergo second dredge-up during the transition, so that

$$M_{c,DU} = 0.44M_{c,He} + 0.448, \quad (86)$$

while lower mass stars have

$$M_{c,DU} = M_{c,He}. \quad (87)$$

Stars with $M_{c,He} \geq 2.25$ on the EAGB would become an NS or BH before the TPAGB was reached. Thus if $M_{c3} \geq 1.438$, given by $M_{c,He} = 2.25$ in equation (86), the star cannot exist with $k_3 = 6$, and we set it up so that it immediately becomes an NS or BH by setting $M_{c3} = M_{c,SN}$ (see equation 75 of Paper I) in equation (86). Therefore

$$M_{c,He} = \begin{cases} (M_{c3} + 0.35)/0.773 & M_{c3} \geq 1.438 \\ (M_{c3} - 0.448)/0.44 & 0.8 < M_{c3} < 1.438 \\ M_{c3} & M_{c3} \leq 0.8 \end{cases},$$

and $M_{c,He} = M_{c,BAGB}$, so that $M_{0,3}$ can be found by solving equation (66) of Paper I. The age of the star is $t_3 = t_{DU3}$ by equation (70) of Paper I. At this stage it is possible that $M_{0,3} < 0$ if M_{c3} is less than the minimum allowed core mass for the start of the TPAGB. This could happen in the rare event of an extremely low-mass COWD gaining only a very small envelope to make it a TPAGB star. If this occurs, then we simply add the small amount of mass to the WD so that $k_3 = 11$ and $M_{0,3} = M_3$.

If $k_3 \in \{8, 9\}$, we set $M_{0,3}$ and t_3 so that the new star begins life at the end of the naked helium star MS. $M_{0,3}$ must be found by a bisection method, because some of the parameters involved depend on the chosen value of $M_{0,3}$. At each iteration we find the luminosity at the end of the main sequence, L_{THe}, by putting $\tau = 1$ in equation (80) of Paper I, and the HeGB luminosity corresponding to M_{c3}, calculated with equation (84) of Paper I, for the current guess of $M_{0,3}$. We iterate until the two values agree to within a difference of 10^{-4}. Once $M_{0,3}$ is determined, we set the age, $t_3 = t_{HeMS3}$, using equation (79) of Paper I.

2.8 The evolution algorithm

The initial state of a binary system is described by the masses, M_1 and M_2, of the component stars, and the period, P, and eccentricity, e, of the orbit. A choice must also be made for the metallicity, Z, of the stars. In general, the system begins with both stars on the ZAMS, but it is possible to start the binary-star evolution (BSE) algorithm with the stars in an evolved state. The stars are each assumed to have an initial spin frequency on the ZAMS, independent of the properties of the orbit (given by equation 108 of Paper I); however, options exist to begin the stars in corotation with the orbit or with any given value. A number of input parameters and options exist for the BSE code, many of which have been introduced in the preceeding sections. These are summarized in Table 3, along with their ranges and default values.

Each star has its own stellar evolution time-step, δt_i, (given by equation 112 of Paper I) which includes restrictions that prevent the star changing its mass by more than 1 per cent, or its radius by more than 10 per cent. For binary evolution it is particularly important to keep the time-steps relatively small so that the radius of the primary does not increase too much over any one time-step. This aids identification of the time when the star first fills its Roche lobe, if indeed it does. We also calculate an orbital time-step such that the angular momentum of the system changes by 2 per cent,

$$\delta t_b = 0.02\frac{J_{orb}}{|\dot{J}_{orb}|}, \quad (88)$$

and take the actual binary evolution time-step when the system is in a detached state to be

$$\delta t = \min(\delta t_1, \delta t_2, \delta t_b). \quad (89)$$

We evolve the system forward by this time, implementing the necessary tidal and braking mechanisms as well as evolving each star according to the SSE prescription given in Paper I. If by virtue of the stars growing in size, or the orbital separation shrinking, the periastron separation is less than the combined radii of the two stars, then the stars collide and the system is dealt with according to the prescription described in Section 2.7.

If the primary fills its Roche lobe, then we interpolate within the last time-step until the radius of the star only just exceeds its Roche lobe radius ($1 \leq R_1/R_{L1} \leq 1.002$). The system enters RLOF, and we treat it according to Section 2.6. First, we test for dynamical mass transfer and deal with it if necessary, by merging or CE evolution; otherwise the mass transfer is steady. We set the time-step during RLOF to

$$\delta t_{RL} = k_m P, \quad (90)$$

where initially

$$k_m = \delta t\frac{10^{-3}}{P}, \quad (91)$$

Table 3. Input parameters and options in the BSE algorithm set by the user. Column 2 gives the range of values that each parameter may assume (suggested range if bracketed), and default values are given in Column 3. The relevant section where each parameter or option is discussed is given in Column 4 (note that some parameters are introduced in Paper I).

Parameter	Range	Default	Section
β_W	$(0.125 \rightarrow 7.0)$	0.5	2.1
α_W	$(0.0 \rightarrow 2.0)$	1.5	2.1
μ_W	$0.0 \rightarrow 1.0$	1.0	2.1
B_W	$(0.0 \rightarrow 10^6)$	0.0	2.1
ϵ	$-1.0 \rightarrow 1.0$	0.001	2.6.6
α_{CE}	$(0.5 \rightarrow 10.0)$	3.0	2.7.1
σ_k km s^{-1}	$0.0 \rightarrow \infty$[a]	190.0	A1
Tidal Evolution	on/off	on	2.3
Eddington Limit	on/off	off	2.6.6
Stellar Winds	on/off	on	7.1 of Paper I
η	$(0.0 \rightarrow 2.0)$	0.5	7.1 of Paper I

[a] A value of zero corresponds to no velocity kick.

where δt is the previous time-step for the detached system. After implementing mass transfer, and any mass loss due to stellar winds, and adjusting the separation accordingly, as well as implementing the tidal and braking mechanisms, we check whether the primary still fills its Roche lobe. If $R_1 < R_{L1}$, then the system leaves RLOF to evolve once more as a detached binary. If $R_1 \geq R_{L1}$ and $R_2 \geq R_{L2}$, a contact system has formed and we treat this as either a collision or CE evolution depending on the nature of the stars involved. Otherwise we allow the time-step to grow by a factor of 2, until R_1/R_{L1} is such that $\delta M_1/M_1 = 0.005$, i.e.

$$k_m = \min\left(2k_m, \frac{0.005M_1}{|\delta M_1|}\right), \tag{92}$$

and the RLOF process is repeated.

When CE evolution leaves a surviving binary system, we continue the evolution with the new orbital parameters. If at any point the stars merge, we follow the evolution of the resulting single star. If either star explodes as a supernova and the resultant velocity kick disrupts the binary, we evolve the system forward as two single stars that do not interact.

The CPU time required by the BSE algorithm to evolve 500 000 binaries up to the age of the Galaxy is approximately 20 h, or 0.144 s per binary, on a Sun SparcUltra10 workstation (containing a 300-MHz processor).

3 SOME EXAMPLES AND COMPARISONS

To illustrate the BSE algorithm, we present some example evolutionary scenarios, concentrating in particular on Algol and cataclysmic variable evolution. These examples also serve to demonstrate the sensitivity of binary evolution to the choice of model parameters where, unless otherwise specified, the default values given in Table 3 are used. In addition, we take a selection of evolution scenarios previously outlined by other authors, and we compare the results of their models with those of the BSE algorithm.

3.1 Algol evolution

Consider a system in which the initial masses are 2.9 and 0.9 $M_\odot$ in an 8-d orbit with $e = 0.7$. In this example $Z = 0.02$ and $\alpha_{CE} = 3$. Fig. 1 shows the evolution of the binary stars in the Hertzsprung–Russell diagram. On the MS tidal friction arising from convective damping of the tide raised on the 0.9-$M_\odot$ secondary acts to circularize the system, so that at a time $T = 413$ Myr, when the 2.9 $M_\odot$ primary reaches the end of its MS lifetime, the eccentricity has fallen to 0.28 and P to 3 d. The radius of the primary then increases rapidly as it evolves across the HG until $R_1 = 6.2\,R_\odot$ when it fills its Roche lobe. By then, $P = 2.7$ d and the orbit has circularized (position a in Fig. 1). Mass transfer proceeds on a thermal time-scale, with the secondary accreting 80 per cent of the transferred mass (limited by its thermal time-scale), until the primary reaches the end of the HG with $M_1 = 0.53\,M_\odot$, $M_2 = 2.74\,M_\odot$ and $P = 17$ d. During this phase the equilibrium radius of the primary has exceeded its Roche lobe by as much as a factor of 2. Mass transfer continues as the primary begins to ascend the GB, but now on a nuclear time-scale which allows the secondary to accrete all the transferred mass, until the primary's envelope mass becomes so small that it shrinks inside its Roche lobe (position b). Fig. 2 shows the intrinsic spin of the stars and the spin of the orbit as a function of the eccentricity, up to this point. We see clearly that

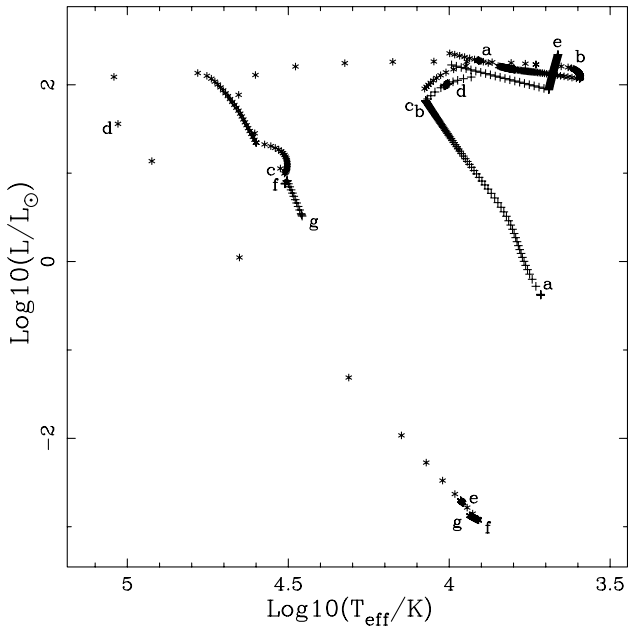

Figure 1. Hertzsprung–Russell diagram showing the evolution of a 2.9-$M_\odot$ star ($*$ points) and a 0.9-$M_\odot$ star ($+$ points) in a binary system with an initial orbit of $P = 8$ d and $e = 0.70$. The letters represent various times in the evolution of the binary system (see text for details). Each point represents an iteration of the BSE algorithm, except in regions of high density, i.e., rapid evolution.

corotation is achieved as the orbit circularizes. When RLOF ends, $M_1 = 0.42\,M_\odot$, $M_2 = 2.85\,M_\odot$ and $P = 30$ d. While the primary was transferring mass on the HG the mass ratio of the system inverted, $q_1 < 1$, so that the more evolved component is now the less massive. This is the well-known Algol paradox (Crawford 1955; Hoyle 1955). Many semidetached Algol systems have since been observed and their parameters determined (e.g. Popper 1980). These include RY Gem: $M_1 = 2.6\,M_\odot$, $M_2 = 0.6\,M_\odot$ and $P = 9.3$ d, and TT Hya: $M_1 = 2.6\,M_\odot$, $M_2 = 0.7\,M_\odot$ and $P = 6.95$ d, both of which could easily be explained by this example. Fig. 3 shows the evolution of the mass of the stars with the orbital period up to the end of the Algol phase of evolution.

Shortly after the mass-transfer phase has ended, the GB primary loses all of its envelope leaving a 0.42-$M_\odot$ HeMS star with a 2.85-$M_\odot$ MS companion, which would be a blue straggler in a star cluster (position c). The naked helium star evolves to the HeGB and then to a 0.417-$M_\odot$ COWD after losing its helium envelope (position d). The MS star, now the primary, evolves to the GB and fills its Roche lobe (position e) when the period has reduced to 18 d as a result of the transfer of angular momentum from the orbit to the spin of the star. As $q_1 = 6.83 > q_{crit}$, the mass transfer is dynamical, a CE forms and leaves a binary containing the COWD and the 0.416-$M_\odot$ He core of the primary in an orbit of 0.04 d. The HeMS star evolves to fill its Roche lobe (position f), which has shrunk by gravitational radiation, and transfers 0.1 $M_\odot$ of He-rich material to the COWD before the system reaches a contact state at $P = 1$ min (position g). The two stars merge to a single HeGB star.

3.2 A cataclysmic variable

Next, we use a binary with initially $M_1 = 6.0\,M_\odot$ and $M_2 = 1.3\,M_\odot$, $P = 630$ d, and a circular orbit, $e = 0.0$, to give a quick illustration of CV formation and evolution. In this example

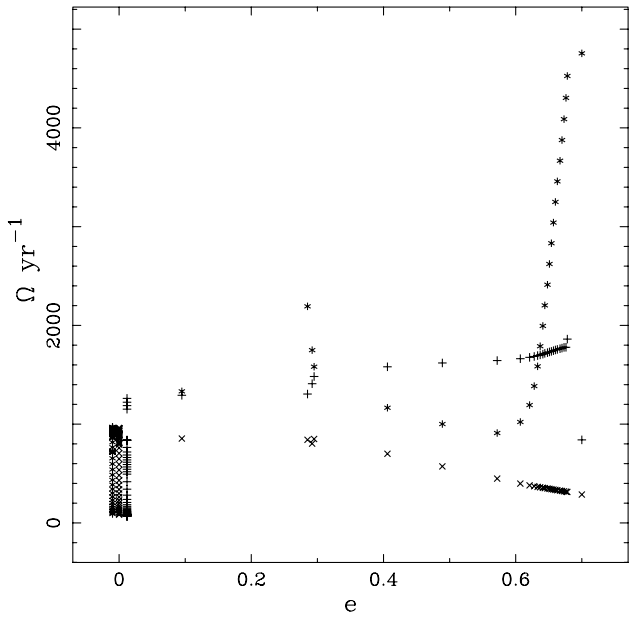

Figure 2. The evolution of the spins of the primary (∗ points) and secondary (+ points) stars, and the orbital spin (× points), as a function of the eccentricity of the orbit for the example of Algol evolution, shown until the end of the first phase of mass transfer. The points at zero eccentricity have been slightly displaced so that the corotation of the stars with the orbit can be clearly seen.

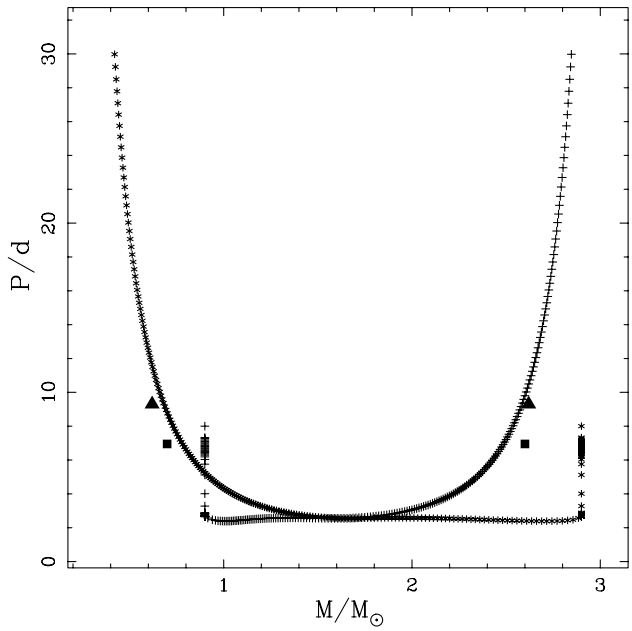

Figure 3. The evolution of stellar mass with binary period for the example of Algol evolution, until the end of the first phase of mass transfer. The primary mass decreases from 2.9 $M_\odot$ to 0.42 $M_\odot$ (∗ points) and the secondary mass increases from 0.9 $M_\odot$ to 2.85 $M_\odot$ (+ points), while the period initially decreases owing to circularization of the orbit, and then increases as a result of the nearly conservative mass transfer. The observed parameters for the Algol systems RY Gem (solid triangles) and TT Hya (solid squares) are also shown.

$Z = 0.02$, $\alpha_{\rm CE} = 1$ and $\epsilon = 0.001$. The relatively large orbital period gives the 6.0-$M_\odot$ primary enough room to evolve on to the EAGB before filling its Roche lobe 78 Myr after the evolution began. At this point the tides raised on the convective envelope of the primary have moderately decreased the orbital period, offset slightly by orbital changes owing to 0.1 $M_\odot$ lost from the primary, none of which has been accreted by the MS companion. Because $q_1 = 4.5 > q_{\rm crit}$, mass transfer is dynamical and a common envelope forms. The He core of the primary and the MS secondary spiral together until their orbital period is reduced to 0.63 d, at which point the envelope has been driven off.

The primary is now a HeHG star of mass 1.5 $M_\odot$, and very soon evolves to fill its Roche lobe again, resulting in another CE system. Once again the cores do not coalesce before the envelope is removed, and a binary consisting of a 0.94 $M_\odot$ COWD and a 1.3-$M_\odot$ MS star in a circular orbit of 0.45 d emerges. Gravitational radiation acts to reduce the orbital period, until at $T = 303$ Myr the MS primary fills its Roche lobe and a CV is formed. Mass transfer is steady and proceeds on a nuclear time-scale, driven in part by gravitational radiation and, when the primary mass is reduced below 1.25 $M_\odot$ and the primary develops a convective envelope, magnetic braking and tidal friction. As the primary evolves across the HG it transfers mass on a thermal time-scale, now driven by the evolution. Throughout RLOF the mass transfer rate remains below $10^{-7}\,M_\odot\,{\rm yr}^{-1}$, low enough that nova explosions at the surface of the white dwarf have allowed only 0.1 per cent of the transferred material to be accreted. RLOF ends with the primary on the GB just before it loses the remainder of its envelope, becoming a low-mass HeWD of $M_1 = 0.158\,M_\odot$. The orbital period is now 4.5 d, and a gravitational radiation time-scale of 10^{14} yr means that the double-degenerate system cannot coalesce within the age of the Galaxy. Fig. 4 shows the radius of each star and the corresponding Roche lobe radius, as a function of the stellar mass, during the CV phase of evolution.

3.3 Sensitivity to model parameters

To give an idea of how sensitive the final state of the system is to changes in the initial binary parameters and the physical parameters that govern the evolution, we first reconsider the Algol example described above. If the WD–HeMS system emerged from the CE with a separation increased by only a few per cent, then the COWD would accrete 0.15 $M_\odot$ of He-rich material and explode as an ELD SNIa before the system evolved into contact. Such an increase in separation could easily be achieved by a less than 10 per cent change to $\alpha_{\rm CE}$, well within its uncertainty, or small changes in the initial period and/or eccentricity of the system.

There is no doubt that major changes to the outcome would result if we neglected to model tidal evolution for this example, but to do so for a system that is initially eccentric with a short period would not be physically correct. However, for the purpose of comparison, we can examine the evolution of a system that begins with the same component masses and semilatus rectum but in a circular orbit, i.e., $P = 2.9$ d. Apart from the initial circularization phase, this example, evolved with the tidal evolution activated, follows a virtually identical path to that of the above example (a result we will discuss further in Section 4.2.3). If tidal evolution is not activated, and therefore any spin–orbit coupling is neglected, the orbit experiences a greater degree of expansion during RLOF, so that $P = 25$ d at the end of the Algol phase. The wider orbit translates to a lower mass-transfer rate during this phase, which

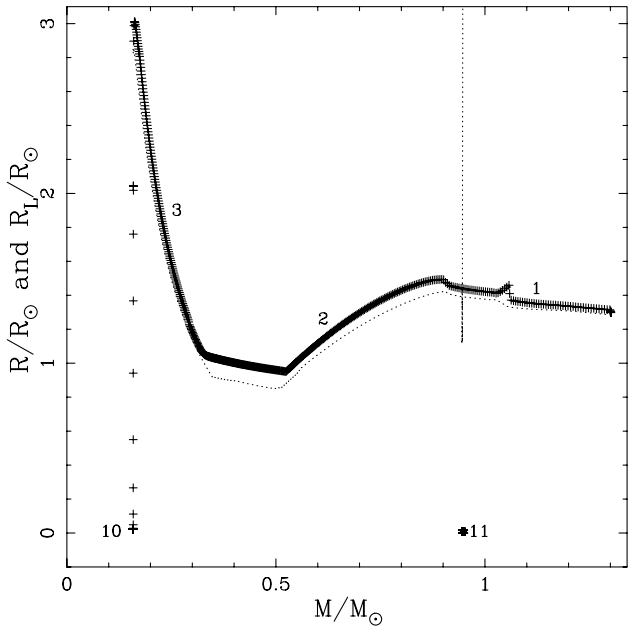

Figure 4. The evolution of stellar radius (+ points for the primary and ∗ points for the COWD secondary) with mass during a typical phase of CV evolution. The numbers indicate the evolution state of each star. Dotted lines are the Roche lobe radii for each star. Note that the COWD accretes little material as its Roche lobe radius shrinks and then expands.

means that more mass is accreted by the companion. The subsequent evolution still leads to a CE when the original secondary has reached the GB, but in this case a lower value of $\alpha_{\rm CE}$ is required if a COWD–HeMS binary is to emerge with $P = 0.04$ d.

If the CV example presented above had a common-envelope efficiency of $\alpha_{\rm CE} = 3$, less energy is required to drive off the CE, and the WD–MS binary forms with a larger orbital period of 3.0 d. This allows the MS primary to evolve to the GB before it fills its Roche lobe, so that dynamical mass transfer leads to another CE phase in which the WD and the giant core coalesce to form an EAGB star. A CV is not formed at all. If the metallicity of the component stars is taken to be $Z = 0.001$, rather than $Z = 0.02$, the system coalesces after the first instance of CE evolution and forms an EAGB star. This is also the case if the tidal evolution is not followed.

3.4 Comparison with other authors

The Algol example described by Tout et al. (1997) begins with initial masses of 3.2 and 2.0 $M_\odot$ and a circular 5-d orbit. The primary fills its Roche lobe on the HG, and mass transfer proceeds until it has lost its envelope on the GB, at which point it is a 0.318-$M_\odot$ naked helium star in a 170-d orbit with a 4.65-$M_\odot$ MS companion. The MS star evolves to the AGB, by which time the secondary has become a COWD, before filling its Roche lobe which results in CE evolution and the production of a double-degenerate WD binary in a 35-min orbit. Gravitational radiation decreases the size of the orbit so that steady mass transfer from the less massive WD begins and an AM CVn system is formed. The same binary evolved with the BSE algorithm also forms an Algol system, but the first phase of RLOF ends when the primary is in the CHeB stage and loses its envelope to become a 0.49-$M_\odot$ HeMS star with a 4.7-$M_\odot$ MS companion. Tidal friction within the system has restrained the growth of the separation during mass transfer, so that the orbital period at this stage is only 110 d. As a result, the new primary fills its Roche lobe on the GB, and the CE evolution that follows leads to coalescence and the formation of a single CHeB star. An AM CVn system is not produced from this set of initial conditions when tides are included.

Tout et al. (1997) describe a scenario for the formation of a CV with initial masses of 7.0 and 1.0 $M_\odot$ in a circular orbit of $P = 1200$ d. In this example, $Z = 0.02$ and $\alpha_{\rm CE} = 1$. They find that the 7.0-$M_\odot$ primary fills its Roche lobe on the AGB when its mass has fallen to 5.36 $M_\odot$. The ensuing CE produces a 1.014-$M_\odot$ COWD (they did not distinguish ONeWDs) in a 35-h orbit with the 1.0-$M_\odot$ MS star. The MS star then fills its Roche lobe, as magnetic braking reduces orbital separation, resulting in steady mass transfer with nova explosions on the WD surface. Evolution with the BSE algorithm leads to a similar outcome, but with differences in the states of the stars and the orbit. The 7.0-$M_\odot$ primary fills its Roche lobe earlier on the AGB when its mass has only fallen to 6.8 $M_\odot$, and the CE produces a 1.183-$M_\odot$ ONeWD in an 18-h orbit with the 1.0-$M_\odot$ MS star. Once again, a CV with nova outbursts is formed when the MS primary fills its Roche lobe. In this case the differences between Tout et al. and the BSE algorithm are primarily due to improvements in the single-star evolution model.

As a final example, we consider the formation of the double neutron star binary described by PZV. In their model, stellar evolution is performed using a simple prescription based on models with $Z = 0.02$. They assume no kick in a supernova explosion, and their treatment of CE evolution is similar to that of Iben & Livio (1993), discussed in Section 2.7.1. Tidal evolution is not included in their model, but eccentric orbits are instantaneously circularized when the radius of either star exceeds 1/5 of the separation at periastron. The initial binary has masses 13.1 and 9.8 $M_\odot$ separated by 138 $R_\odot$ in a circular orbit. Mass transfer, which begins when the primary has evolved to the HG, becomes dynamical when the primary reaches the GB, leading, via CE evolution, to the formation of a binary composed of a 3.7-$M_\odot$ He star and an 18.7-$M_\odot$ MS companion separated by 411 $R_\odot$. The He star then undergoes a supernova explosion, which leaves a 1.34-$M_\odot$ NS remnant and widens the orbital separation to 463 $R_\odot$. Another phase of dynamical mass transfer, when the 18.7 $M_\odot$ star fills its Roche lobe, leads to a CE from which the NS emerges with a 4.6-$M_\odot$ He star companion, separated by 1.6 $R_\odot$. When the new He star explodes as a supernova, a double NS binary forms with $P = 0.5$ d.

This example evolved with the BSE algorithm forms a binary consisting of a 3.1-$M_\odot$ HeMS star separated from an 11.7-$M_\odot$ MS companion by 60 $R_\odot$ after the first CE phase. The separation in this instance is much smaller, because not as much mass is transferred and because tides cause the spin of each star to synchronize with the binary period so that the orbit does not expand during mass transfer. Next, the HeMS star evolves to the HeGB before a supernova explosion leaves a 1.33-$M_\odot$ NS and widens the separation to 67 $R_\odot$. The second phase of CE evolution then leads to coalescence of the NS and the 2.63-$M_\odot$ He core, which creates an unstable Thorne–Żytkow object. However, if the initial binary consists of masses 13.6 and 7.7 $M_\odot$ separated by 100 $R_\odot$, the evolution proceeds along a similar path to that described by PZV, forming a double NS binary with $P = 1$ d. This system coalesces in 300 Myr through gravitational radiation. If a velocity kick at supernova is included in the model, then the final state of the system depends on the magnitude of the kick and the relative positions of the two stars when the explosion occurs.

4 THE EFFECT OF TIDES ON BINARY EVOLUTION

The examples in the previous section have shown that the evolution of a binary is sensitive to the inclusion of tidal evolution in the binary algorithm. This is true even for initially circular orbits. It is instructive to investigate and quantify the systematic effect of tides within a population of binaries. We do this by using the rapid evolution code to generate a series of large binary populations, from which we calculate the formation rate of interesting individual species, such as X-ray binaries, double-degenerates and symbiotic stars, and events such as type Ia SNe. The results for populations with and without tidal friction can be compared. In addition, it is useful to investigate the influence of various uncertain parameters in the binary algorithm, such as the common-envelope efficiency parameter. Comparison with observations and work of others hopefully constrains the value of some of these parameters. The statistics of theoretical binary populations have been presented and discussed by many authors in the past. Examples include Han (1998): the formation of double-degenerates, type Ia SNe and CVs; Portegies Zwart & Yungelson (1998): the formation of binary neutron stars; de Kool (1992) and Politano (1996): formation of CVs; Yungelson et al. (1995): the formation of symbiotic stars with a WD secondary; Iben, Tutukov & Yungelson (1995): low-mass X-ray binaries in the Galactic disc; Han et al. (1995): the formation of CVs, Algols, double-degenerates and symbiotic stars, and Pols & Marinus (1994): the production of blue stragglers. These studies are all flawed by the fact that no attempt was made to model the tidal circularization and synchronization of the binary orbit as it evolves and, in particular, the interaction of the intrinsic spin of the stars with the orbital period.

4.1 Method

Our aim is to evolve a population of binaries according to chosen distributions of primary mass, secondary mass and orbital separation, in conjunction with a realistic birth rate function and, from this population, to calculate birth rates and expected numbers in the Galaxy for various individual binary populations and interesting events.

We first set up a grid of initial binary parameters M_1, M_2 and a within the limits:

$$M_1 : 0.8 \rightarrow 80\,\mathrm{M}_\odot,$$

$$M_2 : 0.1 \rightarrow 80\,\mathrm{M}_\odot,$$

$$a : 3.0 \rightarrow 10^4\,\mathrm{R}_\odot,$$

with the $n_\mathcal{X}$ grid points of parameter $\mathcal{X}$ logarithmically spaced,

$$\delta \ln \mathcal{X} = \frac{1}{n_\mathcal{X} - 1}(\ln \mathcal{X}_{\max} - \ln \mathcal{X}_{\min}). \tag{93}$$

For each set of initial parameters we evolve the binary system to an age of 15 Gyr, or until it is destroyed. Each phase of the evolution is followed in detail according to the BSE algorithm. The lower limit on the primary mass is determined by the lowest mass star that will change appreciably in size within 15 Gyr, and systems with $M_2 > M_1$ are not evolved. If a particular binary system j evolves through a phase that is to be identified with a certain individual binary population i, such as CVs, then the system makes a contribution

$$\delta r_j = S\Phi(\ln M_{1j})\varphi(\ln M_{2j})\Psi(\ln a_j)\delta \ln M_1 \delta \ln M_2 \delta \ln a \tag{94}$$

to the rate r_i at which that particular population is born. This rate depends on the star formation rate S, the primary mass distribution $\Phi(\ln M_1)$, the secondary mass distribution $\varphi(\ln M_2)$, and the separation distribution $\Psi(\ln a)$. The number of population i in the Galaxy at any time T is then given by the sum of $\delta r_j \times \Delta t_{ji}$ for all systems j that lived for a time Δt_{ji} as a member of that population, where we assume that the interval began before T, and that T is the end-point of the binary evolution.

4.1.1 The mass distributions

Our primary-mass distribution is the IMF of Kroupa, Tout & Gilmore (1993), derived from the stellar distribution towards both Galactic poles as well as the distribution of stars within 5.2 pc of the Sun,

$$\xi(m) = \begin{cases} 0 & m \leq m_0 \\ a_1 m^{-1.3} & m_0 < m \leq 0.5 \\ a_2 m^{-2.2} & 0.5 < m \leq 1.0 \\ a_2 m^{-2.7} & 1.0 < m < \infty \end{cases}, \tag{95}$$

where $\xi(m)\,\mathrm{d}m$ is the probability that a star has a mass, expressed in solar units, between m and $m + \mathrm{d}m$. The distribution is normalized according to

$$\int_0^\infty \xi(m)\,\mathrm{d}m = 1 \tag{96}$$

so that, for $m_0 = 0.1$, $a_1 = 0.290\,56$ and $a_2 = 0.155\,71$. Then

$$\Phi(\ln M_1) = M_1 \xi(M_1). \tag{97}$$

The percentage of stars with mass greater than $80\,\mathrm{M}_\odot$ is less than 0.005 and hence our upper mass limit for the grid.

If the component masses are to be chosen independently from the IMF, then the secondary-mass distribution is

$$\varphi(\ln M_2) = M_2 \xi(M_2). \tag{98}$$

However, there is observational evidence (Eggleton et al. 1989; Mazeh et al. 1992; Goldberg & Mazeh 1994) to support correlated masses, i.e.

$$\varphi(\ln M_2) = \frac{M_2}{M_1} = q_2, \tag{99}$$

which corresponds to a uniform distribution of the mass ratio q_2, for $0 < q_2 \leq 1$.

4.1.2 The separation distribution

We take this to be

$$\Psi(\ln a) = k = \text{constant}, \tag{100}$$

between the limits 3 and $10^4\,\mathrm{R}_\odot$. Normalization gives $k = 0.123\,28$. This distribution is contrary to the findings of Eggleton et al. (1989), but it facilitates comparison with other models (e.g. Yungelson, Livio & Tutukov 1997; Han 1998) without upsetting the results. We chose the upper limit with a view to including all separations for which a binary system is likely to experience some form of mass exchange interaction within the

lifetime of the Galaxy (Yungelson et al. 1995). This was not achieved for all classes of binaries (see Section 4.2.2). The choice of lower limit is rather simplistic, and a dependence on binary mass might be more realistic.

4.1.3 Star formation rate

We assume that one binary with $M_1 \geq 0.8\,\mathrm{M}_\odot$ is born in the Galaxy per year. Therefore

$$S\int_{M_1=0.8}^{M_1=\infty} \Phi(m)\,\mathrm{d}m = 1, \tag{101}$$

which gives $S = 7.6085\,\mathrm{yr}^{-1}$. We fix this rate over the lifetime of the Galaxy. It is in rough agreement with the birth rate of WDs in the Galaxy, $\chi_{\mathrm{WD}} \approx 2\times10^{-12}\,\mathrm{pc}^{-3}\,\mathrm{yr}^{-1}$ (Phillips 1989), when we note that only stars with $M > 0.8\,\mathrm{M}_\odot$ can evolve to white dwarfs in the age of the Galaxy, and that all stars are in binaries and assume an effective Galactic volume of $V_{\mathrm{gal}} = 5\times10^{11}\,\mathrm{pc}^3$. The same assumptions regarding the star formation rate have been made previously (e.g. Iben & Tutukov 1984; Han 1998) facilitating comparison with the results of these studies.

To estimate an effective Galactic volume, we use values for the Galactic disc of $L_{V,\mathrm{disc}} = 1.2\times10^{10}\,\mathrm{L}_\odot$ and $(M/L)_{\mathrm{disc}} = 5$ for the visual luminosity and mass-to-light ratio (Binney & Tremaine 1987) to give $M_{\mathrm{disc}} = 6\times10^{10}\,\mathrm{M}_\odot$ for the mass in visible stars. We combine this with the local mass density of stars, $\rho_\odot = 0.1\,\mathrm{M}_\odot\,\mathrm{pc}^{-3}$ (Kuijken & Gilmore 1989), to give $V_{\mathrm{gal}} = 6\times10^{11}\,\mathrm{pc}^3$.

4.1.4 Binary population models

We construct a variety of models, each with slightly different assumptions for the initial conditions of the population or the parameters that govern the evolution. Our standard is Model A, in which the secondary mass is chosen according to a uniform distribution of the mass ratio (see equation 99) and the metallicity of the stars is $Z = 0.02$. All binaries are initially circular, with each star having ZAMS rotation as given by equation (108) of Paper I, and tidal synchronization is followed in detail. The common-envelope efficiency parameter is set at $\alpha_{\mathrm{CE}} = 3$, so that the treatment of CE evolution in this model is similar to that of Iben & Livio (1993, although the dependence on core and envelope mass in the two treatments remains somewhat different). Model B differs from Model A by not including tidal evolution. For Model C the tides are taken into account, but we use $\alpha_{\mathrm{CE}} = 1$. Model D is the same as Model A, except that the secondary mass is chosen independently from the same IMF as the primary.

The assumption that all stars within the population are born with the same composition is somewhat naive: nucleosynthesis in successive generations of stars enriches the gas from which they form as the Galaxy evolves. Currently it is uncertain whether a definite age-metallicity relation exists for stars in the Galactic disc, but it is clear is that there is a large scatter in metallicity at any given age (McWilliam 1997). From the data of Edvardsson et al. (1993) the age–metallicity relation for the solar neighbourhood can be represented in terms of the relative iron abundance by

$$[\mathrm{Fe/H}] = 0.35x - 0.4\tau - (1.73 + 0.35x)\tau^{20}, \tag{102}$$

where $\tau = t/T_{\mathrm{gal}}$ is the fractional time since formation of the star in terms of the current Galactic age. A star born now has $\tau = 0$. The scatter in the data is reproduced by a random variable x uniform in the range $-1 \leq x \leq 1$. The metallicity can be obtained from

$$[\mathrm{Fe/H}] \simeq \ln(Z/\mathrm{Z}_\odot) \tag{103}$$

with $Z_\odot = 0.02$. This relation shows that solar composition is within the limits of the scatter for the most recent 80 per cent of the Galaxy's life, but that for older populations the metallicity drops sharply to much lower values. While it would be interesting to construct a model with a $Z(t)$ dependence, this is beyond the scope of this work. To represent an older population, we simply take the metallicity of the stars in Model E to be $Z = 0.0001$.

Finally, to investigate the changes produced when tidal circularization, as well as synchronization, is acting on the population, our Model F differs from Model A by allowing binaries to form in eccentric orbits. We choose the initial eccentricity from a thermal distribution (Heggie 1975)

$$f(e) = 2e, \tag{104}$$

between the limits 0 and 1. Model G also allows eccentric orbits, but the process of circularization is according to the model by PZV, as described in Section 3.

The characteristics of each model are summarized in Table 4. All models assume the default values given in Table 3, unless specified otherwise. This means that a velocity kick is imparted to an NS or BH at birth (as described in Section 2.5), and the Eddington limit is not imposed during mass transfer in any of these models (see Section 2.6.6). We set the wind accretion parameter to $\beta_{\mathrm{W}} = 0.5$ in all cases, and the stars are not assumed to be in corotation with the orbit on the ZAMS.

For each model we use 100 grid points in each dimension so that, recalling that only systems with $q_2 \leq 1$ need be evolved, a total of 6.54×10^5 different binaries are evolved in each case. We find that a finer grid spacing does not alter the results within the tolerance set by the quoted errors. For each system we slightly displace the initial parameters from their grid positions so that a smooth distribution in mass and separation is achieved. This is done uniformly about each grid point, after selection of a random variable, with no overlap between parameters attached to adjoining grid points.

4.2 Results

Table 5 lists the formation rates, as number per year in the Galactic disc, of various interesting stars, binaries and events. We calculate these assuming an age for the Galactic disc of 12 Gyr (Eggleton et al. 1989; Phelps 1997; Knox, Hawkins & Hambly 1999), and that all stars are born in binaries. Also listed is an estimate of the percentage error in the formation rate of the individual populations calculated from the standard deviation produced by repeated runs of Model A, each with a different seed for the random number

Table 4. Model parameters.

	TIDES	α_{CE}	e	M_2	Z
A	ON	3.0	0.0	eq. (99)	0.0200
B	OFF	3.0	0.0	eq. (99)	0.0200
C	ON	1.0	0.0	eq. (99)	0.0200
D	ON	3.0	0.0	eq. (98)	0.0200
E	ON	3.0	0.0	eq. (99)	0.0001
F	ON	3.0	$f(e)$	eq. (99)	0.0200
G	PZV	3.0	$f(e)$	eq. (99)	0.0200

generator. Errors associated with systems that involve the formation of an NS or BH are generally larger owing to the velocity kick distribution. The eccentricity distribution used in Models F and G introduces an additional degree of uncertainty in the results; however, repeated runs of Model F show that the percentage error exceeds that quoted in Table 5 for only a few cases, and never by more than a factor of 2.

4.2.1 *Definitions of binary class*

In our models a blue straggler star (BSS) is an MS star that, by accreting mass or by merging, appears older than the standard MS lifetime applicable to its mass. This phase of evolution lasts until the star moves off the MS. Cataclysmic variables (CVs) have a WD secondary with a non-degenerate Roche lobe-filling companion. These we divide into subcategories: classical CV (CV class) if $k_1 \leq 1$, GK Persei systems (GK Per, e.g. Crampton, Cowley & Fisher 1986) if $k_1 = 2$, symbiotic-like binaries (CV Symb) if $3 \leq k_1 \leq 6$, and subdwarf B binaries (sdB) if $7 \leq k_1 \leq 9$. Binaries in which an MS secondary is accreting from a Roche lobe-filling companion are termed *Algol*. If the mass ratio of the primary, $q_1 = M_1/M_2$, is greater than unity, then the system is pre-Algol; if the primary is an MS star and $q_1 < 1$, then this is an MS Algol; otherwise the system is a cold Algol, if the secondary has $M_2 \leq 1.25\,\mathrm{M}_\odot$, or a hot Algol, if $M_2 > 1.25\,\mathrm{M}_\odot$.

X-ray binaries have an NS or a BH secondary accreting material from either the stellar wind of the companion or by RLOF, with an accretion luminosity $L_\mathrm{X} > \mathrm{L}_\odot$. The primary star may be of any type. If the material is accreted via an accretion disc, the accretion luminosity is given by

$$L_\mathrm{X} = \frac{GM_2\dot{M}_2}{2R_2}. \tag{105}$$

If the primary is an MS star with $M_1 < 2\,\mathrm{M}_\odot$, the system is a low-mass X-ray binary (LMXB); if the primary is a WD, then it is a white dwarf X-ray binary (WDXB); otherwise it is a massive X-ray binary (MXRB). These sources are divided into transient (t) or persistent (p) according to the criteria of van Paradijs (1996): for a

Table 5. Formation rates per year in the Galactic disc of various events and systems.

Model	A	B	C	D	E	F	G	per cent err
BSS	1.295×10^{-1}	1.138×10^{-1}	1.248×10^{-1}	5.049×10^{-2}	1.839×10^{-1}	1.181×10^{-1}	1.367×10^{-1}	0.31
CV class	1.987×10^{-2}	1.292×10^{-2}	2.120×10^{-2}	1.820×10^{-2}	3.080×10^{-2}	1.889×10^{-2}	3.973×10^{-2}	3.65
GK Per	1.398×10^{-2}	1.165×10^{-2}	1.671×10^{-2}	1.679×10^{-3}	3.709×10^{-2}	1.374×10^{-2}	3.460×10^{-3}	0.93
CV Symb	7.858×10^{-4}	1.423×10^{-4}	2.450×10^{-3}	1.898×10^{-4}	1.027×10^{-2}	8.527×10^{-4}	4.440×10^{-4}	2.73
sdB	1.135×10^{-2}	1.398×10^{-2}	2.189×10^{-3}	1.090×10^{-3}	1.729×10^{-2}	1.047×10^{-2}	1.125×10^{-2}	0.49
pre Algol	1.248×10^{-1}	1.040×10^{-1}	1.244×10^{-1}	8.807×10^{-2}	1.861×10^{-1}	1.112×10^{-1}	2.082×10^{-1}	0.07
MS Algol	2.861×10^{-2}	2.981×10^{-2}	2.864×10^{-2}	1.558×10^{-2}	2.784×10^{-2}	2.485×10^{-2}	1.077×10^{-2}	0.32
cold Algol	1.313×10^{-2}	1.145×10^{-2}	1.293×10^{-2}	7.007×10^{-3}	3.718×10^{-2}	1.222×10^{-2}	2.255×10^{-3}	1.11
hot Algol	4.910×10^{-2}	4.593×10^{-2}	4.458×10^{-2}	1.018×10^{-2}	9.049×10^{-2}	4.430×10^{-2}	2.780×10^{-2}	0.18
NS LMXBp	3.487×10^{-6}	1.362×10^{-7}	2.219×10^{-7}	5.481×10^{-6}	1.010×10^{-5}	1.071×10^{-6}	4.906×10^{-6}	37.56
BH LMXBp	3.601×10^{-6}	1.696×10^{-6}	1.561×10^{-6}	3.686×10^{-6}	2.563×10^{-5}	3.865×10^{-6}	5.349×10^{-5}	25.36
NS MXRBp	7.481×10^{-4}	5.014×10^{-4}	6.307×10^{-4}	1.434×10^{-5}	6.096×10^{-4}	7.214×10^{-4}	5.164×10^{-4}	1.37
BH MXRBp	1.057×10^{-4}	1.612×10^{-5}	1.092×10^{-4}	2.043×10^{-6}	2.425×10^{-4}	1.085×10^{-4}	1.132×10^{-4}	3.77
NS WDXBp	1.639×10^{-3}	2.028×10^{-3}	1.686×10^{-4}	8.393×10^{-5}	3.563×10^{-3}	1.426×10^{-3}	1.347×10^{-3}	0.55
BH WDXBp	2.764×10^{-4}	3.513×10^{-4}	2.885×10^{-5}	4.987×10^{-6}	4.951×10^{-4}	2.400×10^{-4}	2.085×10^{-4}	7.62
NS LMXBt	2.359×10^{-5}	5.640×10^{-6}	1.253×10^{-6}	2.537×10^{-5}	4.198×10^{-5}	9.087×10^{-6}	3.654×10^{-5}	21.27
BH LMXBt	9.172×10^{-6}	1.691×10^{-6}	4.854×10^{-6}	6.552×10^{-6}	2.323×10^{-5}	6.542×10^{-6}	2.283×10^{-5}	20.87
NS MXRBt	7.345×10^{-4}	8.048×10^{-4}	8.122×10^{-4}	1.823×10^{-5}	1.568×10^{-3}	7.149×10^{-4}	6.515×10^{-4}	1.41
BH MXRBt	5.447×10^{-5}	2.320×10^{-5}	8.706×10^{-5}	2.564×10^{-6}	2.560×10^{-4}	5.823×10^{-5}	4.471×10^{-5}	2.81
NS WDXBt	8.963×10^{-4}	1.088×10^{-3}	7.332×10^{-5}	7.325×10^{-5}	2.296×10^{-3}	7.753×10^{-4}	6.918×10^{-4}	0.29
BH WDXBt	6.531×10^{-4}	8.299×10^{-4}	8.357×10^{-5}	1.017×10^{-5}	1.237×10^{-3}	5.636×10^{-4}	5.784×10^{-4}	1.78
S-Symb	5.353×10^{-3}	5.091×10^{-3}	5.370×10^{-3}	2.712×10^{-4}	6.356×10^{-3}	4.100×10^{-3}	4.305×10^{-3}	1.79
D-Symb	4.322×10^{-2}	4.701×10^{-2}	4.302×10^{-2}	5.748×10^{-3}	3.782×10^{-2}	3.494×10^{-2}	3.763×10^{-2}	0.23
nHe MSC	6.441×10^{-3}	1.929×10^{-3}	2.160×10^{-3}	1.657×10^{-3}	1.649×10^{-2}	5.591×10^{-3}	5.059×10^{-3}	0.94
gnt MSC	3.366×10^{-3}	3.639×10^{-3}	3.432×10^{-3}	1.093×10^{-3}	4.809×10^{-3}	3.075×10^{-3}	8.166×10^{-4}	4.75
WDWD DD	1.131×10^{-1}	1.229×10^{-1}	7.572×10^{-2}	1.334×10^{-2}	2.290×10^{-1}	8.631×10^{-2}	7.902×10^{-2}	0.16
WDNS DD	8.577×10^{-4}	8.982×10^{-4}	5.265×10^{-4}	2.088×10^{-5}	2.842×10^{-3}	7.986×10^{-4}	7.537×10^{-4}	1.10
NSNS DD	7.384×10^{-5}	8.192×10^{-5}	2.785×10^{-5}	6.972×10^{-7}	1.604×10^{-4}	7.587×10^{-5}	7.295×10^{-5}	5.11
He DDRch[a]	1.997×10^{-2}	2.385×10^{-2}	6.782×10^{-3}	2.344×10^{-3}	5.361×10^{-2}	1.927×10^{-2}	1.619×10^{-2}	1.21
CO DDRch	2.942×10^{-3}	3.598×10^{-3}	1.549×10^{-4}	8.558×10^{-5}	4.959×10^{-3}	2.538×10^{-3}	2.144×10^{-3}	0.43
NS DDRch	5.724×10^{-5}	6.826×10^{-5}	2.381×10^{-5}	5.096×10^{-7}	1.062×10^{-4}	5.884×10^{-5}	5.240×10^{-5}	6.12
He LMWD	1.671×10^{-1}	1.709×10^{-1}	9.715×10^{-2}	1.138×10^{-1}	2.985×10^{-1}	1.658×10^{-1}	1.466×10^{-1}	0.42
CO LMWD	7.019×10^{-3}	7.622×10^{-3}	1.351×10^{-3}	1.564×10^{-3}	1.085×10^{-2}	6.597×10^{-3}	3.002×10^{-3}	1.78
He SNIa	2.818×10^{-3}	8.100×10^{-3}	3.217×10^{-4}	7.214×10^{-4}	2.702×10^{-2}	2.677×10^{-3}	1.242×10^{-3}	1.68
ELD SNIa	1.560×10^{-2}	1.994×10^{-2}	5.193×10^{-3}	1.665×10^{-3}	3.227×10^{-2}	1.490×10^{-2}	1.102×10^{-2}	0.61
CO SNIa	2.567×10^{-3}	2.627×10^{-3}	2.109×10^{-4}	1.125×10^{-4}	2.720×10^{-3}	2.442×10^{-3}	1.890×10^{-3}	0.59
AIC	3.738×10^{-3}	3.975×10^{-3}	9.771×10^{-4}	1.364×10^{-4}	6.286×10^{-3}	3.442×10^{-3}	3.029×10^{-3}	0.35
SNII	1.724×10^{-2}	1.592×10^{-2}	1.940×10^{-2}	1.142×10^{-2}	2.848×10^{-2}	1.810×10^{-2}	1.921×10^{-2}	1.75
SNIIa	3.551×10^{-4}	1.453×10^{-4}	6.189×10^{-5}	7.054×10^{-6}	6.840×10^{-5}	2.851×10^{-4}	1.228×10^{-4}	1.67
SNIb/c	1.403×10^{-2}	1.361×10^{-2}	1.304×10^{-2}	4.043×10^{-3}	2.026×10^{-2}	1.313×10^{-2}	1.510×10^{-2}	0.19

[a] DDRch systems are a subset of the corresponding DDs.

critical luminosity

$$\log\left(\frac{L_{\rm X,crit}}{\rm L_\odot}\right) = \begin{cases} 1.62 + 1.07(P/{\rm h}) & {\rm NS\ \ secondary} \\ 2.22 + 1.07(P/{\rm h}) & {\rm BH\ \ secondary}\,, \end{cases} \quad (106)$$

if $L_{\rm X} > L_{\rm X,crit}$, the X-ray source is persistent; otherwise it is a soft X-ray transient (SXT) analogous to a dwarf nova (see Section 2.6.6). SXT outbursts are caused by an instability in the accretion disc, the temperature of which is affected by X-ray heating. The main effect of this X-ray heating, taken into account in the calculation of equation (106), is to make the flow of material through the accretion disc stable to substantially lower mass transfer rates than for dwarf novae systems.

Symbiotic stars are classed as systems with secondaries of $k_2 \leq 12$ that accrete material from the stellar wind of a giant primary at a rate high enough to produce an accretion luminosity that exceeds either $10\,{\rm L_\odot}$ (Yungelson et al. 1995) or 1 per cent of the primary luminosity – whichever is the smaller. Equation (105) is used to calculate the accretion luminosity. D-type symbiotics (D-Symb) are long-period systems containing a Mira-like cool star primary ($k_1 = 6$). They are characterized by extensive circumbinary dust shells. Shorter period symbiotics with a normal giant primary ($k_1 < 6$) are S-type (S-Symb). MS stars accreting from a Roche lobe-filling giant could also appear to be symbiotic stars (Kenyon 1986), but here we include them in the cold Algol population. Miscellaneous RLOF systems with a non-degenerate primary ($k_1 < 10$) are nHe MSC if the secondary is a helium star ($7 \leq k_2 \leq 9$), and gnt MSC if the secondary is giant-like ($2 \leq k_2 \leq 6$).

Double-degenerate (DD) binaries that consist of two WDs are WDWD DD, while those containing a WD and either an NS or BH are WDNS DD. If the system is composed of an NS–NS, NS–BH or BH–BH pair, it is an NSNS DD. DD systems with a Roche lobe-filling WD (AM CVn systems) are He DDRch, if the primary is a HeWD, or CO DDRch otherwise. NS–NS binaries that evolve into contact and coalesce are NS DDRch. As a result of binary interaction, it is possible to form WDs of mass less than the lowest mass WD that can be formed from single-star evolution in the lifetime of the Galaxy, $M \lesssim 0.5\,{\rm M_\odot}$. These low-mass white dwarfs (LMWDs) are recorded as either He LMWD or CO LMWD.

We also count various types of supernovae. HeWDs that explode when their mass exceeds $0.7\,{\rm M_\odot}$ are recorded as He SNIa, as are HeWD mergers. COWDs that explode as a possible type Ia SN in an edge-lit detonation, once $0.15\,{\rm M_\odot}$ of He-rich material has been accreted by the WD, are ELD SNIa, while COWDs that explode because their mass exceeds the Chandrasekhar limit are CO SNIa. Supernovae that leave no remnant from a primary with $k_1 \leq 9$ are SNIIa. AIC represents the accretion-induced collapse of a Chandrasekhar mass ONeWD to an NS. Supernovae that produce an NS or BH from a primary with $8 \leq k_1 \leq 9$ are SNIb/c. All others are normal type II SNe, or SNII.

Supernovae are effectively instantaneous *events*, so there is no record of how long they last, whereas the remainder of the populations are *systems* and must exist for a non-zero amount of time to contribute to the birth rate. We also count double NS binaries that enter RLOF (NS DDRch) as events, because they always coalesce immediately as possible γ-ray bursts. Each binary may contribute to the rate of more than one population if it evolves through a series of phases identified with the individual populations listed in Table 5. The expected numbers presently in the Galactic disc for all the individual populations that exist as systems for a finite time are listed in Table 6. These can be converted to space densities by dividing by the effective Galactic volume $V_{\rm gal} = 6 \times 10^{11}\,{\rm pc^3}$, which has been normalized to the local mass density of stars.

4.2.2 *Comparison of model results*

Comparison of Models A and B reveals that most populations show differences in their formation rates that are greater than the errors, but surprisingly few exhibit significant differences. Fig. 5 shows the parameter space for the formation of all CV types when the initial mass of one component star is fixed at $3.2\,{\rm M_\odot}$. The systems that form in Model A only, Model B only and in both are distinguished. There is no special reason for the choice of $3.2\,{\rm M_\odot}$ as an illustrative example other than that a wide variety of systems are formed in this case. Systems with low-mass ZAMS companions ($M_2 < 0.5\,{\rm M_\odot}$) are CV class, while GK Per systems are formed with high-mass ZAMS primaries ($M_1 > 7.5\,{\rm M_\odot}$). The sdB systems form in two main regions of the parameter space: small orbital separation ($a < 30\,{\rm R_\odot}$) and large orbital separation ($a > 500\,{\rm R_\odot}$). The remainder, those occupying the middle region of the diagram, are either CV class, GK Per or CV Symb, with a large number of the systems evolving through a combination of these phases. It is evident from Fig. 5 that the CV population behaves as expected when tidal evolution is allowed in the model. Wider systems are brought into an interaction distance by the action of tidal synchronization, while closer systems, that formed CVs without tides, now get too close and coalesce during the common-envelope (CE) phase that is an integral part of CV formation.

As a typical example of classical CV formation in Model A, let us consider stars of masses 2.0 and $0.2\,{\rm M_\odot}$ in an orbit with initial separation $100\,{\rm R_\odot}$. The more massive star evolves to fill its Roche lobe on the EAGB when the separation has fallen to $70\,{\rm R_\odot}$ (owing to tidal interaction), a CE forms, and a HeHG star separated from the $0.2\text{-}{\rm M_\odot}$ MS star by $1.1\,{\rm R_\odot}$ emerges. The HeHG star evolves to a COWD, and shortly afterwards the MS star fills its Roche lobe, creating a classical CV. The same system evolved with Model B has expanded to $a = 105\,{\rm R_\odot}$ (owing to stellar wind mass-loss) when the first phase of RLOF begins. As a result the post-CE binary is too wide to interact within $T_{\rm gal}$. However, if the same masses are evolved from a closer initial separation of $50\,{\rm R_\odot}$, in Model A the stars coalesce during CE, while Model B produces a classical CV.

A typical CV Symb system can form from a $3.2\text{-}{\rm M_\odot}$ star and a $1.0\text{-}{\rm M_\odot}$ star initially separated by $180\,{\rm R_\odot}$. RLOF first occurs when the primary has evolved to the EAGB and tides have reduced the separation to $160\,{\rm R_\odot}$. Mass transfer is dynamical, so that a CE forms from which a close binary consisting of a HeHG and an MS star emerges. The helium star evolves to a COWD and a second phase of RLOF begins when the companion reaches the HG. This time the mass transfer proceeds on a thermal time-scale, so that when the new primary reaches the GB its mass has dropped to $0.3\,{\rm M_\odot}$, and a second CE phase is avoided. Stable mass transfer then continues on the GB until the primary loses its envelope and a DD system is born. This system has evolved through both a GK Per and a CV Symb phase. If it were to be evolved without tidal interaction, the binary formed after the CE phase would be wider. The new primary would still fill its Roche lobe on the HG, but only when closer to the GB, so that upon reaching the GB a second CE occurs in which the system coalesces. Thus a GK Per phase still exists, but the CV Symb phase does not.

Unlike the other types of CV, the sdB population increases in formation rate in Model B. As already mentioned, there are two

Table 6. Present number in the Galactic disc of various systems.

Model	A	B	C	D	E	F	G
BSS	6.999×10^{7}	4.444×10^{7}	6.993×10^{7}	4.439×10^{7}	8.823×10^{7}	8.023×10^{7}	6.128×10^{7}
CV class	2.532×10^{7}	3.594×10^{7}	3.554×10^{7}	9.908×10^{7}	3.995×10^{7}	2.550×10^{7}	2.565×10^{7}
GK Per	7.242×10^{6}	2.775×10^{6}	8.155×10^{6}	1.184×10^{6}	2.001×10^{6}	6.953×10^{6}	9.842×10^{5}
CV Symb	7.070×10^{5}	1.255×10^{3}	2.503×10^{6}	1.849×10^{5}	4.781×10^{4}	7.982×10^{5}	2.486×10^{5}
sdB	3.298×10^{4}	6.635×10^{4}	5.548×10^{3}	3.335×10^{3}	5.054×10^{4}	3.047×10^{4}	8.599×10^{3}
pre Algol	6.396×10^{6}	1.262×10^{7}	6.405×10^{6}	3.122×10^{6}	2.411×10^{6}	5.614×10^{6}	7.313×10^{5}
MS Algol	6.081×10^{6}	1.178×10^{7}	6.077×10^{6}	3.423×10^{6}	3.806×10^{6}	5.432×10^{6}	2.115×10^{5}
cold Algol	6.784×10^{6}	1.020×10^{7}	6.795×10^{6}	4.658×10^{6}	9.008×10^{6}	6.007×10^{6}	4.516×10^{5}
hot Algol	7.132×10^{6}	8.216×10^{6}	7.148×10^{6}	3.680×10^{6}	6.790×10^{6}	6.320×10^{6}	5.034×10^{5}
NS LMXBp	4.191×10^{0}	1.112×10^{1}	3.451×10^{0}	7.690×10^{1}	4.409×10^{2}	1.331×10^{0}	4.388×10^{1}
BH LMXBp	9.140×10^{1}	4.106×10^{1}	5.016×10^{1}	3.001×10^{1}	8.553×10^{2}	6.998×10^{1}	2.196×10^{3}
NS MXRBp	2.810×10^{3}	2.608×10^{3}	1.600×10^{3}	8.178×10^{1}	3.987×10^{3}	2.531×10^{3}	2.494×10^{2}
BH MXRBp	2.335×10^{2}	2.992×10^{1}	1.439×10^{2}	3.333×10^{0}	1.876×10^{2}	2.673×10^{2}	1.288×10^{1}
NS WDXBp	1.233×10^{5}	1.494×10^{5}	1.116×10^{4}	7.550×10^{3}	2.871×10^{5}	1.055×10^{5}	1.023×10^{5}
BH WDXBp	1.554×10^{4}	2.145×10^{4}	1.841×10^{3}	3.066×10^{2}	2.947×10^{4}	1.469×10^{4}	1.353×10^{4}
NS LMXBt	2.854×10^{4}	1.871×10^{4}	4.131×10^{3}	1.396×10^{5}	5.545×10^{4}	2.238×10^{4}	1.760×10^{5}
BH LMXBt	7.240×10^{4}	1.085×10^{4}	4.260×10^{4}	5.072×10^{4}	1.343×10^{5}	4.405×10^{4}	2.456×10^{5}
NS MXRBt	1.785×10^{5}	1.511×10^{5}	5.432×10^{4}	8.452×10^{3}	7.547×10^{4}	1.630×10^{5}	2.962×10^{5}
BH MXRBt	4.829×10^{4}	7.947×10^{3}	9.105×10^{4}	2.818×10^{3}	7.353×10^{4}	6.671×10^{4}	1.432×10^{5}
NS WDXBt	2.802×10^{6}	3.406×10^{6}	2.079×10^{5}	2.031×10^{5}	6.925×10^{6}	2.423×10^{6}	2.177×10^{6}
BH WDXBt	3.223×10^{6}	4.161×10^{6}	4.313×10^{5}	5.088×10^{4}	6.099×10^{6}	2.843×10^{6}	2.920×10^{6}
S-Symb	2.363×10^{2}	1.946×10^{2}	2.713×10^{2}	2.858×10^{1}	4.470×10^{2}	1.378×10^{2}	1.271×10^{2}
D-Symb	3.389×10^{3}	3.837×10^{3}	3.369×10^{3}	3.369×10^{2}	5.044×10^{3}	2.702×10^{3}	2.939×10^{3}
nHe MSC	1.497×10^{4}	1.017×10^{4}	2.116×10^{3}	4.578×10^{3}	4.402×10^{4}	1.156×10^{4}	1.572×10^{4}
gnt MSC	4.609×10^{4}	7.355×10^{4}	4.390×10^{4}	1.456×10^{4}	1.292×10^{4}	3.182×10^{4}	5.554×10^{2}
WDWD DD	6.018×10^{8}	6.028×10^{8}	4.919×10^{8}	5.759×10^{7}	1.041×10^{9}	1.219×10^{8}	4.048×10^{8}
WDNS DD	2.725×10^{5}	1.866×10^{5}	4.090×10^{4}	1.192×10^{3}	6.959×10^{5}	1.800×10^{5}	2.955×10^{5}
NSNS DD	2.427×10^{6}	2.160×10^{6}	1.307×10^{6}	7.949×10^{4}	8.313×10^{6}	2.367×10^{6}	2.249×10^{6}
He DDRch	3.076×10^{7}	2.913×10^{7}	1.003×10^{7}	3.959×10^{6}	1.353×10^{8}	2.858×10^{7}	2.371×10^{7}
CO DDRch	2.465×10^{7}	3.299×10^{7}	1.261×10^{6}	7.225×10^{5}	4.125×10^{7}	2.127×10^{7}	1.879×10^{7}

main regions of the parameter space shown in Fig. 5 from which sdB systems form. First, consider the population formed from close orbits which can be characterized by a binary of initial masses 3.2 and 1.0 $M_\odot$ separated by 20 $R_\odot$. The primary fills its Roche lobe on the HG, and its mass has fallen to 0.6 $M_\odot$ by the time it reaches the GB so that CE evolution is avoided and stable mass transfer continues. Eventually it loses its entire envelope to become a HeMS star. The companion evolves to the GB and fills its Roche lobe, by which time the HeMS star has become a COWD and the resulting CE evolution leaves a COWD/HeMS pair in a close orbit. When the new HeMS evolves to fill its Roche lobe, a sdB system is formed. The population formed from wider orbits involves a slightly more complicated path represented by a binary with $M_2 = 3.2\,M_\odot$, $M_1 = 10.0\,M_\odot$ and $a = 500\,R_\odot$. A first phase of RLOF begins when the more massive star is on the HG with the mass transfer becoming dynamical when it reaches the GB. The ensuing CE leaves an MS/HeMS pair separated by 10 $R_\odot$. After the helium star evolves to the helium GB, it fills its Roche lobe and mass transfer proceeds until all the envelope is lost and the star becomes an ONeWD. The MS star now begins a third phase of RLOF when it reaches the HG. During this phase the ONeWD accretes enough material to swell up and become a TPAGB star, so that shortly afterwards the system evolves into another CE from which a close HeMS/ONeWD pair emerges. Yet another phase of RLOF begins when the new HeMS star fills its Roche lobe and the sdB system is born. Mass transfer continues until an AIC changes the ONeWD to an NS. The increase in Model B birth rate for the sdB population is explained by the cluster of additional systems about $M_2 = 2.6\,M_\odot$ and $a = 20\,R_\odot$. These evolve via a stable

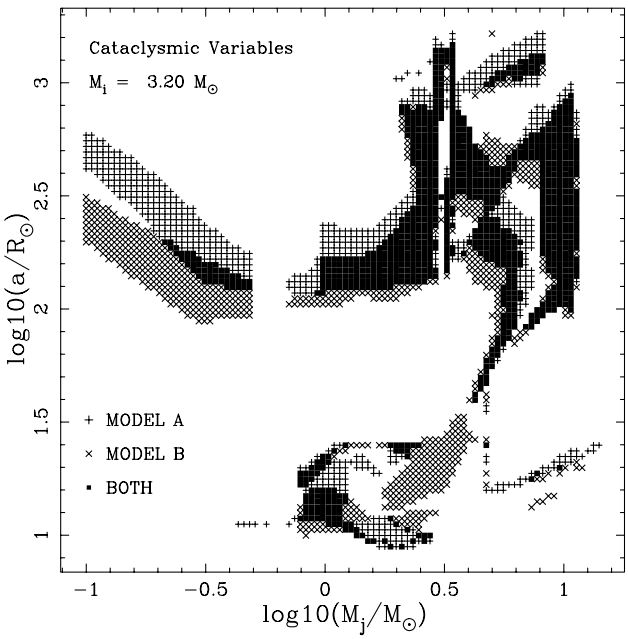

Figure 5. The region of parameter space from which cataclysmic variables (CVs) form when the initial mass of one star is fixed at 3.2 $M_\odot$. Systems formed from Model A are shown as + symbols, from Model B as × symbols, with any overlap as filled squares. The indices i and j can assume the value of either 1 or 2, depending on which mass represents the primary star on the ZAMS, i.e., if the 3.2-$M_\odot$ star is the more massive, then $i = 1$ and $j = 2$.

RLOF phase followed by two instances of CE evolution which produce a close HeMS–COWD pair. When the helium star expands to fill its Roche lobe, the sdB phase begins. If tidal evolution is included, the system formed after the first CE is much closer, so that coalescence occurs during the second CE.

A decrease in the common-envelope efficiency parameter (Model C, $\alpha_{CE} = 1$) increases the CV birth rate, because wider systems are brought within an interaction distance after the CE phase. Thus systems that do not interact in Model A can do so in Model C. This is countered to some degree by closer systems that would interact in Model A now coalescing. The net effect is an increase in production. It could be argued that a combination of Models B and C would produce CV birth rates similar to those of Model A.

Comparing the birth rates of Algols in Models A, B and C reveals no significant variation. This is expected, because RLOF generally begins while the primary is still on the MS when tides have had little effect on the orbit, and also because a CE phase is not involved. The gnt MSC systems that form 55 per cent of the population consist of a GB primary and a HG secondary, while the remaining 45 per cent are GB primary and GB secondary. In most cases the GB–GB systems have previously been GB–HG, and before that were Algols. The general evolution path for these systems begins with RLOF while the primary is on the HG and the secondary on the MS, the HG and GB lifetimes of the primary increase as it loses mass on the HG, mass transfer has reduced q_1 below q_{crit} when the primary reaches the GB, and the secondary evolves to the HG and then the GB while the Roche lobe-filling primary is still on the GB. Of the miscellaneous RLOF systems with helium star secondaries, 51 per cent have an MS primary and a HeMS secondary, and 42 per cent a HeMS primary and secondary.

The birth rate of LMXBs shows an order of magnitude decrease when either Model B or Model C is compared to Model A. With tides a typical LMXB formation scenario begins with a primary mass somewhere in the range 10 to 12 $M_\odot$, a low-mass companion with $M_2 \simeq 1.0\,M_\odot$ and $P \simeq 1000$ d. The massive primary evolves to the EAGB before filling its Roche lobe and forming a CE system from which a fairly close HeHG–MS pair emerges. The helium star explodes in a supernova that leaves an NS. This may increase or decrease the separation, depending on the size of the velocity kick. After some time the MS star evolves to fill its Roche lobe, by which time any eccentricity induced in the orbit by the supernova has been removed by the tides and a persistent NS LMXB is formed. If tides are not included, then the orbit of the HeHG–MS pair is much wider, so that the second RLOF phase occurs when the primary is on the GB, a CE forms, and a DD NS–HeWD binary is produced. On the other hand, if $\alpha_{CE} = 1$, then the orbit of the HeHG–MS pair is much closer after the initial CE so that the HeHG star fills its Roche lobe resulting in another CE in which the two stars coalesce. There is an increase in the LMXB birth rate for Model D, for which the secondary mass is chosen from the same IMF as the primary, because massive stars are more likely to have low-mass companions, increasing the number of systems that can become LMXBs. This is compensated by a corresponding decrease in the MXRB birth rate. All the remaining binary systems show a drop in birth rate for Model D, because more systems form with low q_2, decreasing the likelihood of interaction.

Interestingly, the formation rate of DD systems increases when the tides are not used. Han (1998) finds that a phase of stable RLOF followed by CE evolution (RLOF + CE) and a combination of two CE phases (CE + CE) are the two main channels for forming DDs, with the former channel more likely to occur for close orbits. Adding tides to the model removes many systems from the closer

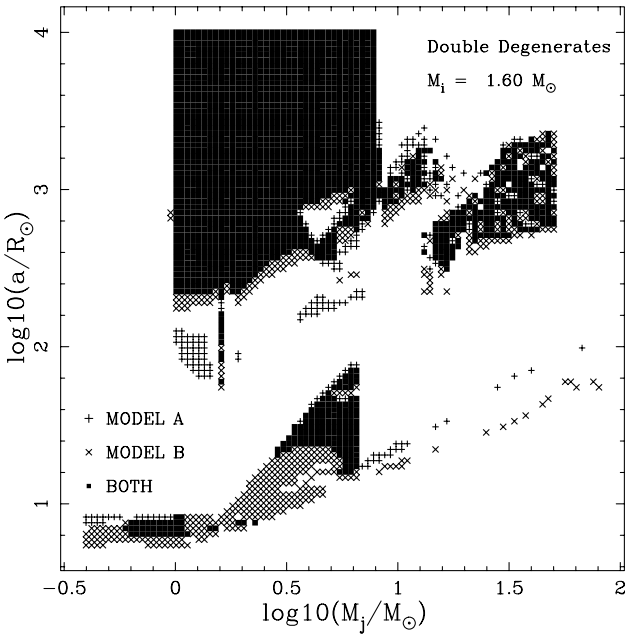

Figure 6. The region of parameter space from which double-degenerate (DD) binaries form when the initial mass of one star is fixed at 1.6 $M_\odot$. Systems formed from Model A are shown as + symbols, from Model B as × symbols, with any overlap as filled squares. The unstable behaviour of some near equal-mass systems is due to the relatively short lifetime of the GB stage. In this case there is a range of separations where the first phase of RLOF begins with both stars on the GB and CE gives a HeWD–HeWD pair. If the mass of either star changes slightly, then one star is still on the MS when RLOF begins and the subsequent evolution is altered.

RLOF + CE channel, because the separation decreases while the secondary evolves on the HG and GB, after the first RLOF phase, so that the CE produces a much closer pair of HeMS stars. This pair then evolves into contact before a DD can form. Fig. 6 shows the parameter space in the M_j–a plane for DD formation in Models A and B when the initial mass of one star is fixed at 1.6 $M_\odot$. The systems with $M_1 > 8.0\,M_\odot$ are WD–NS binaries that survive the supernova kick, while the range of close systems with $a \lesssim 100\,R_\odot$ are RLOF + CE WD–WD binaries, of which there are noticeably more formed in Model B. A typical RLOF + CE WDWD DD formation scenario in Model B begins with $M_1 = 2.2\,M_\odot$, $M_2 = 1.6\,M_\odot$ and $P = 2$ d. The primary fills its Roche lobe on the HG when $P = 1.9$ d. RLOF ends on the GB just before the primary becomes a CHeB star, loses what little is left of its envelope, and moves to the HeMS. Now $M_1 = 0.35\,M_\odot$, $M_2 = 3.45\,M_\odot$ and $P = 60$ d. The orbit has widened as a result of the conservative mass transfer. The more massive star (now assuming the role of the primary) evolves to the GB and overflows its Roche lobe on a dynamical time-scale, so that a CE forms from which a HeMS–HeMS pair emerges with $P = 0.1$ d. Both of these evolve to WDs in a close COWD–COWD DD system. If the same initial parameters are evolved with tides, the system has $P = 30$ d just before the CE, so that a closer HeMS–HeMS pair forms. This evolves into contact before either star can become a WD. If the same masses are evolved with a longer initial period, $P \simeq 240$ d, then a DD forms via the CE + CE channel in Model B. In this case the primary fills its Roche lobe on the EAGB, CE evolution ensues, and a HeHG star with $M_1 = 0.6\,M_\odot$ in an orbit of $P = 6$ d with the MS star emerges. The HeHG star evolves to a COWD. The MS star later fills its Roche lobe on the GB, leading to another CE and the

formation of a HeWD–COWD DD system with $P = 0.03$ d. Evolving this case with Model A leaves a closer binary after the first CE, so that the second CE ends in coalescence of the two stars. Systems with wider initial orbits can survive the second CE phase to produce a DD binary when either Model A or B is used. Even wider systems form a WDWD DD with no interaction, but these have much longer periods than those formed via CE, and are not easily detected.

Inspection of Fig. 6 reveals a large empty region in parameter space between the close group of systems that form DDs via RLOF + CE and the wider group of systems that form DDs via CE + CE. In this gap the initial period is short enough that the second CE leads to coalescence in both Models A and B. However, pockets of DDs do exist in Model A, because stable RLOF can occur on the HG. Mass transfer reduces the primary mass and actually causes a net increase in the separation. This phase of RLOF, coming after the first CE, is non-conservative, so that under the influence of tidal synchronization the separation initially decreases. As the primary mass is reduced further and the strength of the tides weakens, the orbit starts to expand. When the primary reaches the GB, a second CE occurs, but the orbit is wide enough, and the size of the primary small enough, that coalescence is avoided and a DD formed. This is, however, a very unstable region of phase space. If the initial separation is reduced slightly the RLOF phase after the first CE occurs on the MS, the primary mass falls until it develops a convective envelope when dynamical mass transfer leads to coalescence. A slightly larger initial separation means that the RLOF phase starts on the GB before the star has lost any mass, so it is much larger and the CE ends in coalescence. If M_1 is increased slightly, the RLOF phase after the first CE still starts on the HG but, owing to a larger q_1, leads to dynamical mass transfer and coalescence. A reduction in M_1 means the primary takes longer to fill its Roche lobe before the first CE, so that the tides give a greater reduction in the separation, the system formed after the CE is closer, and the next RLOF phase starts on the MS, once more ending in coalescence. With Model B these regions do not occur at all because the orbit is always closer when the second CE forms, so that the binary never survives.

The lower metallicity population, Model E, has increased birth rates in almost all cases compared with Model A. This behaviour can be primarily attributed to the shorter nuclear lifetimes of lower metallicity stars with $M \lesssim 9\,\mathrm{M}_\odot$ (see fig. 5 of Paper I). For example, a solar-mass star with $Z = 0.0001$ evolves to a WD cooling track in half the time it takes a solar-mass star with $Z = 0.02$. This gives it more chance of interacting with its companion when in a relatively wide orbit. Model E represents a very young population that would have formed soon after a galaxy condensed.

It should be noted that the choice of separation distribution $\Psi(\ln a)$ and its limits, particularly the upper cut-off, affects the calculated birth rates and numbers. Only the BSS and D-Symb populations generate any members from initial separations greater than $10^4\,\mathrm{R}_\odot$, but these are rare and so do not affect the absolute numbers very much.

4.2.3 *The role of semilatera recta*

Figs 7 and 8 show the parameter space of CV, Algol and X-ray binaries that are formed for Models A and F respectively when the initial mass of one star is fixed at $3.2\,\mathrm{M}_\odot$. In Model F we form binaries with eccentric orbits and, as expected, this means that systems with wider orbits can interact at periastron and contribute

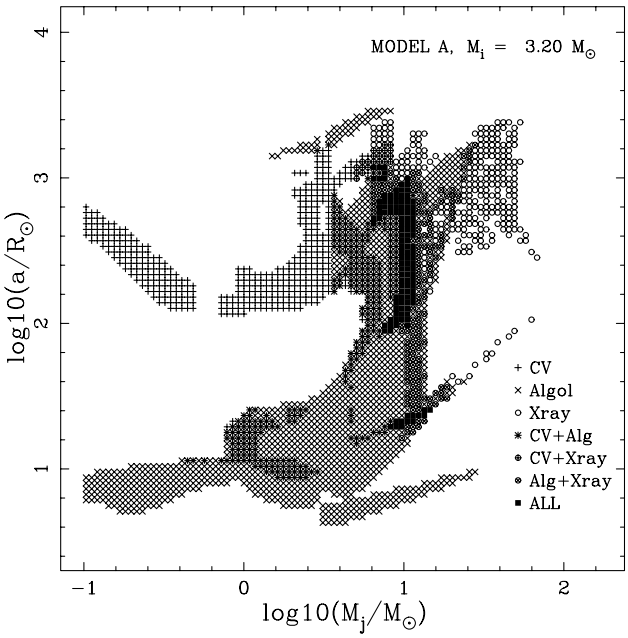

Figure 7. The region of parameter space from which CV, Algol and X-ray binaries form when the initial mass of one star is fixed at $3.2\,\mathrm{M}_\odot$ in Model A.

to the rates. This does not automatically lead to an increase in formation rates, because closer systems are more likely to be destroyed by a collision or coalescence. If we plot semilatus rectum on the vertical axis of Fig. 8, then it appears virtually identical to Fig. 7. Therefore, if a distribution of orbital angular momentum or l is used to determine the initial state of each binary, rather than one of semimajor axis or period, the results do not depend on the form of any chosen eccentricity distribution. In fact, eccentricity need not be a free parameter. This becomes evident when considering

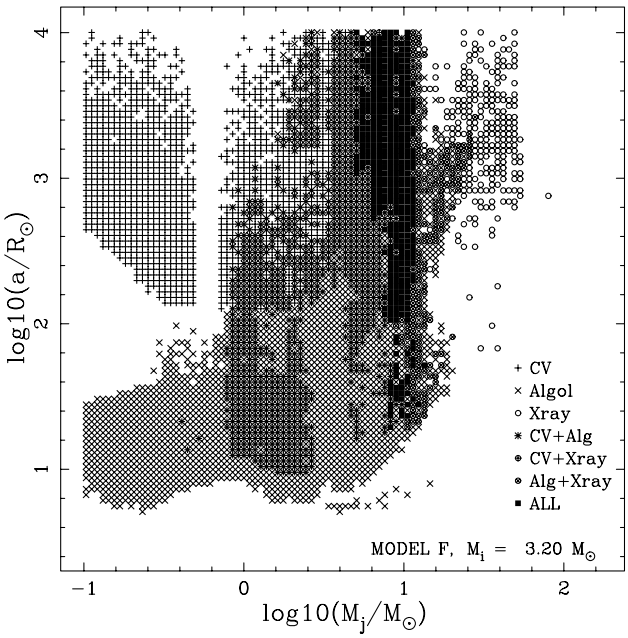

Figure 8. The region of parameter space from which CV, Algol and X-ray binaries form when the initial mass of one star is fixed at $3.2\,\mathrm{M}_\odot$ in Model F.

that tidal interaction conserves angular momentum and that almost all systems circularize before RLOF. Therefore (see equation 4) systems with the same initial l end up in a circular orbit with the same separation when RLOF starts, and their subsequent evolution will be identical. The only instances where the initial eccentricity distribution does matter are binary populations in which tidal interaction is weak, such as wide binaries that may avoid RLOF (e.g. the barium stars; see Karakas et al. 2000).

The circularization method of Model G usually has increased formation rates, because it acts to bring systems closer, making them more likely to interact. Unlike Model F, none of the angular momentum is absorbed by the stars, so that systems do not get so close and, as a result, fewer are destroyed.

The relative fractions of blue stragglers, cataclysmic variables, Algols, persistent low-mass X-ray binaries and double-degenerates as a function of time for Model A are shown in Fig. 9, assuming that all binaries were born in a single burst of star formation. This represents the probability of a binary observed in a star cluster being of a particular type. Each population is a combination of its subpopulations, as listed in Table 5. The peak in the blue straggler distribution at approximately 5000 Myr is primarily due to a decrease in progenitor systems, and its timing depends on the ratio of the mean binary separation, which remains constant, to the radius of the largest MS star, which decreases in time (Hurley et al. 2001). Both the CV and DD probabilities show a steady increase in time, reflecting both the long-lived nature typical of these systems and the constant production of WDs from the evolving mass distribution. As the existence of LMXBs is directly linked to the production of NSs or BHs, it is no surprise that their probability distribution peaks at an early age. The probability of observing an

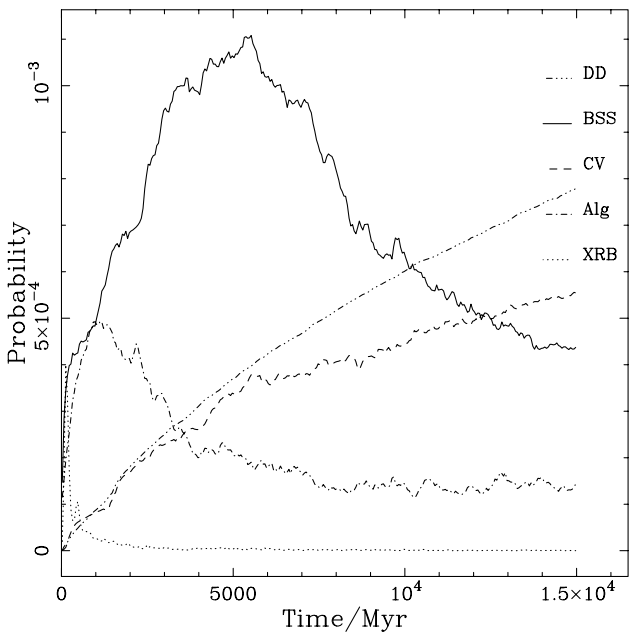

Figure 9. The probability, as a function of time, of a binary being found as a member of certain individual populations of Model A. We assume that all stars are born at the same time. The individual populations shown are: blue stragglers (full line), cataclysmic variables (dashed line), Algols (dot-dashed line), persistent X-ray binaries (dotted line) and double-degenerates (dash-dot-dot-dot line). Each population includes contributions from each of its subpopulations listed in Table 5. The numbers for double-degenerates have been reduced by a factor of 10, and the numbers for persistent X-ray binaries have been increased by a factor of 10.

Algol also shows a peak that is linked to the evolution of massive stars, as these are more likely to fill their Roche lobes on the MS or HG, thus avoiding a common-envelope phase.

4.3 Comparison with observations

To determine whether the parameters of Model A are a good choice, we can compare with observations. For most of the individual binary populations, observational birth rates or numbers in the Galaxy are very uncertain because of selection effects involved when undertaking surveys. However, enough data exist overall to enable a meaningful comparison with the results, from which a decision on the best model parameters can be made. We should add that caution must be exercised when comparing observationally defined classes of binary with the model classes defined in this work. Some overlap between classes necessarily exists, owing in part to the restrictive nature of the theoretical model and to remaining uncertainty about the details of some of these objects in the first place.

4.3.1 Cataclysmic variables

Ritter & Burkert (1986) estimate the CV birth-rate in our Galaxy to be about $10^{-14}\,\mathrm{pc}^{-3}\,\mathrm{yr}^{-1}$ or $6\times10^{-3}\,\mathrm{yr}^{-1}$ if $V_{\mathrm{gal}} = 6\times10^{11}\,\mathrm{pc}^3$. In calculating this rate, they corrected the observed local space density for the selection effect of only a small fraction of CVs being bright enough to be seen even in a distance-limited sample. They assumed that the mass spectrum of WDs in CVs is not too different from that of single WDs. The birth rate of classical CVs in Model A is $2.0\times10^{-2}\,\mathrm{yr}^{-1}$, which is only a factor of 3 greater than this, so that the two are consistent, considering that a binary fraction less than unity would reduce the derived rate. The intrinsic local space density of CVs quoted by Ritter & Burkert (1986) is $(1-2)\times10^{-4}\,\mathrm{pc}^{-3}$ (6 to 12×10^7 in the Galaxy), which they note seems rather high, and can be matched only by the results of Model D. Yungelson et al. (1997) find the present local space density of classical CVs in their model to be about $3\times10^{-5}\,\mathrm{pc}^{-3}$, which is in agreement with the Hertz et al. (1990) observed number, and consistent with the results of all the models except Model D.

4.3.2 Algols

Observational data on Algol systems suffer from the lack of a comprehensive survey aimed at establishing the local space density. The catalogue of eclipsing binaries published by Brancewicz & Dworak (1980) contains parallaxes for 653 systems classified as Algol. Apparent magnitudes for these systems can be obtained from the catalogue of interacting binaries published by Wood et al. (1980), although no mention is made as to the completeness limit of this catalogue. Fig. 10 shows the distribution of the Algol systems that have a primary mass greater than $1\,\mathrm{M}_\odot$ as a function of their apparent magnitude. The apparent brightness of a star is linked to its distance and bolometric luminosity by

$$l = \frac{L}{4\pi d^2}, \tag{107}$$

which defines a volume

$$V = \frac{4\pi}{3}\left(\frac{L}{4\pi l}\right)^{3/2}. \tag{108}$$

Assuming that the stars are uniformly distributed within this

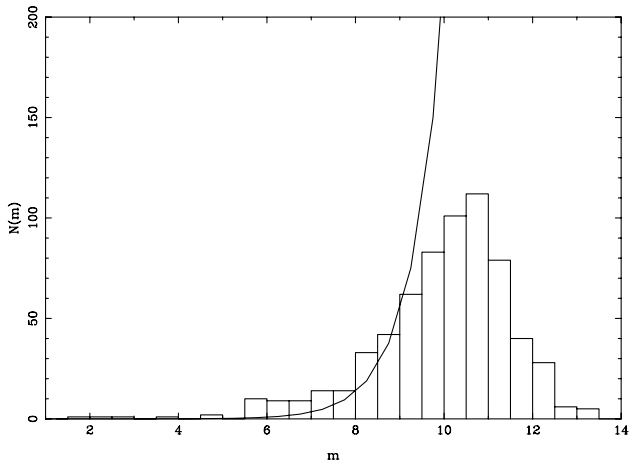

Figure 10. The apparent magnitude distribution of Algol systems identified by Brancewicz & Dworak (1980). The magnitudes are taken from Wood et al. (1980). A best fit to the data for $m \leq 9.5$ is shown by the full line.

volume, the number of stars out to apparent brightness l is

$$N_l(m) = Al^{-3/2}n(m), \tag{109}$$

where A is some constant. The function $n(m)$ depends only on the stellar mass and incorporates such quantities as the mass function, the dependence on luminosity and how long a star of a certain mass remains visible. Integrated over all masses, this is constant in equation (109), so it acts only to normalize the relation.

To determine the completeness limit of the Algol sample, we made a series of least-squares fits of equation (109) to the data, starting from the lowest magnitude bin; each successive fit includes data from the next bin in line. The number of Algol systems in the Brancewicz & Dworak (1980) sample that are brighter than 10th magnitude is 282. A least-squares fit to this subset of the data is shown in Fig. 10, and gives 300 systems brighter than 10th magnitude, which is just consistent with the data within the Poisson error. If we include systems above 10th magnitude in the fit, this leads to a large increase in the rms error between the fitted function and the data, as well as making the two inconsistent within the Poisson error. Therefore it seems safe to assume that the Algol sample is complete to 10th magnitude. This corresponds to a solar-mass primary at the end of the MS being visible to a distance of roughly 180 pc. Returning to the Brancewicz & Dworak sample and counting only systems within this distance with primary mass greater than $1\,\mathrm{M}_\odot$, we find 50 Algol systems corresponding to a local number density of $n \simeq 2 \times 10^{-6}\,\mathrm{pc}^{-3}$, and the number of classical Algols with $M_1 \geq \mathrm{M}_\odot$ currently in the Galaxy is then 1.2×10^6. However, almost half of the systems classified as Algol by Brancewicz & Dworak are assessed to have an extremely unlikely probability of RLOF by Budding (1984), who analysed the semidetached nature of each system. Therefore it is likely that this number is an overestimate. On the other hand, only about 1/3 of all classical Algols are likely to be observed as eclipsing binaries (see Appendix A2 for details). The number of Algols with an MS or subgiant primary more massive than $1\,\mathrm{M}_\odot$ is predicted by Model A to be about 1.4×10^7 (combining the MS, cold and hot Algol populations). This is an order of magnitude greater than the number predicted by observations, but is close enough not to be a major worry when we consider the uncertainties.

4.3.3 *Low-mass X-ray binaries*

The LMXB catalogue compiled by van Paradijs (1995) lists about 80 bright persistent sources in the Galaxy, making no distinction as to whether the compact star is an NS or BH. This number is in good agreement with the results of Model A, and in fair agreement with Model B. The birth rate of persistent NS LMXBs in Model A is similar to the rate found by PZV in their standard model, which includes velocity kicks. The relative distribution of NSs and BHs in X-ray binaries depends on the choice of single star mass above which BHs are formed, rather than NSs (see Section 2.6.6). This mass is not well constrained. It also depends on the assumption that an NS collapses to a BH when it accretes enough material to take its mass above $1.8\,\mathrm{M}_\odot$ (Bombaci 1996; see also Paper I). If the Eddington limit for mass transfer is applied, then the birth rate of persistent NS LMXBs in Model A increases to 3.612×10^{-6}, while the BH LMXB rate drops to 1.446×10^{-6}. The actual number of persistent LMXBs drops in this case, making the model inconsistent with the observations.

4.3.4 *Symbiotic stars*

About 125 symbiotic stars are observed, with WD secondaries about 10 times more prevalent than MS secondaries (Kenyon 1986). Estimates of the total number in the Galaxy range from about 1000 (Boyarchuk 1975) up to 20 000 (Luthardt 1992). Of the known symbiotic stars, roughly 20 per cent are D-Symb, but this is probably biased because these are harder to identify due to dust enshrouding the system. Kenyon (1986) predicts from theory that the total number in the Galaxy should be about 3000 with S-types and D-types contributing equally, although the relative number depends on the period distribution. Yungelson et al. (1995) consider only symbiotics with WD secondaries, and derive a birth rate of $0.073\,\mathrm{yr}^{-1}$, with 3370 present in the Galaxy using their standard model. These numbers are in good agreement with the predicted numbers from all of the models except Model D, which has only about 350. At least 98 per cent of the symbiotics found in each of the models have WD secondaries; the remainder have HeMS secondaries, and the birth rates do not appear to fluctuate significantly between models, except Model D.

As already mentioned, the systems with MS secondaries are part of the cold Algol population, the number of which is typically 7×10^5 when only GB or AGB primaries are considered. This is much larger than the expected number, so perhaps they are observed as symbiotic only for some of the RLOF phase or possibly only a small fraction are observed as symbiotic at all. The birth rate is typically of the order $10^{-2}\,\mathrm{yr}^{-1}$, so an average symbiotic lifetime of 10^4 yr for these MS + giant systems would be consistent with the predicted numbers. The large CV Symb numbers are not consistent with these systems being observed as symbiotic. It could be that they are simply not found, because nova explosions do not occur on the WD surface, and the giant primary probably dominates any light from the accretion disc.

4.3.5 *Double-degenerates*

Maxted & Marsh (1999) have conducted a radial velocity survey to measure the fraction of DDs among hydrogen-line (DA) WDs. They claim that their survey is the most sensitive so far undertaken, in terms of the detection of DDs, yet they found only two systems in a sample of 46 DA WDs, and these two were known to be DD prior to the observations. Their detection efficiency is 80 per cent

or higher for periods less than 10 d, and quickly drops to zero for wider orbits. Thus it seems that the fraction of DDs with $P < 10$ d among DA WDs has a lower limit of $\nu_{\rm WD} \approx 0.04$. This is consistent with the survey of Bragaglia et al. (1991), who find between one and three DDs in a sample of 49 DA WDs. Combining their results with a theoretical model that predicts the period, mass and mass ratio distributions of DDs, Maxted & Marsh (1999) find a 95 per cent probability that the DD fraction lies in the range 0.017 to 0.19, independent of the details of the model used. Saffer, Livio & Yungelson (1998) conducted a radial velocity survey of a sample of 107 DA WDs and 46 sdB stars. The sdB, or helium, stars were included, because they are believed to evolve to the WD cooling track on a relatively short time, following the exhaustion of central helium. From this sample they found a possible 23 binaries, of which 14 are WD + WD, seven are sdB + WD and two are WD + MS. Their detection efficiency is only 70 per cent for periods between 2 and 20 d. Of the 14 possible WD + WD binaries, seven have now been confirmed as DDs (Marsh, private communication) from the sample of 107 DA WDs, so this suggests $\nu_{\rm WD} > 0.07$.

Consideration of all these results together requires a reasonable theoretical model to predict at least $\nu_{\rm WD} \approx 0.05$ for DDs with periods less than 10 d, and $\nu_{\rm WD} \approx 0.1$ when all DDs are taken into account. The frequency of DDs among DA WDs can be converted to a DD birth rate if it is assumed that one DA WD is born per year (Fleming, Liebert & Green 1986; Phillips 1989), equivalent to our one star of $M > 0.8\,{\rm M}_{\odot}$ per year. In terms of the WDWD DD birth rates, both Models A and B satisfy the requirements of the observations: they predict 0.113 and $0.123\,{\rm yr}^{-1}$ respectively when all periods are included; if only DDs with $P < 10$ d are considered, the rates drop to 0.053 and $0.059\,{\rm yr}^{-1}$. Model C is in substantial disagreement with the observations: it predicts $0.076\,{\rm yr}^{-1}$ for all periods and only $0.013\,{\rm yr}^{-1}$ for $P < 10$ d; Model D is even worse. The predicted rate when eccentric orbits are allowed is also low, but the small period rate in this case is still $0.051\,{\rm yr}^{-1}$, in good enough agreement with both Model A and the observations. Han (1998) includes periods up to at least 100 d in his calculation of $0.03\,{\rm yr}^{-1}$ for the DD birth rate, but his model uses $\alpha_{\rm CE} = 1$ (although he accounts for the ionization energy in calculating the envelope binding energy, so this corresponds to a higher and variable $\alpha_{\rm CE}$ in this work).

The period distribution at formation for DDs in Model A is shown in Fig. 11. It has a peak at about 0.05 d. Included are periods for 22 suspected DD binaries provided by Marsh (private communication). To account for the short lives of short-period systems, we also show the period distribution weighted by the corresponding gravitational radiation time-scale for each system. The weighted distribution for Model B shows that the observed distribution is much better represented when tidal evolution is included in the model.

If the merging of two WDs is the progenitor of all type Ia SNe, then it is necessary for an observed population of DDs to contain a certain proportion of very close systems with the combined mass of the components near or above the Chandrasekhar limit. The absence of these systems has proven a major obstacle for the proponents of the WD merger progenitor model (e.g. Saffer et al. 1998). However, the merger time-scale decreases with shorter periods and larger binary masses, and so, as Fig. 11 shows, such systems are less likely to be observed. The statistics of DD searches must be improved before the WD merger progenitor model can be ruled out on this basis. In Model A the percentage of DDs with $P < 10$ d present in the Galaxy now that contain two COWDs, have

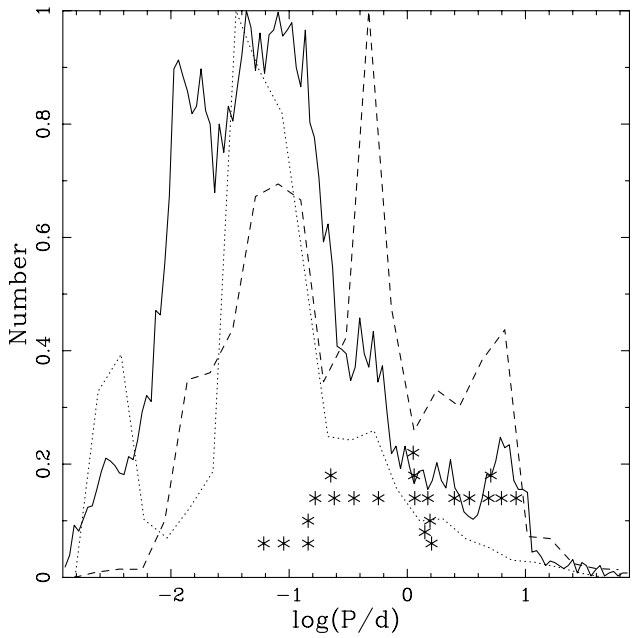

Figure 11. The distribution of periods of WDWD DD systems at formation in Model A (full line). The same distribution weighted by the gravitational radiation time-scale of each system is shown for Model A (dashed line) and Model B (dotted line). Also shown are the periods of 22 observed DD systems (asterisks) provided by Marsh (private communication). Note that the vertical positioning of these points bears no relation to any physical parameters.

$M_1 + M_2 > M_{\rm Ch}$, and will merge within the lifetime of the Galaxy is 0.3. The percentage containing a COWD and a HeWD of mass at least $0.15\,{\rm M}_{\odot}$ that will merge is 2.3. If all periods are included, then the percentages drop by a factor of 10. Considering that 30 DD systems with measured periods are known (Marsh, private communication), we predict that a possible type Ia SNe progenitor should soon be discovered (e.g. Maxted, Marsh & North 2000).

The total number of DDs currently in the Galaxy is predicted by Model A to be 6×10^8. If WDs are detectable for only the first 10^8 yr after formation, then the number drops to 10^7, more than the 3×10^6 predicted by the standard model of Han (1998).

Bragaglia, Renzini & Bergeron (1995) found that, of a sample of 164 DA WDs, 15 were low-mass WDs with $M < 0.4\,{\rm M}_{\odot}$. Low-mass WDs are interesting because they are not predicted by standard theory of single-star evolution, so they are believed to be, or have been, members of close binaries. They are not, however, directly representative of the number of DDs, because they can be produced via other channels of binary interaction, such as in WD/NS binaries. Our theoretical models include WDs with $M < 0.5\,{\rm M}_{\odot}$ in the LMWD populations, so a birth-rate of $0.1\,{\rm yr}^{-1}$ is a lower limit for comparison, and is in good agreement with all models except Model C.

4.3.6 Supernovae

Cappellaro et al. (1997) combined the results of five independent SN searches to obtain a sample of 110 SNe from which they derived the following birth rates for the Galaxy:

$4 \pm 1 \times 10^{-3}\,{\rm yr}^{-1}$ SNIa,

$2 \pm 1 \times 10^{-3}\,{\rm yr}^{-1}$ SNIb/c,

$12 \pm 6 \times 10^{-3}\,{\rm yr}^{-1}$ SNII.

The SNII rate is consistent with all the $Z = 0.02$ models except possibly Models C and G. Note that the increase in type II SNe for the lower metallicity population (Model E) is due to supernovae occurring in lower mass single stars (see table 1 in Pols et al. 1998). An obvious discrepancy lies in the birth rates of SNIb/c, because all the theoretical rates are too high, except for Model D which is in good agreement. This can be reconciled by assuming a binary fraction smaller than unity.

The SNII rate is a fairly robust number, but the SNIb/c rate is sensitive to many of the assumptions underlying the model. In all models other than Model D the majority of SNIb/c come from naked helium stars formed from relatively low-mass progenitors ($10-20\,M_{\odot}$) stripped by binary interaction. In a model containing only single stars with $Z = 0.02$ the SNII rate is the same as for Model A, but the SNIb/c rate is reduced to $2.7 \times 10^{-3}\,\mathrm{yr}^{-1}$, which would be consistent with observations. These single SNe Ib/c come from stars initially more massive than $24\,M_{\odot}$ which become Wolf–Rayet stars prior to explosion. However, this rate is sensitive to the assumed mass-loss rate for red supergiants (see Paper I), as well as to our assumption that BH formation ignites a supernova explosion, both of which are very uncertain. If mass-loss rates are lower or if black holes form without a SN, the SNIb/c rate from single stars would be lower.

4.3.7 *Γ-ray bursts*

The observed rate of γ-ray bursts is about $10^{-6}\,\mathrm{yr}^{-1}$ per galaxy (Piran 1996), which is typically an order of magnitude less than the merger rate of NS binaries found in all models except Model D. Numerical models of NS mergers suggest that the γ-rays produced are beamed and appear only in certain directions (Davies et al. 1994). An optically thick radiation–electron–positron plasma, or *fireball*, with initial energy larger than its rest mass is formed. The fireball is highly aspherical, and expands along the polar axis to form a jet. Only when the fireball reaches ultrarelativistic velocities and its material becomes optically thin, or reacts with the interstellar medium, do the observed γ-rays emerge. If the width of the jet is Θ, then we observe γ-ray bursts from only a fraction $2\Theta^{-2}$ of NSNS mergers (Piran 1996). Portegies Zwart & Yungelson (1998) find the neutron star merger rate in their model to be about $2 \times 10^{-5}\,\mathrm{yr}^{-1}$, which they claim is consistent with the observed rate of γ-ray bursts if the γ-ray emission is beamed into an opening angle of 10°. The same reasoning can reconcile the rates for all our models, except Model D, with the observed rate of γ-ray burst events.

5 CONCLUSIONS

The primary purpose of this paper was to describe in detail a rapid evolution algorithm for binary stars. Recognizing that tidal interaction is an important process in binary evolution, we have also studied its effect on the results of binary population synthesis, and made a global comparison with observations.

The main effects of tides on the evolution of an interacting binary are:

(1) circularization of the orbit, generally well before RLOF occurs, and

(2) the exchange of angular momentum between the orbit and the spins of the components.

Because as a star expands tidal synchronization transfers orbital angular momentum to the stellar rotation, in general the latter effect tends to bring binary components closer together and cause them to follow an evolutionary path similar to that of a closer binary if tides were ignored. However, we find that as a result of the sometimes very convoluted evolutionary paths of interacting binaries, this general principle does not always hold, and it is difficult to summarize the overall effect of tides on binary evolution.

The primary differences in our population synthesis results when tidal evolution within binary systems is ignored are as follows:

(i) a 35 per cent decrease in the birth rate of classical CVs, but a 23 per cent increase in sdB CV production;

(ii) lower birth rates for LMXBs with the persistent NS LMXB rate decreasing significantly, but conversely the number of NS LMXB increases;

(iii) a 10 per cent increase in the birth rate of double-degenerates;

(iv) an increase of 190 per cent in the incidence of exploding HeWDs, and

(v) 55 per cent more Algols currently in the Galaxy.

While these differences may seem substantial, they are generally not enough to confirm one way or another whether tidal evolution helps to explain the observed binary populations. This is mainly due to the lack of comprehensive binary searches and the selection effects involved that make discrimination on the basis of observational evidence a risky business. However, tides are present in binary systems whether we like it or not. One area where neglecting tidal evolution does seem to be in clear conflict with observations is in the incidence of HeWDs that explode as supernovae. This rate is too high by a factor of 2 to be accounted for by either the observed numbers of type Ia or type Ib SNe (see Tout et al. 2001 for further discussion).

The common-envelope efficiency parameter α_{CE} is an uncertain factor in a phase of evolution that is crucial for the production of many types of binary. The failure of the model with $\alpha_{\mathrm{CE}} = 1$ to produce anywhere near enough DDs would seem to favour $\alpha_{\mathrm{CE}} = 3$. Choosing the secondary mass independently of the primary mass does not produce enough DDs, symbiotics or type Ia SN candidates. All in all, the results favour using the properties of Model A. In fact, the standard tidal model, represented by Model A, is not in disagreement with any of the observations, except in the production of too many type Ib/c SNe. This discrepancy could indicate a lower mass-loss rate for helium stars.

A major conclusion of this work must be that it is extremely difficult to set constraints on any of the parameters involved in binary evolution from population synthesis of birth rates and Galactic numbers of the various types of binary. This is certainly true while such a large number of parameters remain uncertain. The task would be simpler if we could find observational tests specific to an individual parameter. For example, Algols do not require CE evolution for formation. Therefore, if observational constraints on the number of Algol systems currently in the Galaxy improve, then this could provide a suitable test for models of mass transfer on a thermal time-scale. The effect of varying additional model parameters, such as the binary enhanced mass loss, and initial conditions, such as the separation distribution, would need to be quantified before such a test could be reliably implemented. This is beyond the scope of this paper, but will be the subject of future work. In terms of tides, it is difficult to isolate direct tests of the tidal evolution model with the type of population synthesis

performed in this paper. In fact, to properly constrain the strength of tidal interaction, it is necessary to study pre-RLOF binaries, as has been done previously by, for example, Zahn (1975, 1977). What we would like to emphasize is that the outcome of binary evolution is sensitive to the physical processes of tidal circularization and synchronization. Therefore any attempt to constrain uncertain parameters in binary evolution by the method of population synthesis must utilize a binary-evolution algorithm that incorporates a working model of tidal evolution, such as that presented here.

An exciting challenge for the future involves attempting to reproduce the individual orbital characteristics of a large number of observed binaries with our binary-evolution model. This will allow multiparameter fitting, and should become a powerful tool as the statistics of binary surveys continue to improve. Our preliminary work in this area has shown that the observed properties of DD binaries are much easier to explain when tidal evolution is included. A detailed exploration of the DD parameter space will be the focus of another paper.

Tidal synchronism is important but, because orbits generally circularize before Roche lobe overflow, the outcome of the interactions of systems with the same semilatus rectum is almost independent of eccentricity. Although the inclusion of a distribution of eccentricities seems natural, it is not necessary in population synthesis of interacting binaries; however, the initial separations should be distributed according to the observed distribution of semilatera recta rather than periods or semimajor axes.

A necessity for the near future is a thorough comparison of our BSE algorithm with the workings of a detailed evolution code (e.g. Nelson & Eggleton 2001). In this way we can improve the algorithm, especially the treatment of the Hertzsprung gap phase, and hopefully add more stringent constraints to many of the evolution variables. Work is already underway to provide more accurate descriptions of the parameters k_2' (see Section 2.3.1) and λ (see Section 2.7.1), through investigation of the detailed stellar models provided by Pols et al. (1998). The algorithm will also be improved by providing options for how angular momentum is lost from the binary system during non-conservative mass transfer (see Section 2.6), reflecting the various possible modes of mass transfer (Soberman, Phinney & van den Heuvel 1997). When this work is completed, we will perform additional population synthesis calculations in order to quantify how the various improvements affect the results presented here.

6 AVAILABILITY OF THE BSE CODE

The BSE algorithm allows the entire evolution of even the most complicated binary systems to be modelled in less than a second of CPU time, rather than the several hours required when using a full stellar evolution code. It is therefore ideal for synthesizing large populations of binary stars, and will prove an extremely useful tool for testing uncertain processes in binary evolution. To obtain a copy of the BSE package described in this paper, send a request to the authors, who will consider providing the FORTRAN subroutines by ftp.

ACKNOWLEDGMENTS

JRH thanks Trinity College and the Cambridge Commonwealth Trust for their support during this work. CAT is very grateful to PPARC for support from an Advanced Fellowship. ORP thanks the Institute of Astronomy, Cambridge for supporting a number of visits undertaken during this work. We thank Peter Eggleton, Sverre Aarseth, Philipp Podsiadlowski and Gerry Gilmore for many helpful suggestions and comments, and the anonymous referee for a number of insightful remarks. We also thank Tom Marsh for making his data on double-degenerate systems available.

REFERENCES

Alexander M. E., 1973, Ap&SS, 23, 459
Bailey V. C., 1999, PhD thesis, Univ. Cambridge
Bailey V. C., Davies M. B., 1999, MNRAS, 308, 257
Beloborodov A. M., 1998, MNRAS, 297, 739
Benz W., Hills J. G., 1992, ApJ, 389, 546
Binney J., Tremaine S., 1987, Galactic Dynamics. Princeton Univ. Press, Princeton
Boffin H. M. J., Jorissen A., 1988, A&A, 205, 155
Bombaci I., 1996, A&A, 305, 871
Bond H. E., Liller W., Mannery E. J., 1978, ApJ, 223, 252
Bondi H., Hoyle F., 1944, MNRAS, 104, 273
Boyarchuk A. A., 1975, in Sherwood V. E., Plaut L., eds, Proc. IAU Symp. 67, Variable Stars and Stellar Evolution. Reidel, Dordrecht, p. 377
Bragaglia A., Greggio L., Renzini A., D'Odorico S., 1991, in Woosley S. E., ed., Supernovae. Springer, New York, p. 599
Bragaglia A., Renzini A., Bergeron P., 1995, ApJ, 443, 735
Branch D., 1998, ARA&A, 36, 17
Brancewicz H. K., Dworak T. Z., 1980, Acta Astron., 30, 501
Brandt N., Podsiadlowski P., 1995, MNRAS, 274, 461
Budding E., 1984, Ap&SS, 99, 299
Cameron A. G. W., Mock M., 1967, Nat, 215, 464
Campbell C. G., 1984, MNRAS, 207, 433
Cappellaro E., Turatto M., Tsvetkov D. Yu., Bartunov O. S., Pollas C., Evans R., Hamuy M., 1997, A&A, 322, 431
Che-Bohnenstengel A., Reimers D., 1986, A&A, 156, 172
Crampton D., Cowley A. P., Fisher W. A., 1986, ApJ, 300, 788
Crawford J. A., 1955, ApJ, 121, 71
Davies M. B., Benz W., Piran T., Thielemann F. K., 1994, ApJ, 431, 742
de Kool M., 1992, A&A, 261, 188
Edvardsson B., Andersen J., Gustafsson B., Lambert D. L., Nissen P. E., Tomkin J., 1993, A&A, 275, 101
Eggleton P. P., 1983, ApJ, 268, 368
Eggleton P. P., Fitchett M., Tout C. A., 1989, ApJ, 347, 998
Faulkner J., 1971, ApJ, 170, L99
Fleming T. A., Liebert J., Green R. F., 1986, ApJ, 308, 176
Fryer C., Kalogera V., 1997, ApJ, 489, 244
Fryer C. L., Benz W., Herant M., 1996, ApJ, 460, 801
Goldberg D., Mazeh T., 1994, A&A, 282, 801
González Pérez J. M., 1999, in Solheim J.-E., Meistas E. G., eds, ASP Conf. Ser. Vol. 169, 11th European Workshop on White Dwarfs. Astron. Soc. Pac., San Francisco, p. 428
Hack M., Engin S., Yilmaz N., Sedmak G., Rusconi L., Boehm C., 1992, A&AS, 95, 589
Han Z., 1998, MNRAS, 296, 1019
Han Z., Eggleton P. P., Podsiadlowski P., Tout C. A., 1995, MNRAS, 277, 1443
Hansen B. M. S., Phinney E. S., 1997, MNRAS, 291, 569
Hartmann D. H., 1996, A&AS, 120, 31
Heggie D. C., 1975, MNRAS, 173, 729
Hertz P., Bailyn C. D., Grindlay J. E., Garcia M. R., Cohn H., Lugger P. M., 1990, ApJ, 364, 251
Hjellming M. S., 1989, PhD thesis, Univ. Illinois, Urbana
Hjellming M. S., Webbink R. F., 1987, ApJ, 318, 794
Hoyle F., 1955, Frontiers of Astronomy. Wm. Heinemann, London, p. 195
Huang S. S., 1956, AJ, 61, 49
Hurley J. R., 2000, PhD thesis, Univ. Cambridge
Hurley J. R., Pols O. R., Tout C. A., 2000, MNRAS, 315, 543, (Paper I)

Hurley J. R., Tout C. A., Aarseth S. J., Pols O. R., 2001, MNRAS, 323, 630
Hut P., 1980, A&A, 92, 167
Hut P., 1981, A&A, 99, 126
Iben I., Jr, Livio M., 1993, PASP, 105, 1373
Iben I., Jr, Tutukov A. V., 1984, ApJS, 54, 335
Iben I., Jr, Tutukov A. V., 1996, ApJS, 105, 145
Iben I., Jr, Tutukov A. V., Yungelson L., 1995, ApJS, 100, 233
Iben I., Jr, Tutukov A. V., Yungelson L., 1996, ApJ, 456, 750
Karakas A., Tout C. A., Lattanzio J. C., 2000, MNRAS, 316, 689
Kaspi V. M., Bailes M., Manchester R. N., Stappers B. W., Bell J. F., 1996, Nat, 381, 584
Kawai Y., Saio H., Nomoto K., 1987, ApJ, 315, 229
Kenyon S. J., 1986, The Symbiotic Stars. Cambridge Univ. Press, Cambridge
Knox R. A., Hawkins M. R. S., Hambly N. C., 1999, MNRAS, 306, 736
Kopal Z., 1978, Dynamics of Close Binary Systems. Riedel, Dordrecht
Kroupa P., Tout C. A., Gilmore G., 1993, MNRAS, 262, 545
Kučinskas A., 1999, Ap&SS, 262, 127
Kuijken K., Gilmore G., 1989, MNRAS, 239, 651
Kuznetsov O. A., Prokhorov M. E., Sazhin M. V., Chechetkin V. M., 1998, Astronomy Reports, 42, 638
Lamers H. J. G. L. M., Snow T. P., Lindholm D. M., 1995, ApJ, 455, 269
Lamers H. J. G. L. M., van den Heuvel E. P. J., Petterson J. A., 1976, A&A, 49, 327
Levato H., 1974, A&A, 35, 259
Livio M., 2000, in Niemeyer J. C., Truran J. W., eds, Type Ia Supernovae: Theory and Cosmology. Cambridge Univ. Press, Cambridge, p. 33
Livne E., Arnett D., 1995, ApJ, 452, 62
Luthardt R., 1992, Reviews Mod. Astron., 5, 38
Lyne A. G., Lorimer D. R., 1994, Nat, 369, 127
Maxted P. F. L., Marsh T. R., 1999, MNRAS, 307, 122
Maxted P. F. L., Marsh T. R., North R. C., 2000, MNRAS, 317, L41
Mazeh T., Goldberg D., Duquennoy A., Mayor M., 1992, ApJ, 401, 265
McWilliam A., 1997, ARA&A, 35, 503
Nelson C. A., Eggleton P. P., 2001, ApJ, 552, 664
Nomoto K., Kondo Y., 1991, ApJ, 367, L19
Nomoto K., Sugimoto D., 1977, PASJ, 29, 765
Paczyński B., 1976, in Eggleton P. P., Mitton S., Whelan J. A. J., eds, Proc. IAU Symp. 73, Structure and Evolution of Close Binary Systems. Reidel, Dordrecht, p. 75
Phelps R., 1997, ApJ, 483, 826
Phillips J. P., 1989, in Torres-Peimbert S., ed., Proc. IAU Symp. 131, Planetary Nebulae. Kluwer, Dordrecht, p. 425
Piran E. S., 1996, in van Paradijs J., van den Heuvel E., Kuulkers E., eds, Proc. IAU Symp. 165, Compact Stars in Binaries. Kluwer, Dordrecht, p. 489
Politano M., 1996, ApJ, 465, 338
Pols O. R., Marinus M., 1994, A&A, 288, 475
Pols O. R., Schröder K. P., Hurley J. R., Tout C. A., Eggleton P. P., 1998, MNRAS, 298, 525
Popper D. M., 1980, ARA&A, 18, 115
Portegies Zwart S. F., Verbunt F., 1996, A&A, 309, 179, (PZV)
Portegies Zwart S. F., Yungelson L. R., 1998, A&A, 332, 173
Pringle J. E., Wade R. A., 1985, Interacting Binary Stars. Cambridge Univ. Press, Cambridge
Rappaport S., Verbunt F., Joss P., 1983, ApJ, 275, 713
Rasio F. A., Shapiro S. L., 1991, ApJ, 377, 559
Rasio F. A., Tout C. A., Lubow S. H., Livio M., 1996, ApJ, 470, 1187
Regős E., Tout C. A., 1995, MNRAS, 273, 146
Ritter H., Burkert A., 1986, A&A, 158, 161
Ruffert M., 1999, A&A, 346, 861
Saffer R. A., Livio M., Yungelson L. R., 1998, ApJ, 502, 394
Saio H., Nomoto K., 1998, ApJ, 500, 388
Skumanich A., 1972, ApJ, 171, 565
Soberman G. E., Phinney E. S., van den Heuvel E. P. J., 1997, A&A, 327, 620
Stępień K., 1995, MNRAS, 274, 1019
Strassmeier K. G., 1996, A&A, 314, 558
Tassoul J.-L., Tassoul M., 1996, Fundam. Cosmic Phys., 16, 337
Terman J. L., Taam R. E., Savage C. O., 1998, MNRAS, 293, 113
Theuns T., Boffin H. M. J., Jorissen A., 1996, MNRAS, 280, 1264
Thorne K. S., Żytkow A. N., 1977, ApJ, 212, 832
Tout C. A., Eggleton P. P., 1988, MNRAS, 231, 823
Tout C. A., Aarseth S. J., Pols O. R., Eggleton P. P., 1997, MNRAS, 291, 732
Tutukov A., Yungelson L., 1996, MNRAS, 280, 1035
van Paradijs J., 1995, in Lewin W. H. G., van Paradijs J., van den Heuvel E. P. J., eds, X-ray Binaries. Cambridge Astrophysics Series, Vol. 26, p. 520
van Paradijs J., 1996, ApJ, 464, L139
van Paradijs J., van den Heuvel E. P. J., Kouveliotou C., Fishman G. J., Finger M. H., Lewin W. H. G., 1997, A&A, 317, L9
Verbunt F., 1984, MNRAS, 209, 227
Webbink R. F., 1984, ApJ, 277, 355
Webbink R. F., 1985, in Pringle J. E., Wade R. A., eds, Interacting Binary Stars. Cambridge Univ. Press, Cambridge, p. 39
Webbink R. F., 1988, in Mikolajewska J., Friedjung M., Kenyon S. J., Viotto R., eds, Proc. IAU Colloq. 103, The Symbiotic Phenomenon. Kluwer, Dordrecht, p. 311
Webbink R. F., Kalogera V., 1997, in Wickramasinghe D. T., Bicknell G. V., Ferrario L., eds, ASP Conf. Ser. Vol. 121, Proc. IAU Colloq. 163, Accretion Phenomena and Related Outflows. Astron. Soc. Pac., San Francisco, p. 828
Whyte C. A., Eggleton P. P., 1985, MNRAS, 214, 357
Wijers R. A. M. J., Davies M. B., Tout C. A., 1996, Proc. NATO ASI, Cambridge, 1995, Evolutionary Processes in Binary Stars. Kluwer, Dordrecht
Wood F. B., Oliver J. P., Florkowski D. R., Koch R. H., 1980, Publ. Dept. of Astron., Univ. of Florida, Vol. I
Woosley S. E., Taam R. E., Weaver T. A., 1986, ApJ, 301, 601
Woosley S. E., Weaver T. A., 1994, ApJ, 423, 371
Yungelson L. R., Livio M., Tutukov A. V., Saffer R. A., 1994, ApJ, 420, 336
Yungelson L., Livio M., Tutukov A., Kenyon S. J., 1995, ApJ, 447, 656
Yungelson L., Livio M., Tutukov A., 1997, ApJ, 481, 127
Zahn J.-P., 1975, A&A, 41, 329
Zahn J.-P., 1977, A&A, 57, 383
Zahn J.-P., 1989, A&A, 220, 112
Zahn J.-P., 1992, in Duquennoy A., Mayor M., eds, Binaries as Tracers of Stellar Formation. Cambridge Univ. Press, Cambridge, p. 253
Zangrilli L., Tout C. A., Bianchini A., 1997, MNRAS, 289, 59

APPENDIX A

A1 Orbital parameters after supernova

Consider a frame of reference in which the pre-supernova centre of mass is at rest, the primary star is about to explode and the secondary is at the origin. The initial orbit is in the *XY*-plane, so that the initial specific angular momentum vector is directed along the positive *Z*-axis, and the separation vector $\boldsymbol{r} = \boldsymbol{r}_1 - \boldsymbol{r}_2$ is directed along the positive *Y*-axis, as shown in Fig. A1. The relative velocity of the stars is

$$\boldsymbol{v} = -v_{\rm orb}(\sin\beta\boldsymbol{i} + \cos\beta\boldsymbol{j}), \tag{A1}$$

where β is the angle between $\boldsymbol{r}$ and $\boldsymbol{v}$, and is such that

$$\sin\beta = \left[\frac{a^2(1-e^2)}{r(2a-r)}\right]^{1/2}, \tag{A2}$$

$$\cos\beta = -\frac{e\sin E}{(1-e^2\cos^2 E)^{1/2}}, \tag{A3}$$

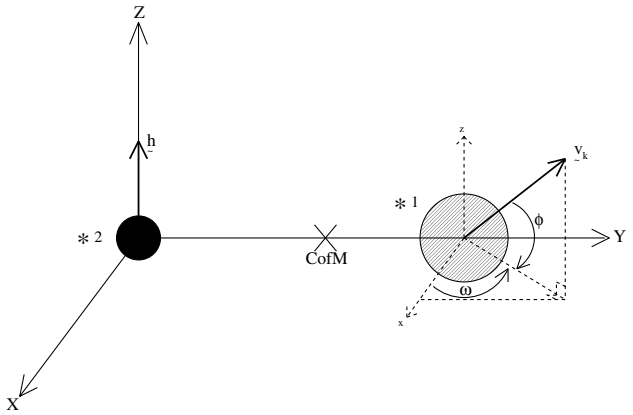

Figure A1. The binary and supernova kick geometry.

and E is the eccentric anomaly in Kepler's equation

$$\mathcal{M} = E - e\sin E \tag{A4}$$

for mean anomaly $\mathcal{M}$, which varies uniformly with time between 0 and 2π. The orbital speed is defined by

$$v_{\rm orb}^2 = \dot{r}^2 + r^2\dot{\theta}^2 = GM_{\rm b}\left(\frac{2}{r} - \frac{1}{a}\right). \tag{A5}$$

As well as losing an amount of mass ΔM_1, the primary is subject to a kick velocity $\boldsymbol{v}_{\rm k}$ during the supernova explosion, so that

$$M_1 \rightarrow M_1' = M_1 - \Delta M_1,$$

$$M_{\rm b} \rightarrow M_{\rm b}' = M_{\rm b} - \Delta M_1,$$

$$\boldsymbol{v}_1 \rightarrow \boldsymbol{v}_1' = \boldsymbol{v}_1 + \boldsymbol{v}_{\rm k},$$

where

$$\begin{aligned}\boldsymbol{v}_{\rm k} &= v_{\rm k}(\cos\omega\cos\phi\boldsymbol{i} + \sin\omega\cos\phi\boldsymbol{j} + \sin\phi\boldsymbol{k}) \quad ,\\ v_{\rm k} &= |\boldsymbol{v}_{\rm k}|.\end{aligned} \tag{A6}$$

Here $\boldsymbol{i}$, $\boldsymbol{j}$ and $\boldsymbol{k}$ are unit vectors in the X, Y and Z directions respectively. We assume that the separation is constant, as the explosion is instantaneous. To find the separation at the moment of explosion, we randomly choose a mean anomaly $\mathcal{M}$ and then solve equation (A4) for the eccentric anomaly E using a Newton–Raphson method. Then

$$r = a(1 - e\cos E \quad , \quad r = |\boldsymbol{r}| \tag{A7}$$

in terms of the initial semimajor axis and eccentricity. This is necessary because the binary is evolved using values averaged over an orbital period, so that the exact separation at any one time is not known for an eccentric orbit.

After the supernova the new relative velocity is

$$\begin{aligned}\boldsymbol{v}_n &= \boldsymbol{v} + \boldsymbol{v}_{\rm k}\\ &= (v_{\rm k}\cos\omega\cos\phi - v_{\rm orb}\sin\beta)\boldsymbol{i} + (v_{\rm k}\sin\omega\cos\phi - v_{\rm orb}\cos\beta)\boldsymbol{j}\\ &\quad + v_{\rm k}\sin\phi\boldsymbol{k}.\end{aligned}$$

From equation (A5) it must be true that

$$v_n^2 = GM_{\rm b}'\left(\frac{2}{r} - \frac{1}{a_n}\right) \tag{A8}$$

for the new orbital parameters, where

$$\begin{aligned}v_n^2 &= |\boldsymbol{v}_n|^2\\ &= v_k^2 + v_{\rm orb}^2 - 2v_{\rm orb}v_{\rm k}(\cos\omega\cos\phi\sin\beta\\ &\quad + \sin\omega\cos\phi\cos\beta).\end{aligned} \tag{A9}$$

This can be solved for the semimajor axis a_n of the new orbit. The specific angular momentum of the new system is

$$\boldsymbol{h}' = \boldsymbol{r}\times\boldsymbol{v}_n, \tag{A10}$$

so it follows from equation (4) that

$$GM_{\rm b}'a_n(1 - e_n^2) = |\boldsymbol{r}\times\boldsymbol{v}_n|^2 \tag{A11}$$

where

$$|\boldsymbol{r}\times\boldsymbol{v}_n|^2 = r^2[v_k^2\sin^2\phi + (v_{\rm k}\cos\omega\cos\phi - v_{\rm orb}\sin\beta)^2]. \tag{A12}$$

This we solve for the new eccentricity e_n of the orbit. If either $a_n \leq 0$ or $e_n > 1$, then the binary does not survive the kick.

The angle ν between the new and old angular momentum vectors is given by

$$\cos\nu = \frac{v_{\rm orb}\sin\beta - v_{\rm k}\cos\omega\cos\phi}{[v_k^2\sin^2\phi + (v_{\rm k}\cos\omega\cos\phi - v_{\rm orb}\sin\beta)^2]^{1/2}}. \tag{A13}$$

An amount of mass ΔM_1 is ejected from the primary, and hence from the system, so that the new centre of mass has a velocity

$$\boldsymbol{v}_{\rm s} = \frac{M_1'}{M_{\rm b}'}\boldsymbol{v}_{\rm k} - \frac{\Delta M_1 M_2}{M_b' M_{\rm b}}\boldsymbol{v} \tag{A14}$$

relative to the old centre of mass frame. This agrees with Brandt & Podsiadlowski (1995) for initially circular orbits. Note that the ϕ used here is $\pi - \phi$ as defined in their coordinate system.

To determine the kick velocity, it is necessary to choose $\boldsymbol{v}_{\rm k}$, the magnitude of $\boldsymbol{v}_{\rm k}$, ϕ, the angle between $\boldsymbol{v}_{\rm k}$ and the orbital plane, and ω, the angle between the projection of $\boldsymbol{v}_{\rm k}$ on to the orbital plane and the X-axis, from appropriate distribution functions. We take the kick speed from a Maxwellian distribution

$$P(v_{\rm k}) = \sqrt{\frac{2}{\pi}}\frac{v_k^2}{\sigma_k^3}{\rm e}^{-v_k^2/2\sigma_k^2}, \tag{A15}$$

with a dispersion of $\sigma_{\rm k} = 190\,{\rm km\,s^{-1}}$ (Hansen & Phinney 1997) based on analysis of various pulsar proper motion samples.

For a variable $\mathcal{X}$ uniformly distributed between 0 and 1 we may write

$$P(v_{\rm k})\,{\rm d}v_{\rm k} = {\rm d}\mathcal{X} \tag{A16}$$

$$\Rightarrow \mathcal{X} = \int_0^{v_{\rm k}} P(v_{\rm k})\,{\rm d}v_{\rm k} = F(v_{\rm k}). \tag{A17}$$

The change of variable

$$u^2 = \frac{v_k^2}{2\sigma_k^2} \tag{A18}$$

gives us

$$F(u) = {\rm Erf}(u) - \frac{2}{\sqrt{\pi}}u\,{\rm e}^{-u^2}, \tag{A19}$$

so that $\mathcal{X} = F(u)$ can be solved for some $\mathcal{X}$, by Newton–Rapshon iteration, to give $v_{\rm k}$.

The kick direction is uniform over all solid angles, so that

$$P(\phi) = \cos\phi \quad , \quad \frac{-\pi}{2} \leq \phi \leq \frac{\pi}{2}, \tag{A20}$$

and ω is uniformly distributed between 0 and 2π.

A2 Eclipsing semidetached binaries

Consider a semidetached system in which a primary of radius R is filling its Roche lobe and is separated from a companion of radius r by a distance a. The angle that a line which is the inner tangent to the surface of both stars makes with the line joining the centres of the stars can be given by

$$\sin\psi = \frac{R+r}{a}. \tag{A21}$$

If we assume that half of the companion must be eclipsed for the light curve to be noticeably changed, and that $R \simeq R_L$, then

$$\sin\psi \simeq \frac{R_L}{a} \approx 1/3. \tag{A22}$$

Define i as the inclination angle between the line of sight and the normal to the orbital plane of the binary. If $i = 0$, then the orbital plane is perpendicular to the line of sight, and the binary will never eclipse; if $i = \pi/2$, then it is edge-on and will always eclipse. The probability of i between i and $i + \mathrm{d}i$ is

$$f(i)\,\mathrm{d}i = k \sin i\,\mathrm{d}i, \tag{A23}$$

for a normalization constant k. Only one orientation of the orbit gives $i = 0$, so it is the least likely case, whereas a full circle of orientations gives $i = \pi/2$. The normalization constraint

$$\int_0^{\pi/2} f(i)\,\mathrm{d}i = 1 \tag{A24}$$

determines $k = 1$. Now the binary eclipses if

$$\pi/2 - \psi < i < \pi/2, \tag{A25}$$

where

$$\psi = \arcsin(1/3) = \frac{\pi}{2} - \arccos(1/3). \tag{A26}$$

Therefore the fraction of systems that are likely to be eclipsing is

$$P = \int_{\arccos(1/3)}^{\pi/2} \sin i\,\mathrm{d}i = 1/3. \tag{A27}$$

This paper has been typeset from a TEX/LATEX file prepared by the author.